Astrofisica Nucleare e Subnucleare

Nuclear Astrophysics - 3

Hertzspung-Russell diagram

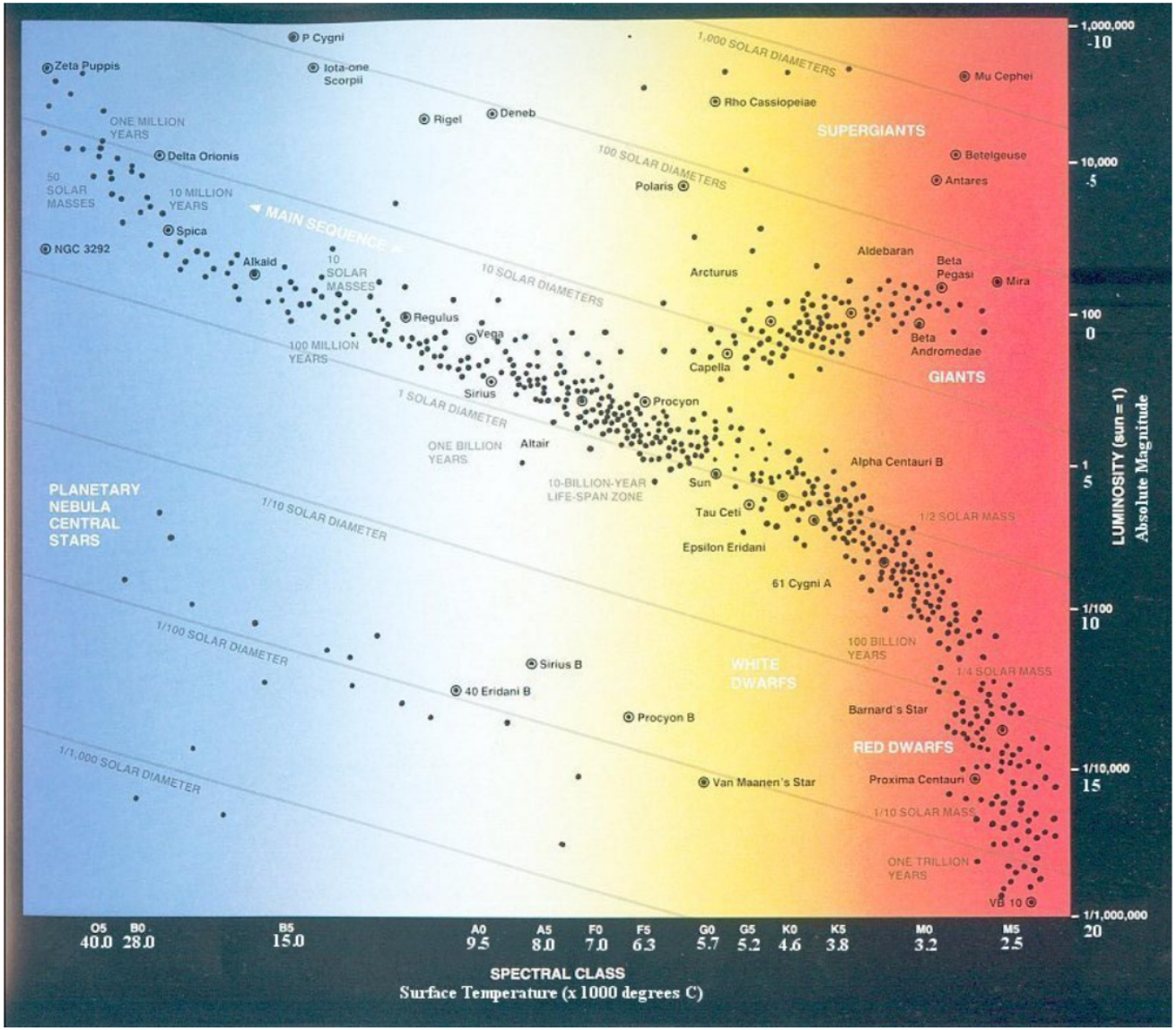

Life of small star (< 1,4 $M_{\odot}$)

Forms in Dust & Gas Cloud

Burns Hydrogen for 10 Billion Years

Becomes Red Giant Star burning Helium for 100 million years

Ejects outer layers and is a planetary nebula for 100,000 years

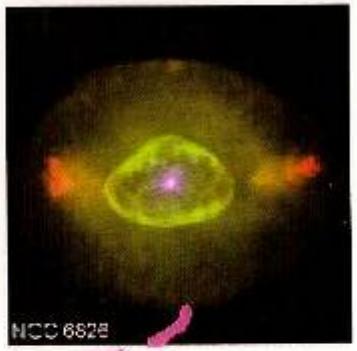

Becomes White Dwarf star for Eternity

Nuclear Binding Energy

Liberated energy is due to the gain in nuclear binding energy.

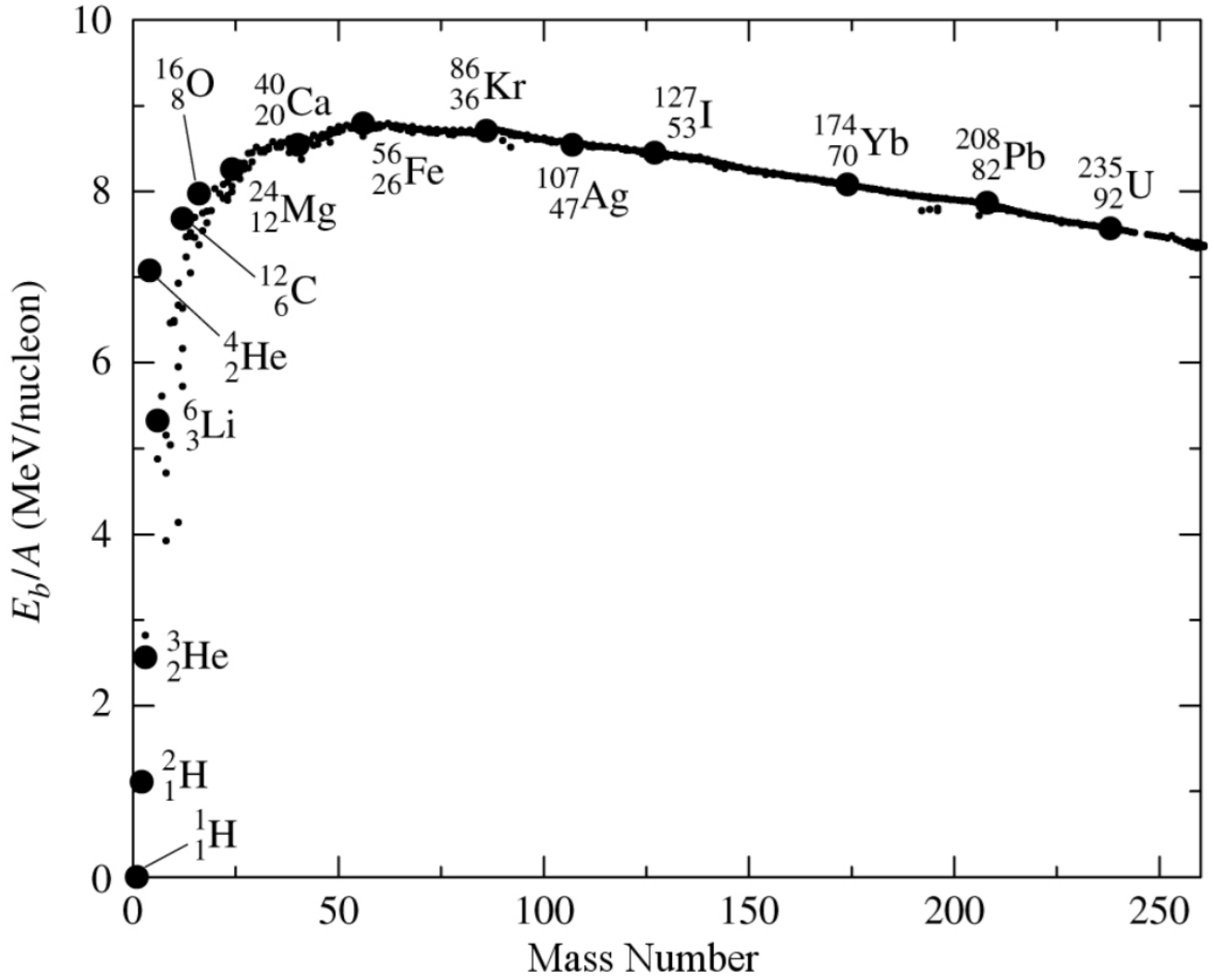

Gamow window

Using definition S factor:

$$\langle \sigma v \rangle = \left(\frac{8}{\pi m}\right)^{1/2} \frac{1}{(kT)^{3/2}} \int_0^\infty S(E) \exp\left[-\frac{E}{kT} - \frac{b}{E^{1/2}}\right] dE$$

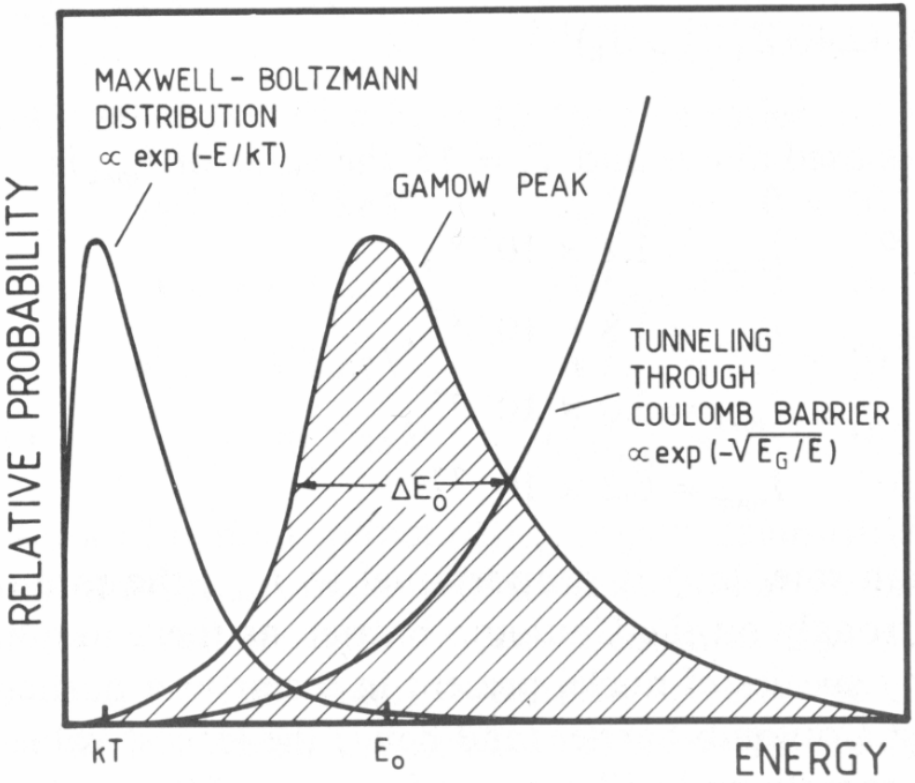

Problem of extrapolation in nuclear astrophysics

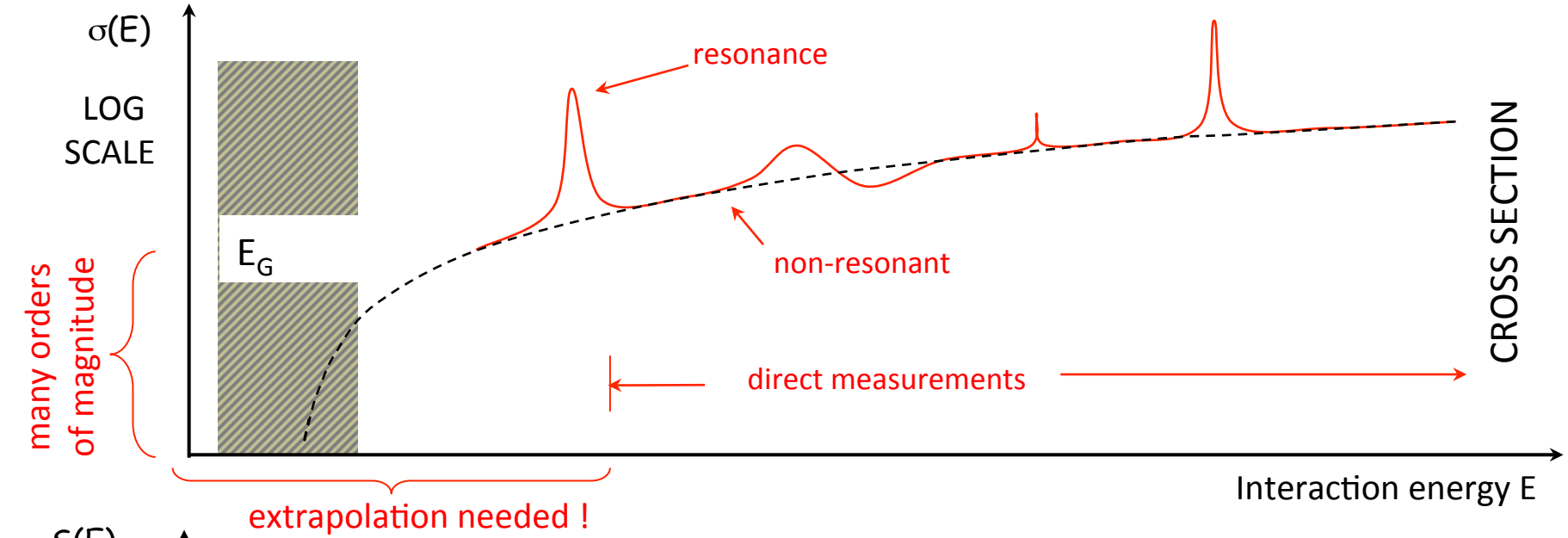

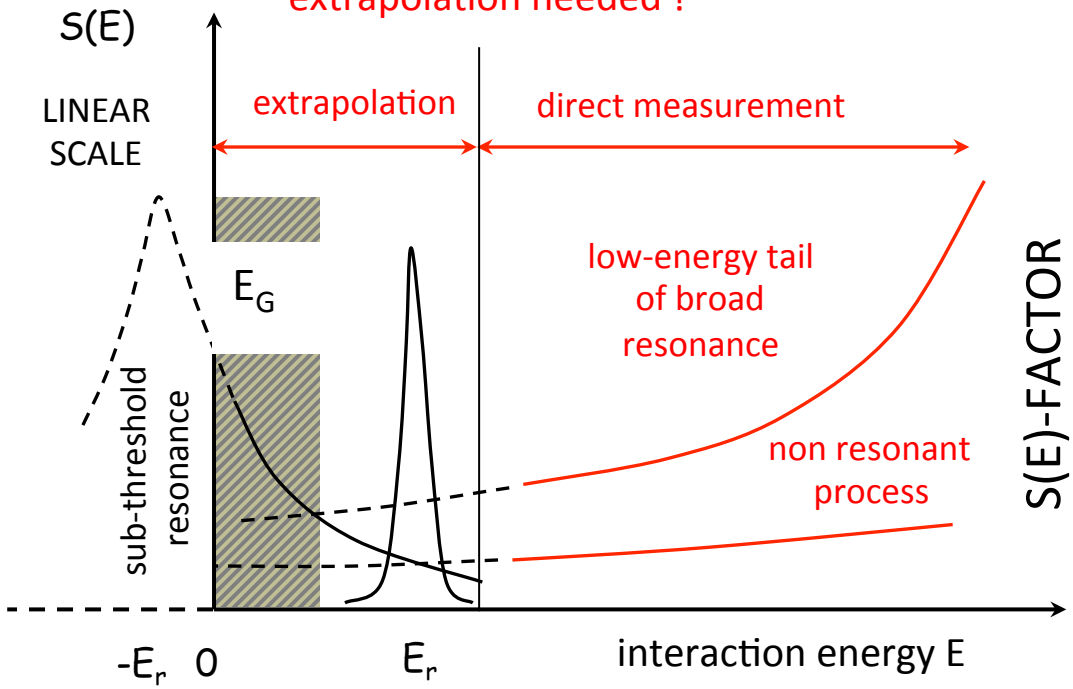

Most of the reactions of astrophysical interest happen via radiative capture.

$^{14}N(p,\gamma)^{15}O$,

$^{12}C(\alpha,\gamma)^{16}C$...

Hydrogen burning: ppI-chain

Step 1: $p + p \rightarrow {}^{2}\mathrm{He}$ (not possible)

$p + p \rightarrow d + e^{+} + \nu_e$

Step 2: $d + p \rightarrow {}^{3}\mathrm{He}$

$d + d \rightarrow {}^{4}\mathrm{He}$ (d abundance too low)

Step 3: ${}^{3}\mathrm{He} + p \rightarrow {}^{4}\mathrm{Li}$ (${}^{4}\mathrm{Li}$ is unbound)

${}^{3}\mathrm{He} + d \rightarrow {}^{4}\mathrm{He} + n$ (d abundance too low)

${}^{3}\mathrm{He} + {}^{3}\mathrm{He} \rightarrow {}^{4}\mathrm{He} + 2p$

$d + d$ not going because Y_d is small and $d + p$ leads to rapid destruction.
${}^{3}\mathrm{He} + {}^{3}\mathrm{He}$ goes because $Y_{^{3}\mathrm{He}}$ gets large as nothing destroys it.

pp chains

Once ^{4}He is produced can act as catalyst initializing the ppII and ppIII chains.

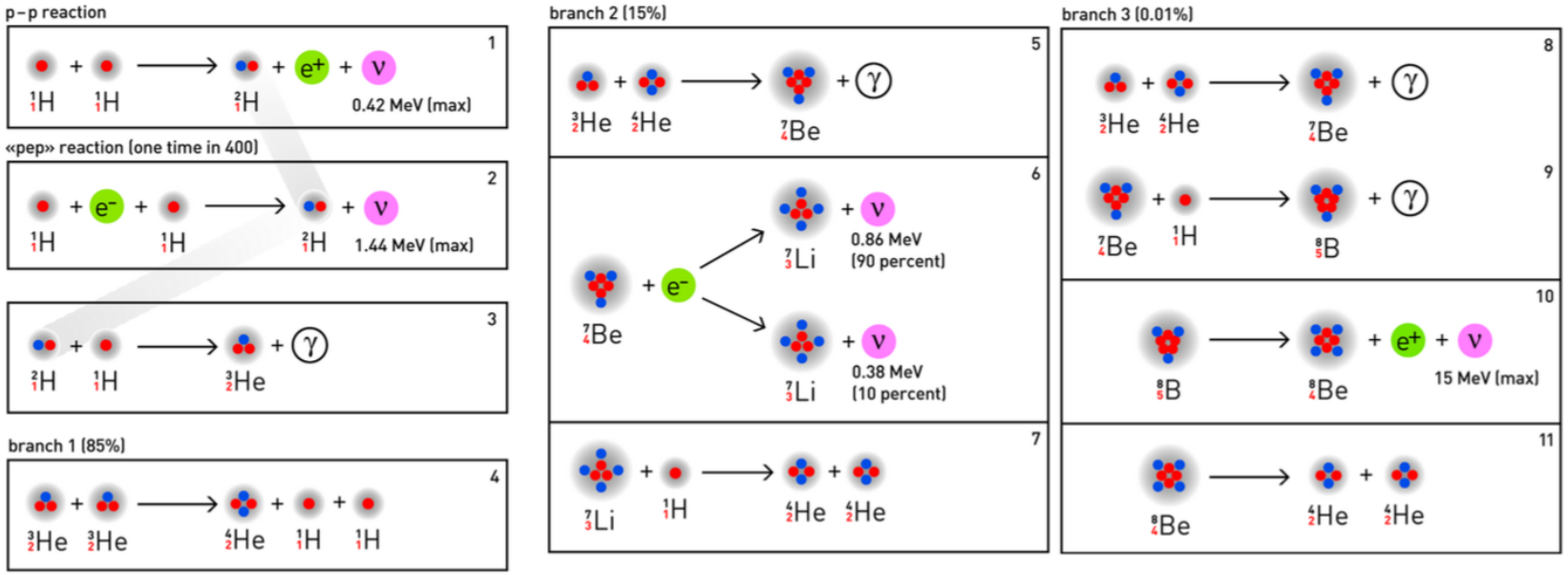

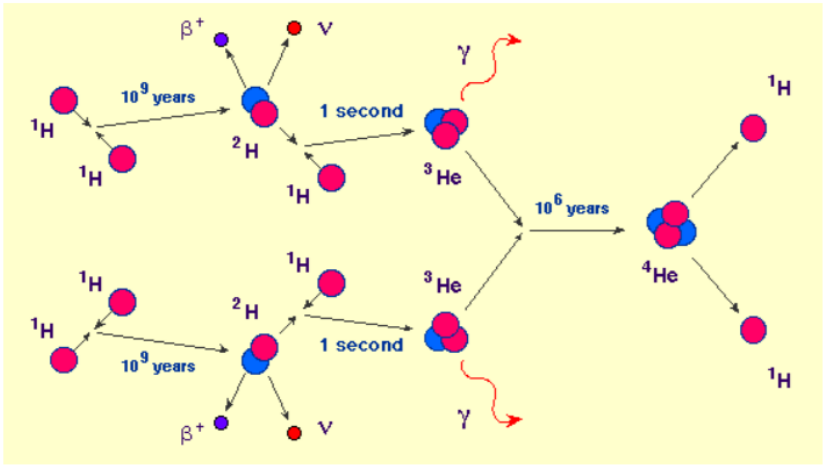

Reaction Network ppI-chain

$$\frac{dY_p}{dt} = -Y_p^2 \frac{\rho}{m_u}\langle\sigma v\rangle_{pp} - Y_d Y_p \frac{\rho}{m_u}\langle\sigma v\rangle_{pd} + Y_3^2 \frac{\rho}{m_u}\langle\sigma v\rangle_{33}$$

$$\frac{dY_d}{dt} = \frac{Y_p^2}{2}\frac{\rho}{m_u}\langle\sigma v\rangle_{pp} - Y_d Y_p \frac{\rho}{m_u}\langle\sigma v\rangle_{pd}$$

$$\frac{dY_3}{dt} = Y_d Y_p \frac{\rho}{m_u}\langle\sigma v\rangle_{pd} - Y_3^2 \frac{\rho}{m_u}\langle\sigma v\rangle_{33}$$

$$\frac{dY_4}{dt} = \frac{Y_3^2}{2}\frac{\rho}{m_u}\langle\sigma v\rangle_{33}$$

Stiff system of coupled differential equations.

The relevant S-factors

$p(p, e^+\nu_e)d$: $S_{11}(0) = (4.00 \pm 0.05) \times 10^{25}$ MeV b

calculated

$p(d, \gamma)^3\mathrm{He}$: $S_{12}(0) = 2.5 \times 10^{-7}$ MeV b

measured at LUNA

$^3\mathrm{He}(^3\mathrm{He}, 2p)^4\mathrm{He}$: $S_{33}(0) = 5.4$ MeV b

measured at LUNA

Laboratory Underground for Nuclear Astrophysics (Gran Sasso).

LUNA program: pp chain

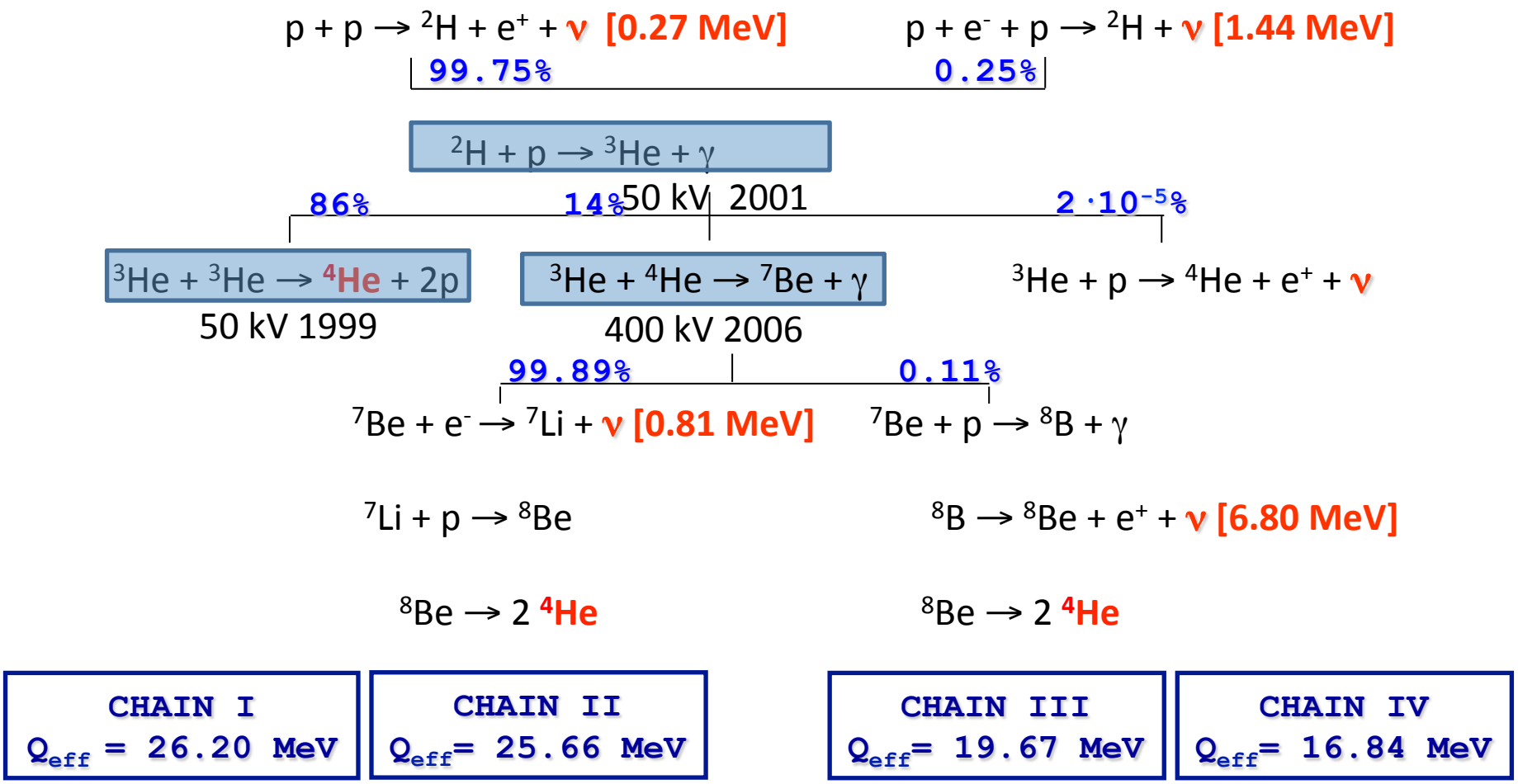

LUNA (Laboratory Underground for Nuclear Astrophysics)

50 kV accelerator @ Gran Sasso – Italy (1400 m rock -> 10^6 shielding factor)

$^3He(^3He,2p)^4He$

R. Bonetti et al.: Phys. Rev. Lett. 82 (1999) 5205

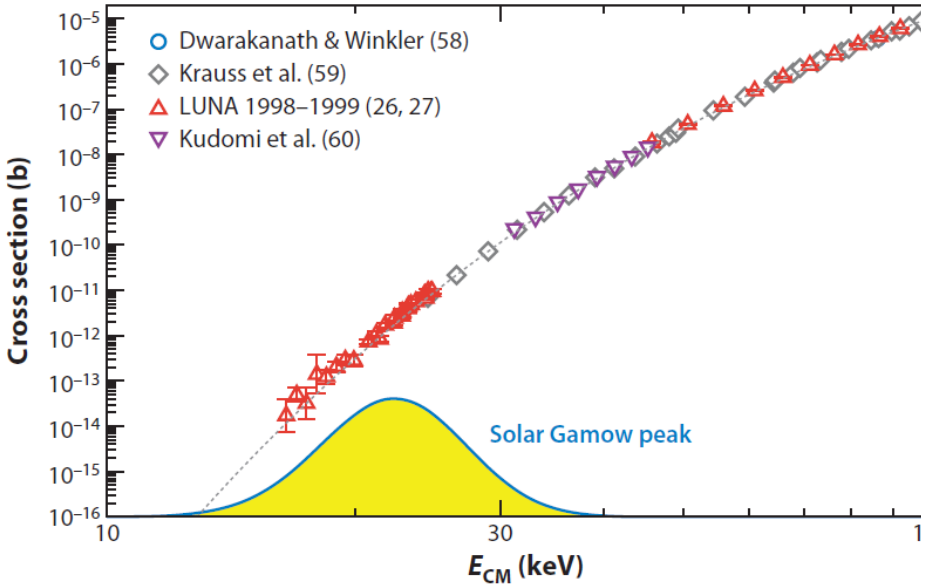

At lowest energy: σ ~ 20 fb → 1 event/month

$d(p,\gamma)^3He$

C. Casella et al.: Nucl. Phys. A706 (2002) 203-216

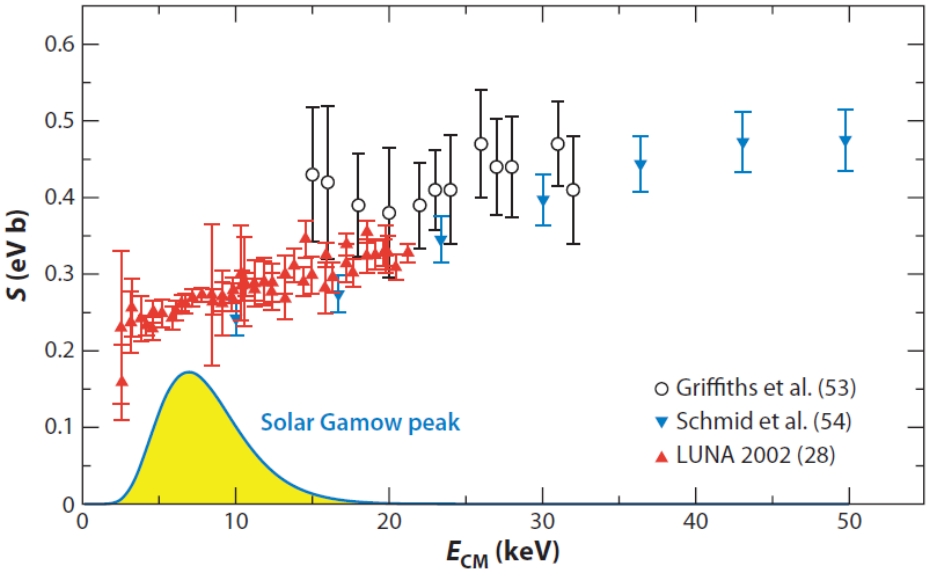

At lowest energy: σ ~ 9 pb → 50 counts/day

No *extrapolation* needed!

The other hydrogen burning: CNO cycle

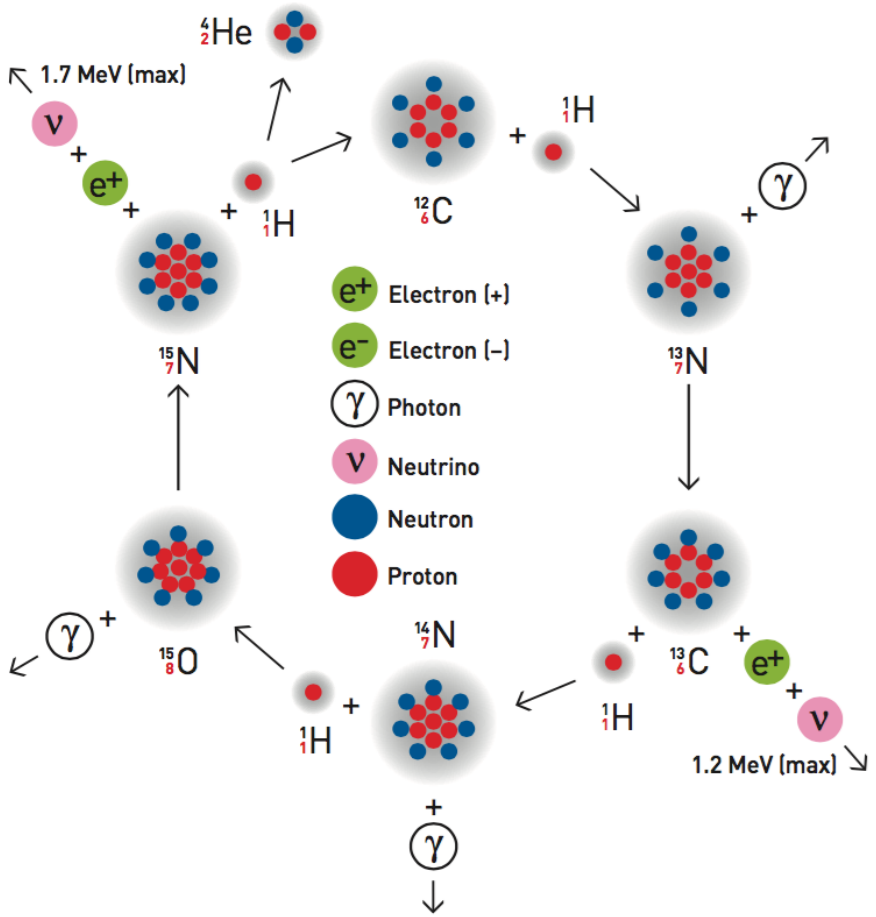

requires presence of ^{12}C as catalyst.

The Carbon Cycle

An alternative way of transmuting hydrogen into helium exists in the carbon cycle, which consists of the following six reactions

$$
\begin{aligned}
&C^{12} + H^1 \longrightarrow N^{13} + \gamma && + 1.95 \text{ Mev } (1.3 \times 10^7 \text{ yrs}) \\
&N^{13} \longrightarrow C^{13} + e^+ + \nu && + 2.22 \text{ Mev } (7 \text{ min}) \\
&C^{13} + H^1 \longrightarrow N^{14} + \gamma && + 7.54 \text{ Mev } (2.7 \times 10^6 \text{ yrs}) \\
&N^{14} + H^1 \longrightarrow O^{15} + \gamma && + 7.35 \text{ Mev } (3.2 \times 10^8 \text{ yrs}) \\
&O^{15} \longrightarrow N^{15} + e^+ + \nu && + 2.71 \text{ Mev } (82 \text{ sec}) \\
&N^{15} + H^1 \longrightarrow C^{12} + He^4 && + 4.96 \text{ Mev } (1.1 \times 10^5 \text{ yrs})
\end{aligned}
\qquad (10.3)
$$

To start with, the collision of a proton with a common carbon nucleus produces a N^{13} particle with emission of a gamma ray. The N^{13} particle is not stable but decays—in seven minutes, on the average—into the heavy carbon isotope with the emission of a positron and a neutrino. Again, the positron disappears together with an electron and the neutrino leaves the star. The next build-up step is taken when a second proton collides with the heavy carbon isotope, forming a common nitrogen nucleus.

Neutrino spectrum (Sun)

This is the predicted neutrino spectrum

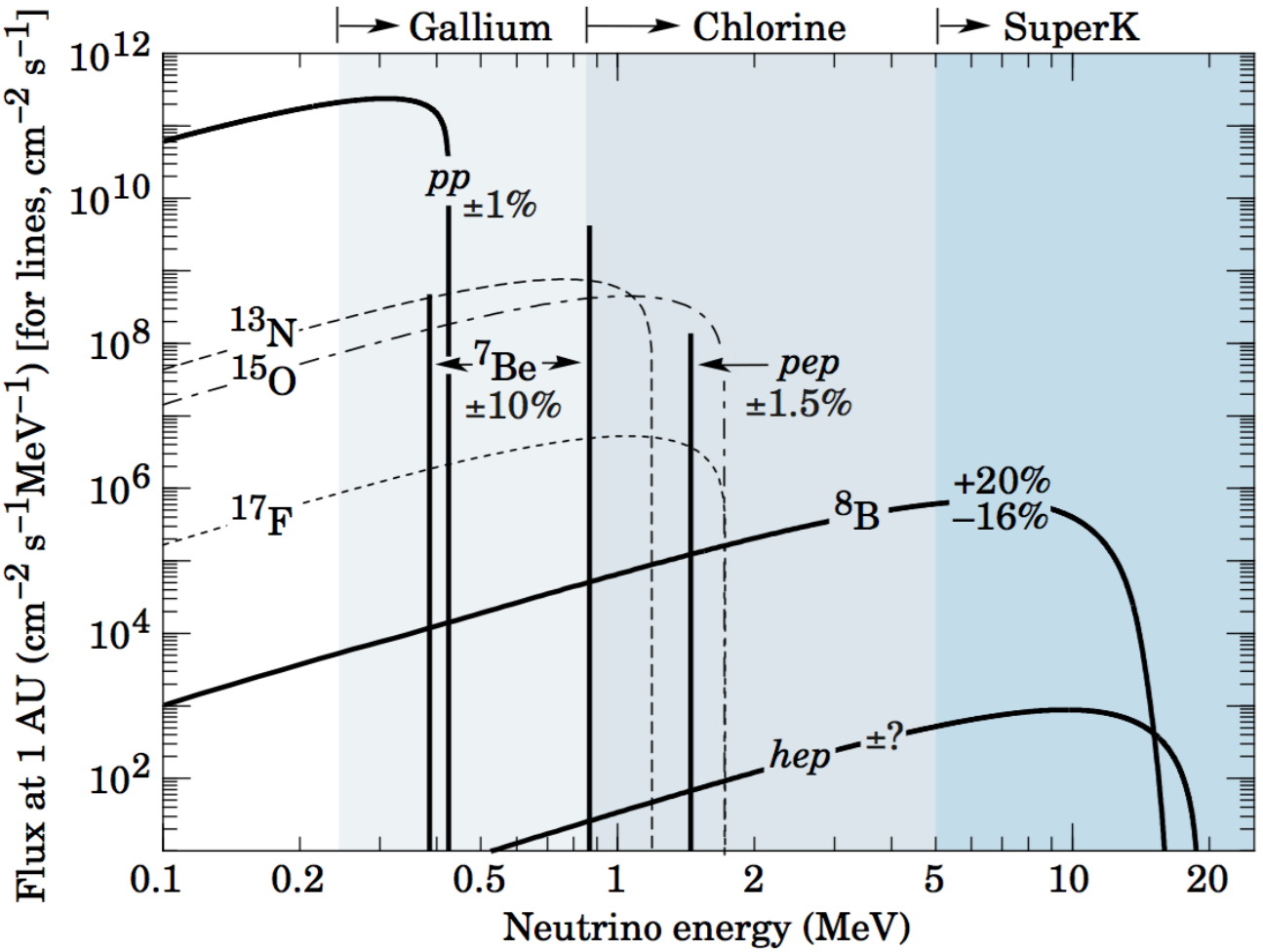

Energy generation: CNO cycle vs pp-chains

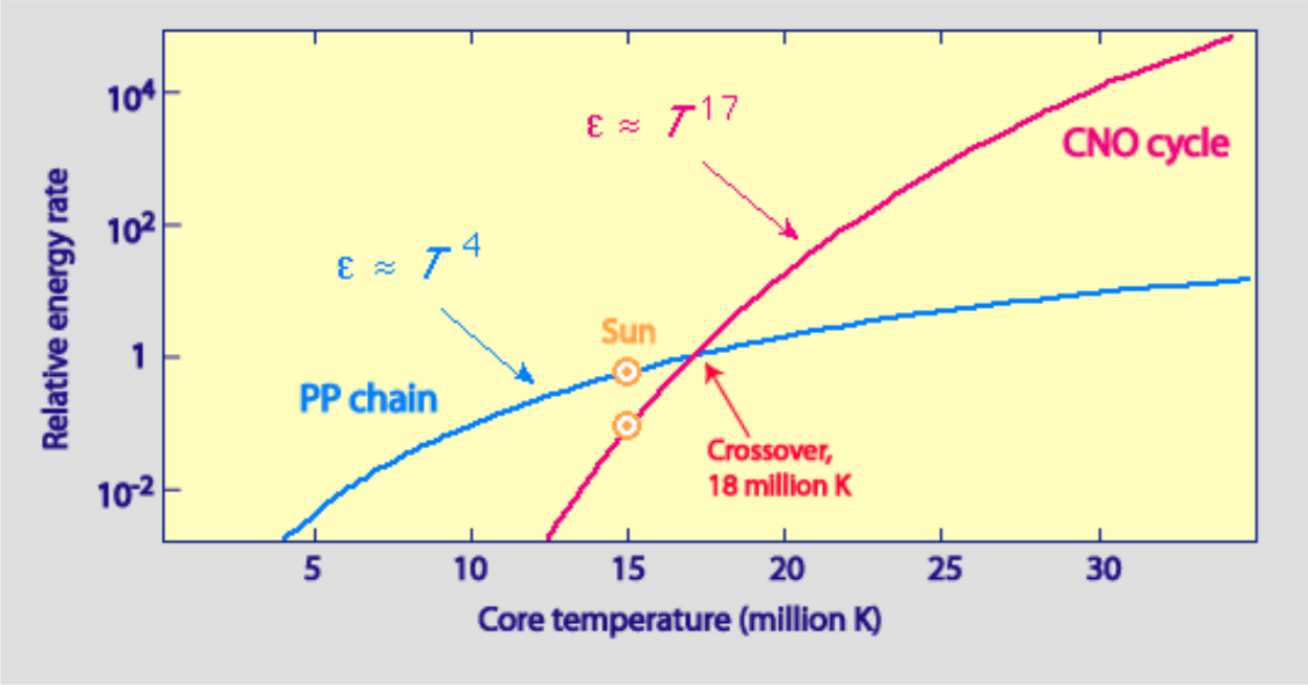

Life of big star (> 1,4 $M_{\odot}$)

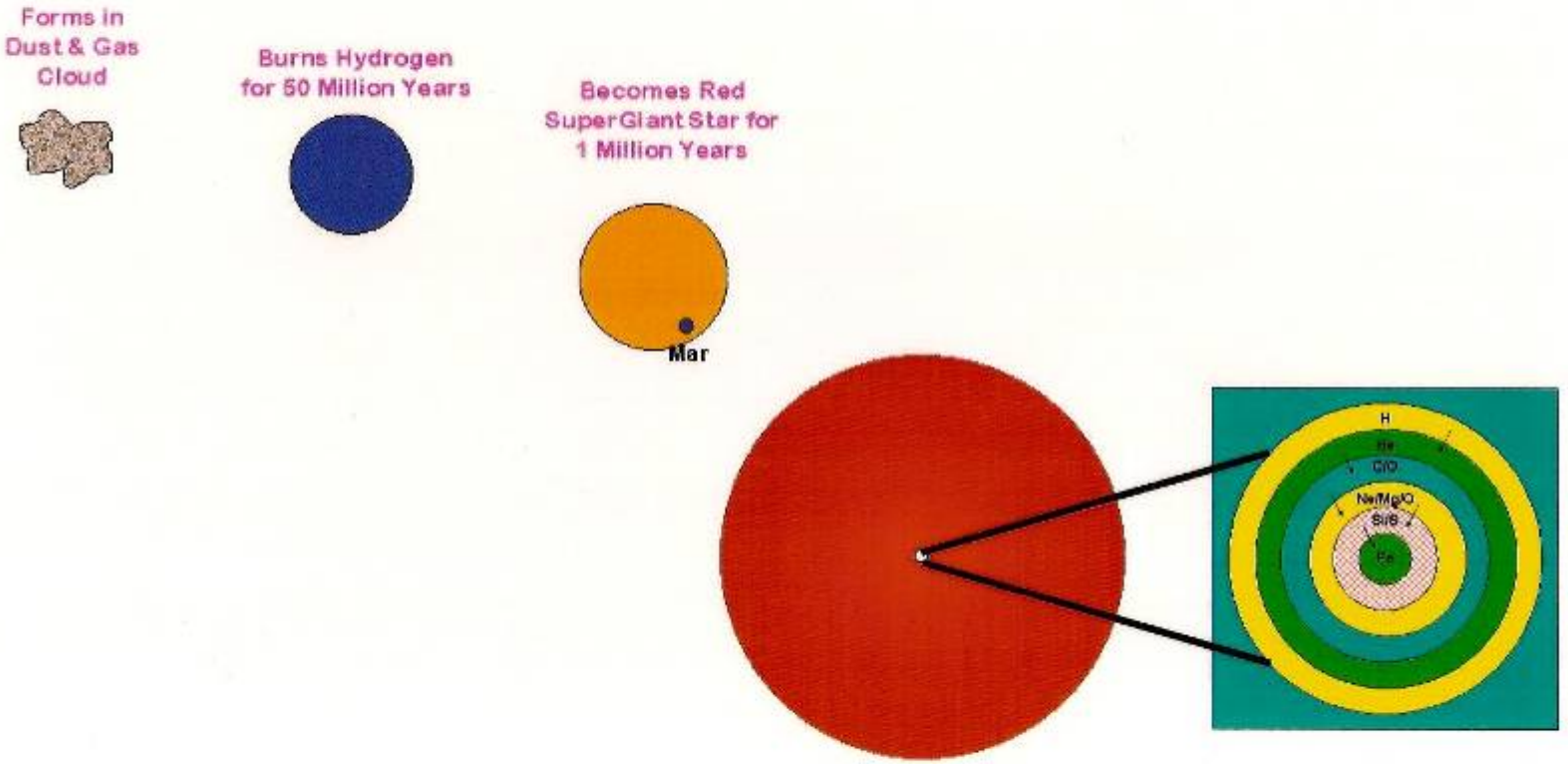

End in Supernovae of type Ib, Ic et II

End of helium burning

Nucleosynthesis yields from stars may be divided into production by stars above and below $9\,\mathrm{M}_\odot$.

stars with $M \lesssim 9\,\mathrm{M}_\odot$ These stars eject their envelopes during helium shell burning producing planetary nebula and white dwarfs. Constitute the site for the s process.

stars with $M \gtrsim 9\,\mathrm{M}_\odot$ These stars will ignite carbon burning under non-degenerate conditions. The subsequent evolution proceeds in most cases to core collapse. These stars make the bulk of newly processed matter that is returned to the interstellar medium.

Consequences

- Stars slightly heavier than the Sun burn hydrogen via CNO cycle.
- CNO cycle goes significantly faster. Such stars have much shorter lifetimes

Mass ($M_\odot$)	lifetime (yr)
0.8	1.4×10^{10}
1.0	1×10^{10}
1.7	2.7×10^{9}
3.0	2.2×10^{8}
5.0	6×10^{7}
9.0	2×10^{7}
16.0	1×10^{7}
25.0	7×10^{6}
40.0	1×10^{6}

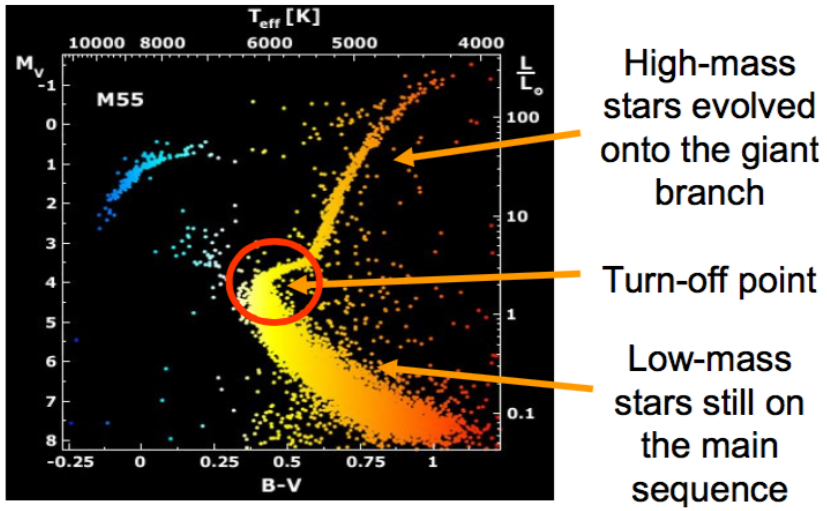

Helium Burning

- Once hydrogen is exhausted the stellar core is made mainly of helium. Hydrogen burning continues in a shell surrounding the core.
- $^4\mathrm{He} + p$ produces $^5\mathrm{Li}$ that decays in 10^{-22} s.
- Helium survives in the core till the temperature become large enough ($T \approx 10^8$ K) to overcome the coulomb barrier for $^4\mathrm{He} + {}^4\mathrm{He}$. The produced $^8\mathrm{Be}$ decays in 10^{-16}. However, the lifetime is large enough to allow the capture of another $^4\mathrm{He}$:

$$3\,{}^4\mathrm{He} \rightarrow {}^{12}\mathrm{C} + \gamma$$

- Hoyle suggested that in order to account for the large abundance of Carbon and Oxygen, there should be a resonance in $^{12}\mathrm{C}$ that speeds up the production.
- $^{12}\mathrm{C}$ can react with another $^4\mathrm{He}$ producing $^{16}\mathrm{O}$

$$^{12}\mathrm{C} + \alpha \rightarrow {}^{16}\mathrm{O} + \gamma$$

- These two reactions make up helium burning.

Hoyle State and tripple α reaction

Red giant structure

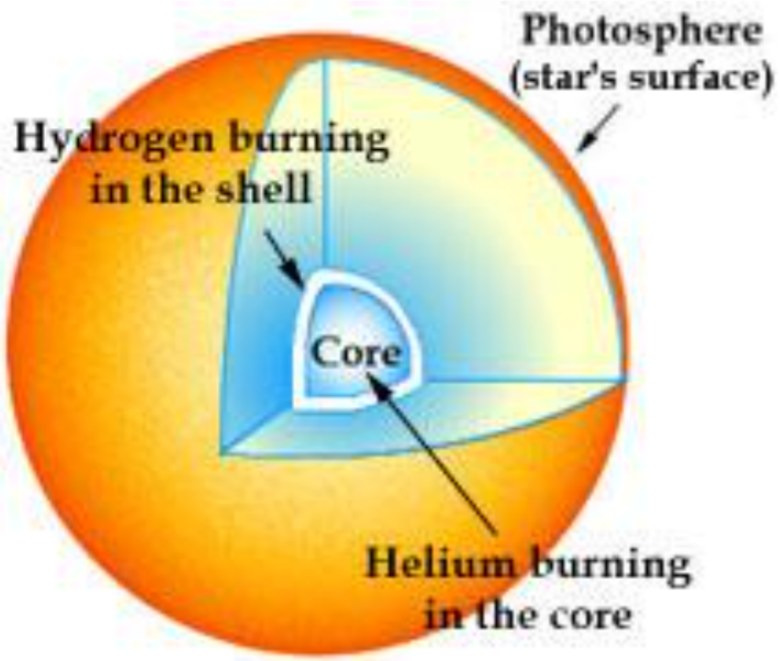

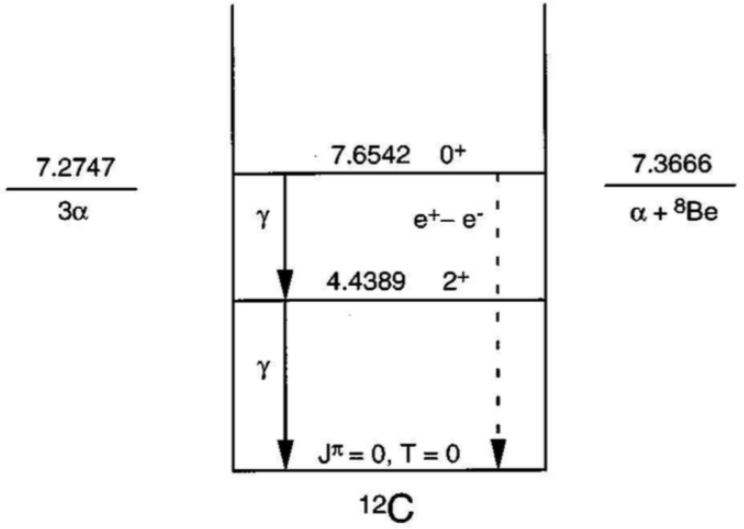

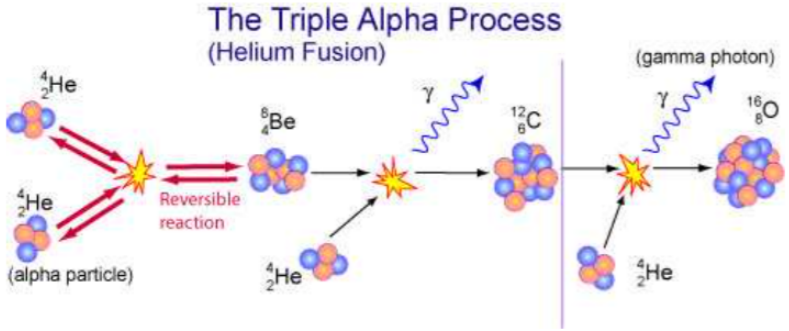

MASSIVE STAR EVOLUTION : $M = 25 M_\odot$

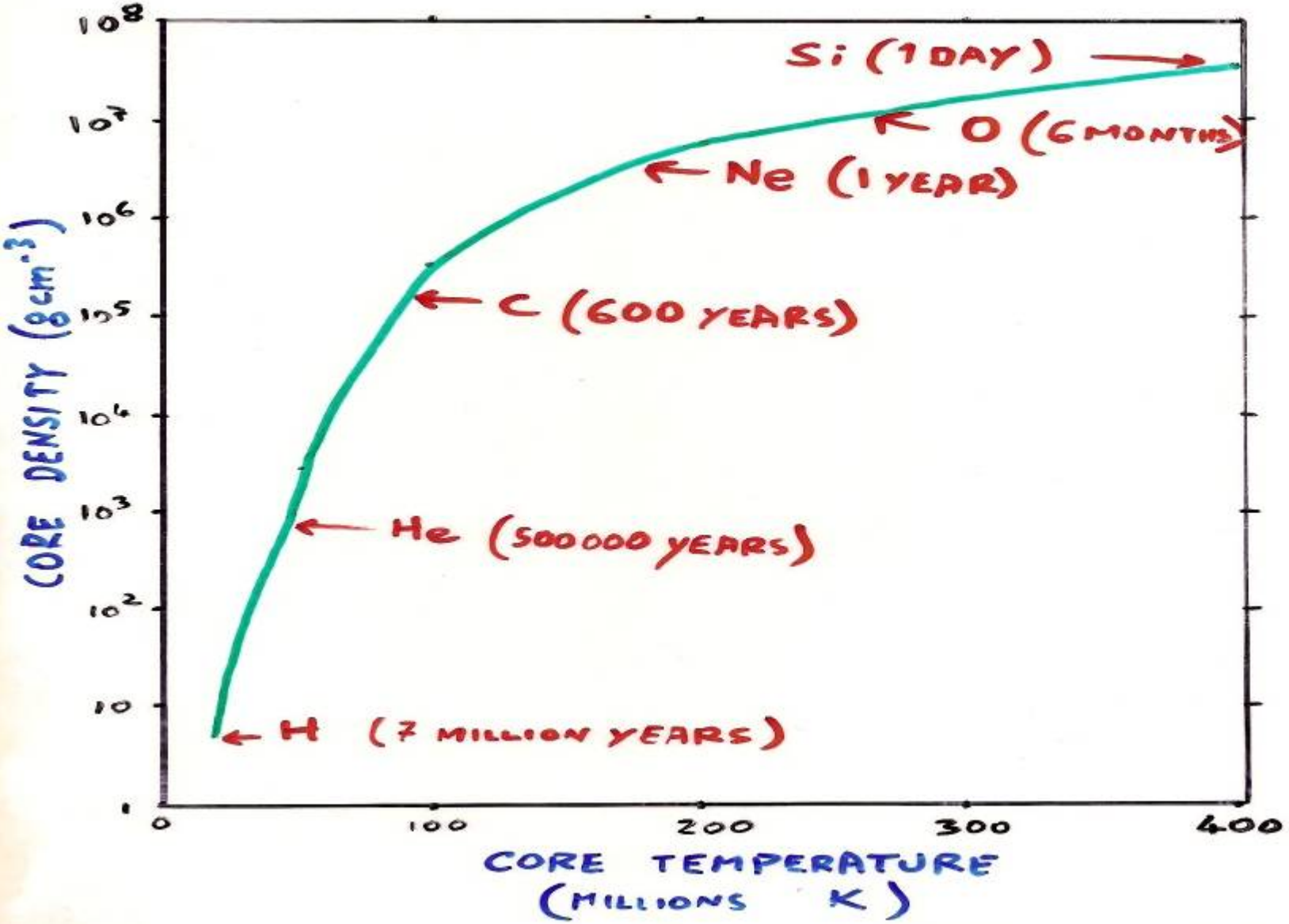

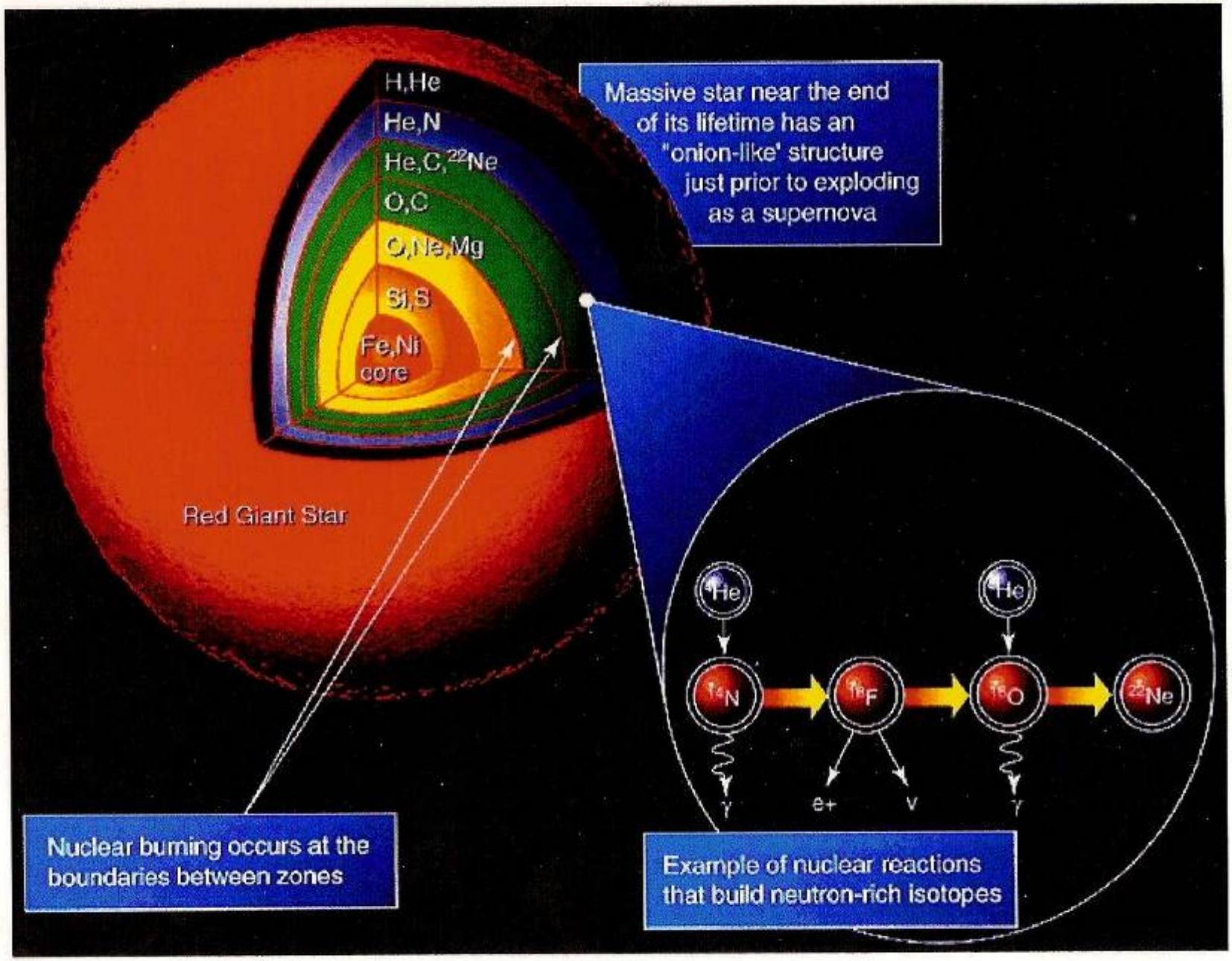
H,He
He,N
He,C,22Ne
O,C
O,Ne,Mg
Si,S
Fe,Ni core
Red Giant Star
Massive star near the end of its lifetime has an "onion-like" structure just prior to exploding as a supernova
Nuclear burning occurs at the boundaries between zones
4He
4He
14N
18F
18O
22Ne
γ
e+
ν
γ
Example of nuclear reactions that build neutron-rich isotopes

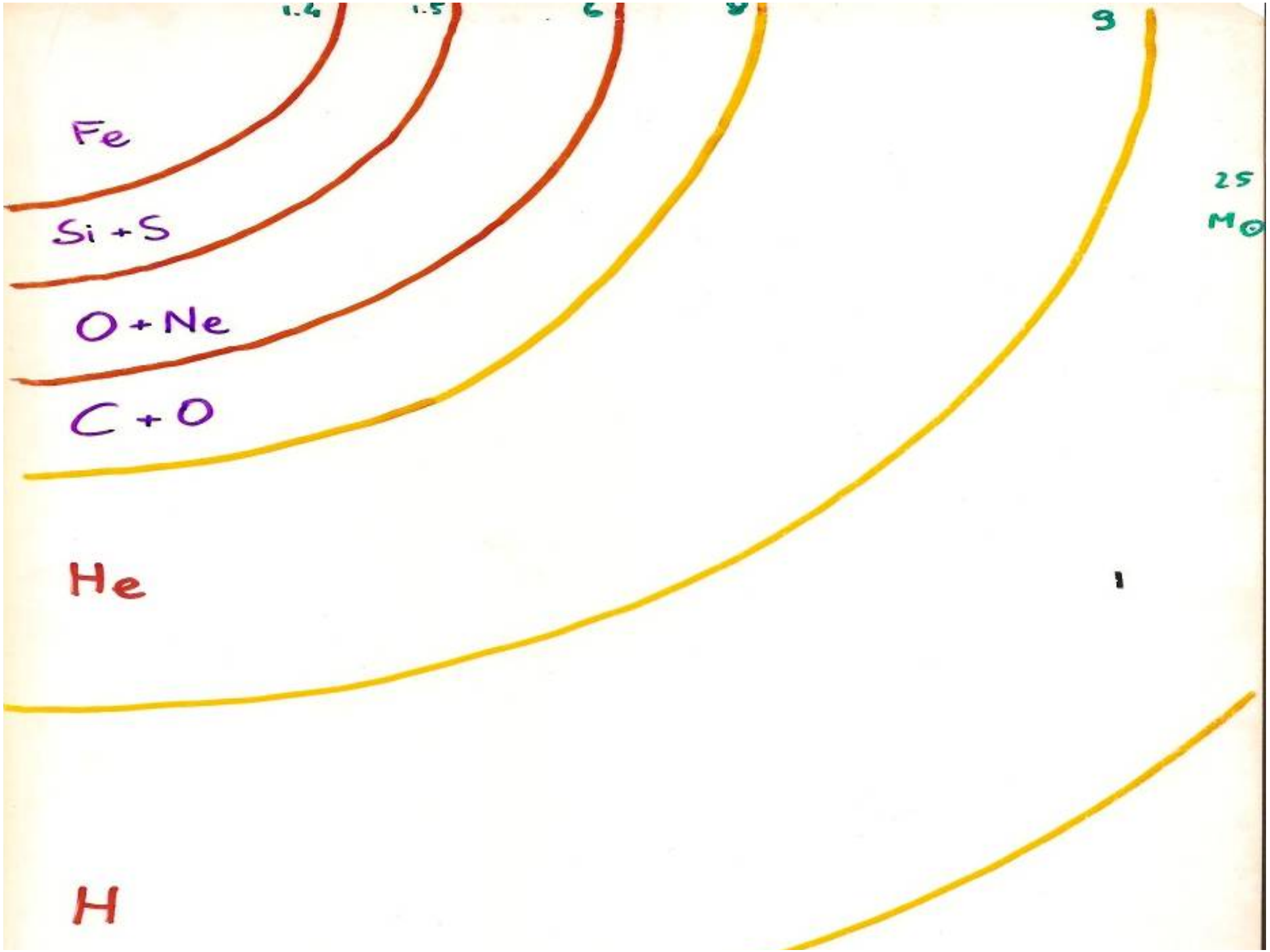
1.4
1.5
2
3
Fe
Si + S
O + Ne
C + O
He
H
25
M⊙

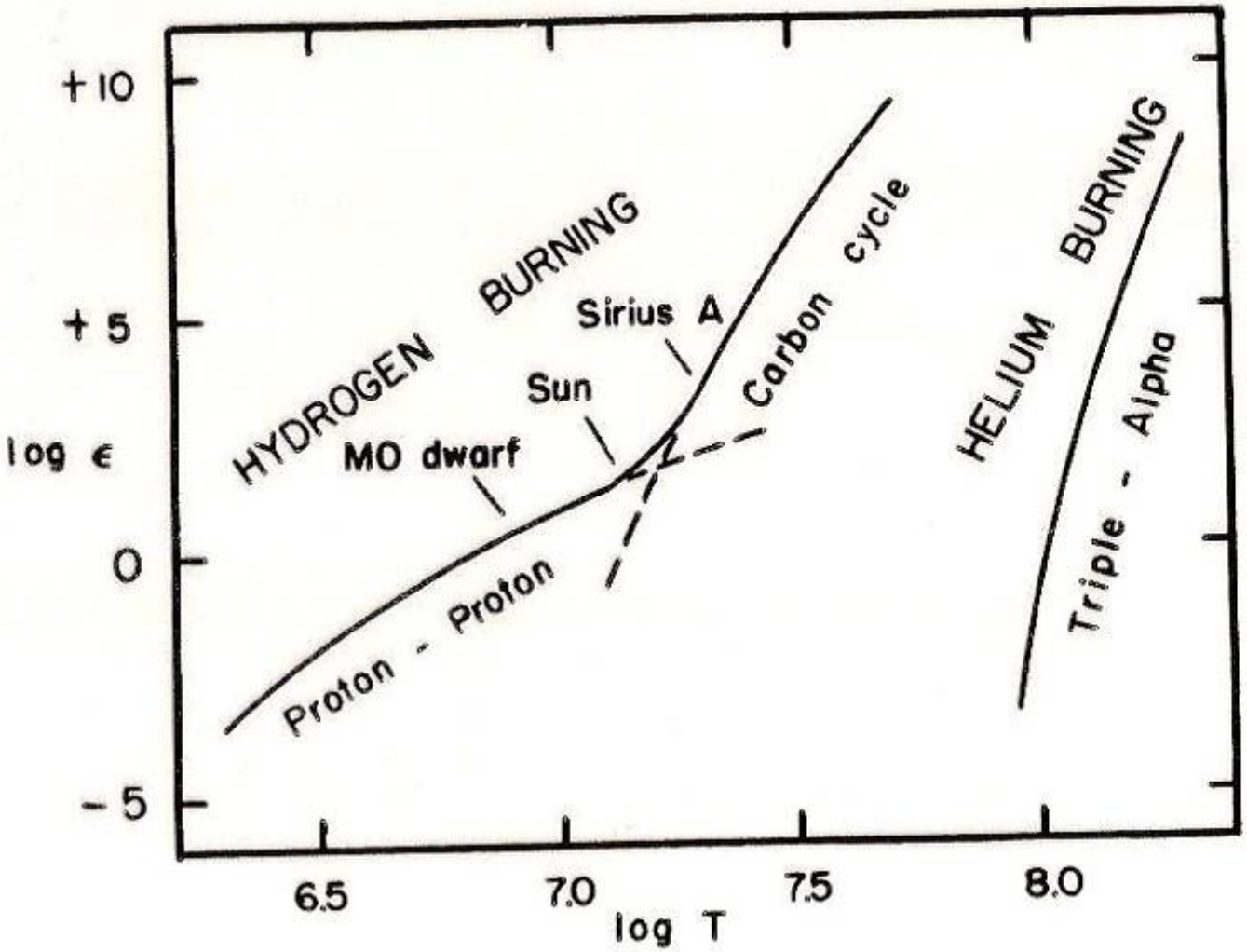

Fig. 10.1. Nuclear energy generation as a function of temperature (with $\rho X^2 = 100$ and $X_{CN} = 0.005X$ for the proton-proton reaction and the carbon cycle, but $\rho^2 Y^3 = 10^8$ for the triple-alpha process).

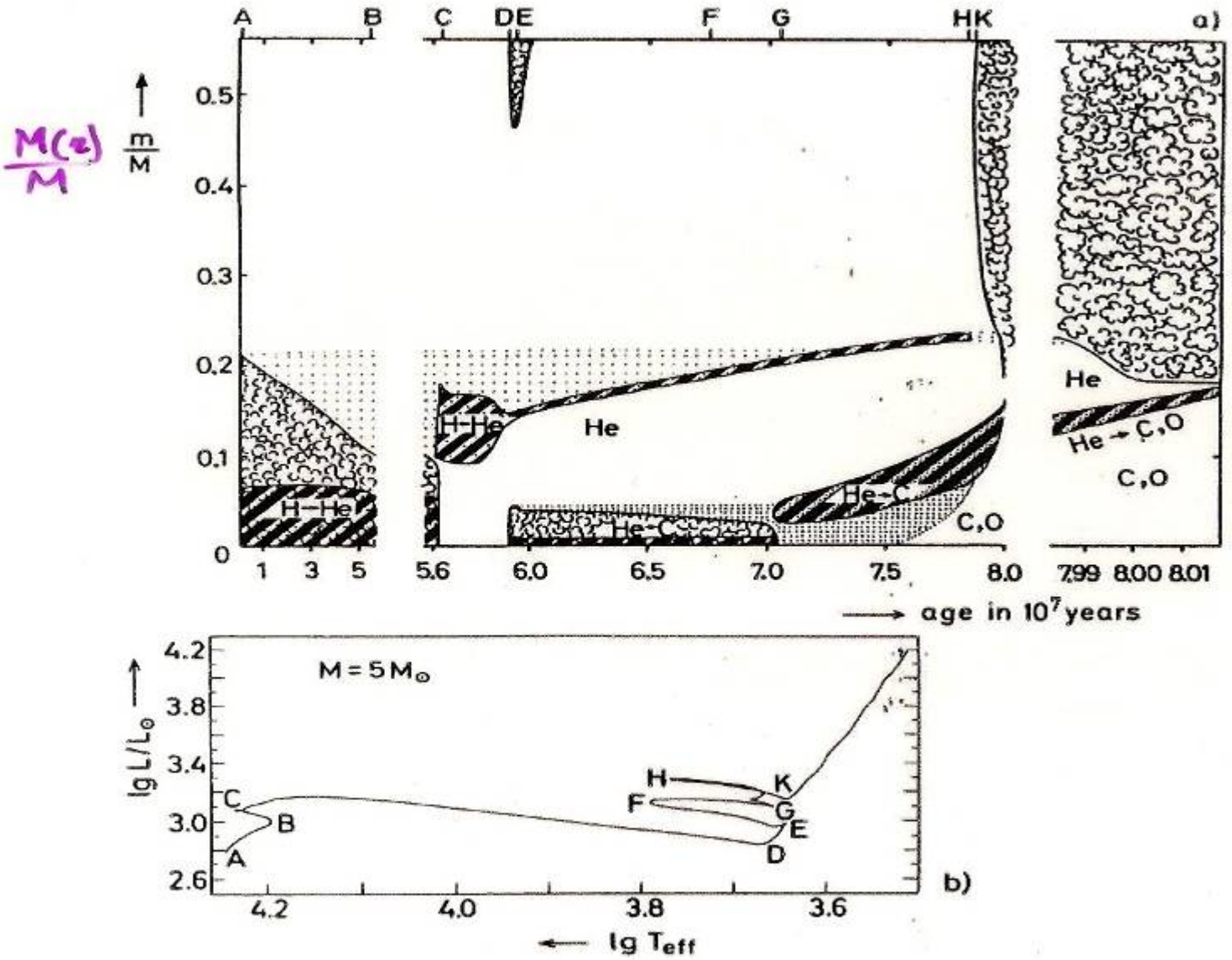

Fig. 31.2. (a) The evolution of the internal structure of a star of $5M_\odot$ of extreme population I. The abscissa gives the age after the ignition of hydrogen in units of 10^7 years; each vertical line corresponds to a model at a given time. The different layers are characterized by their values of m/M. "Cloudy" regions indicate convective areas. Heavily hatched regions indicate where the nuclear energy generation (ε_H or ε_{He}) exceeds 10^3 erg g^{-1} s^{-1}. Regions of variable chemical composition are dotted. The letters $A \ldots K$ above the upper abscissa indicate the corresponding points in the evolutionary track, which is plotted in Fig. 31.2 (b). (After KIPPENHAHN et al., 1965)

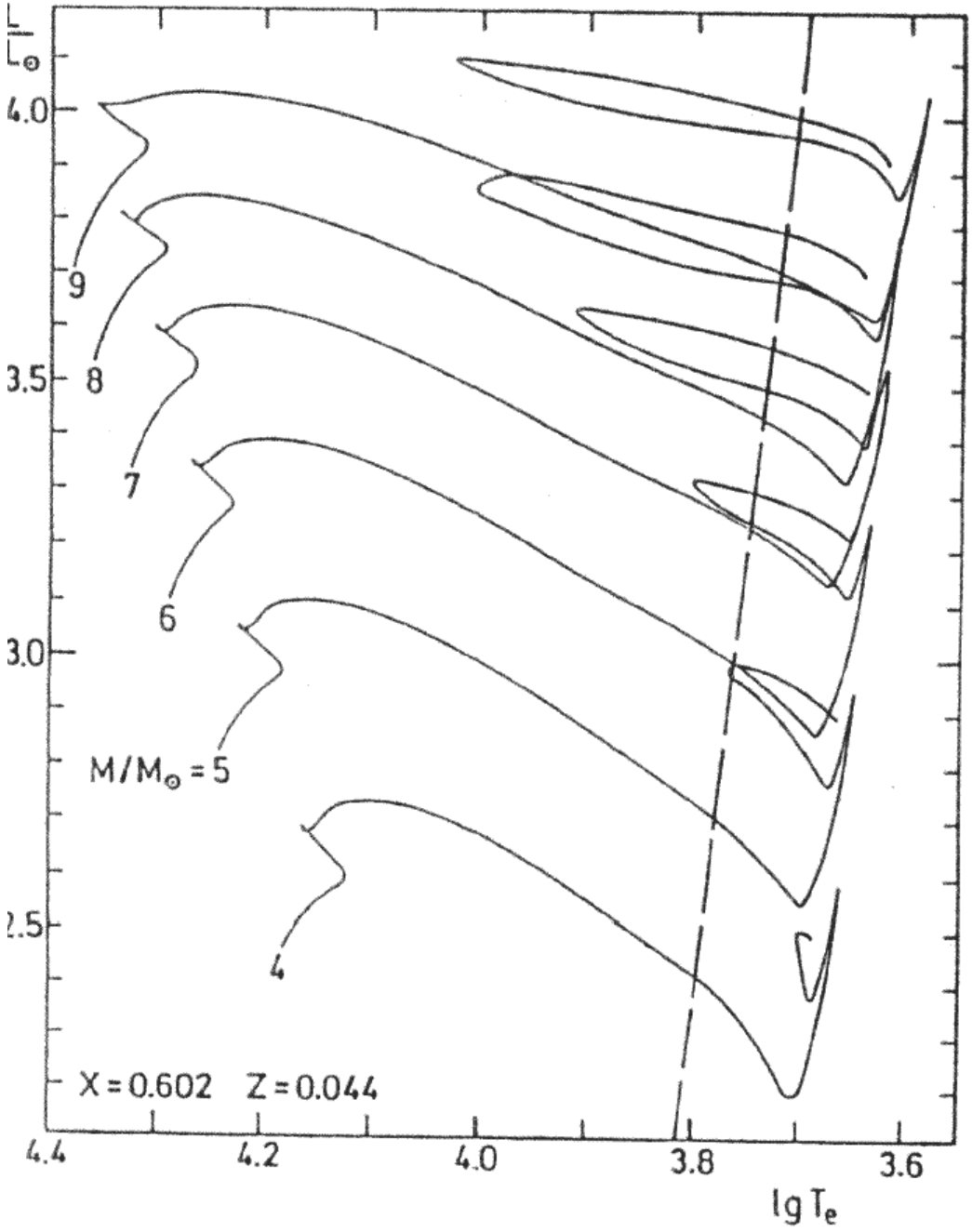

Fig. 31.6. Hertzsprung–Russell diagram with evolutionary tracks for stars in the mass range from $4M_\odot$ to $9M_\odot$ from the main sequence through helium burning (after MATRAKA et al., 1982). The broken line indicates the Cepheid strip

Stellar life

Nuclear burning stages

(e.g., 20 solar mass star)

Fuel	Main Product	Secondary Product	T (10^9 K)	Time (yr)	Main Reaction
H	He	^{14}N	0.02	10^7	$4\,H \xrightarrow{CNO} {}^4He$
He	O, C	^{18}O, ^{22}Ne s-process	0.2	10^6	$3\,He^4 \rightarrow {}^{12}C$; $^{12}C(\alpha,\gamma)^{16}O$
C	Ne, Mg	Na	0.8	10^3	$^{12}C + {}^{12}C$
Ne	O, Mg	Al, P	1.5	3	$^{20}Ne(\gamma,\alpha)^{16}O$; $^{20}Ne(\alpha,\gamma)^{24}Mg$
O	Si, S	Cl, Ar, K, Ca	2.0	0.8	$^{16}O + {}^{16}O$
Si	Fe	Ti, V, Cr, Mn, Co, Ni	3.5	0.02	$^{28}Si(\gamma,\alpha)\ldots$

Stellar Evolution

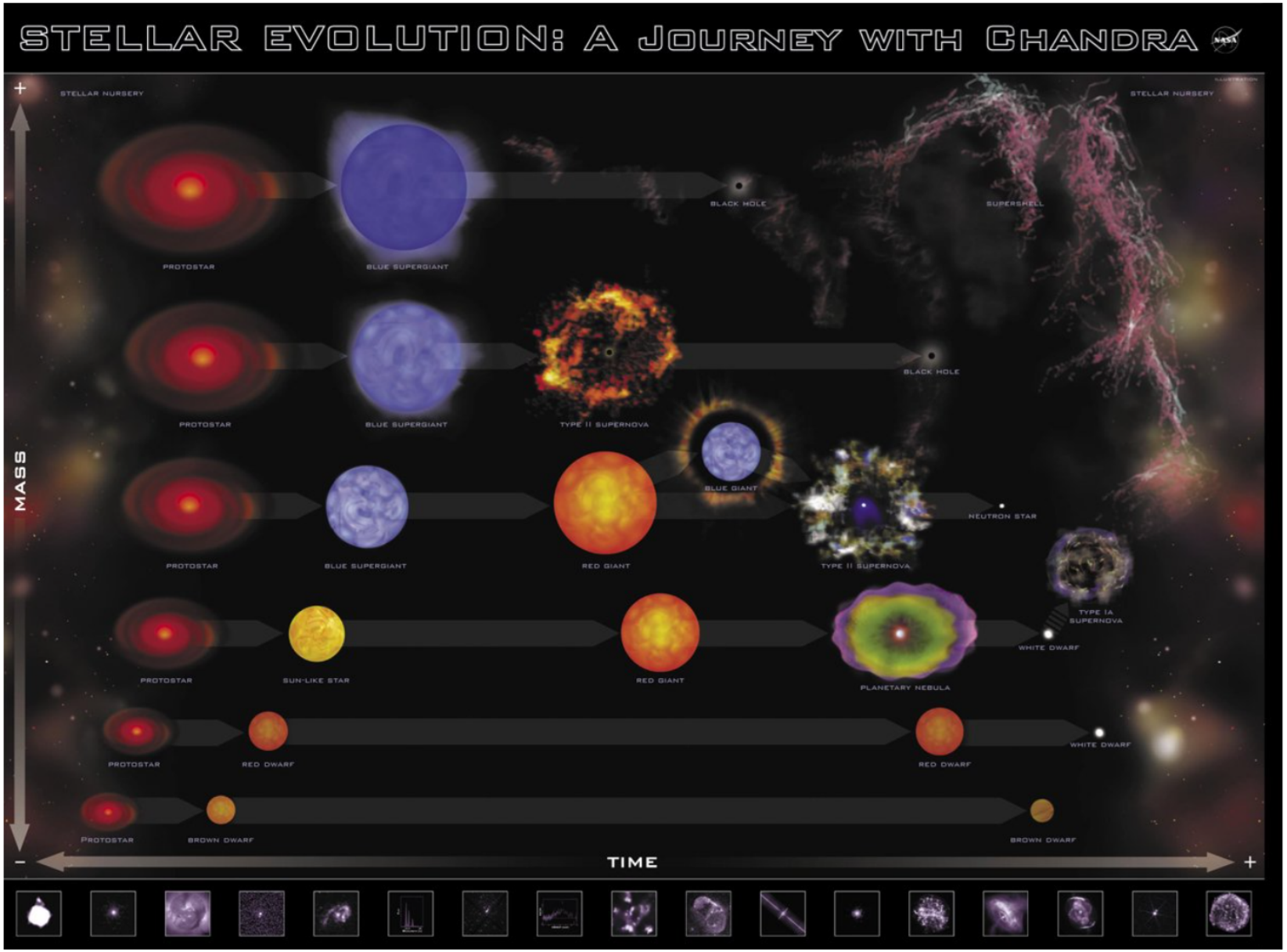

Type Ia vs. Core-Collapse Supernovae

Type Ia	Core collapse (Type II, Ib/c)
• Carbon-oxygen white dwarf (remnant of low-mass star) • Accretes matter from companion 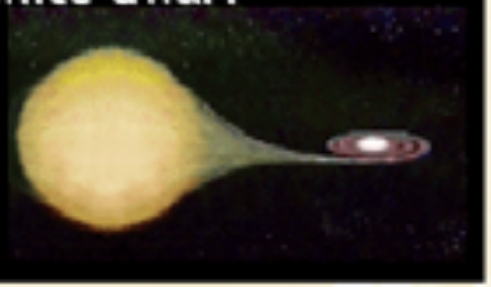	• Degenerate iron core of evolved massive star • Accretes matter by nuclear burning at its surface 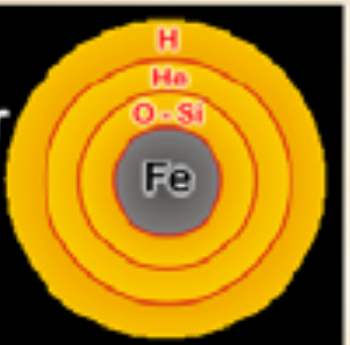
Chandrasekhar limit is reached – $M_{Ch} \approx 1.5\ M_{sun}\ (2Y_e)^2$ COLLAPSE SETS IN	
Nuclear burning of C and O ignites → Nuclear deflagration ("Fusion bomb" triggered by collapse)	Collapse to nuclear density Bounce & shock Implosion → Explosion
Powered by nuclear binding energy	Powered by gravity
Gain of nuclear binding energy ~ 1 MeV per nucleon	Gain of gravitational binding energy ~ 100 MeV per nucleon 99% into neutrinos

SuperNovae Remnants

Vela

Tycho

Cygnus

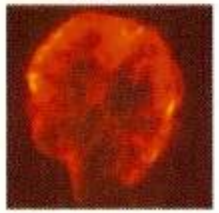

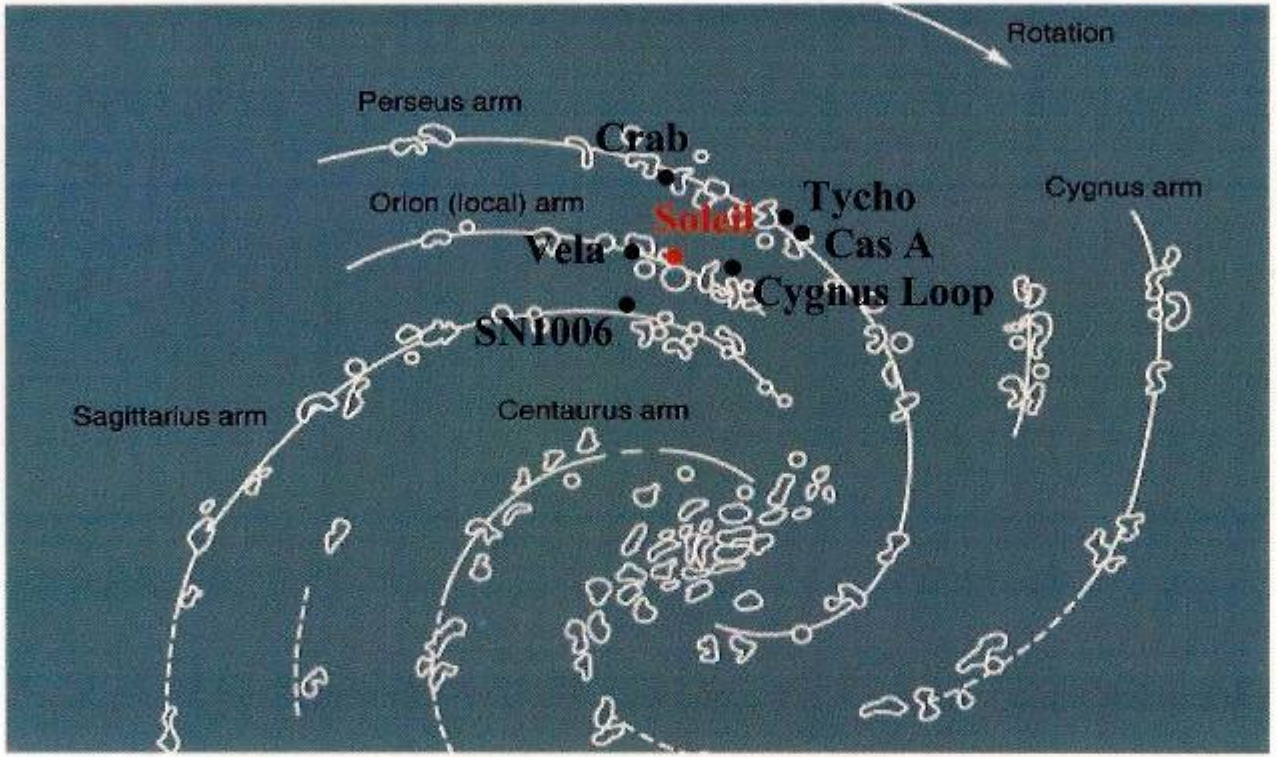

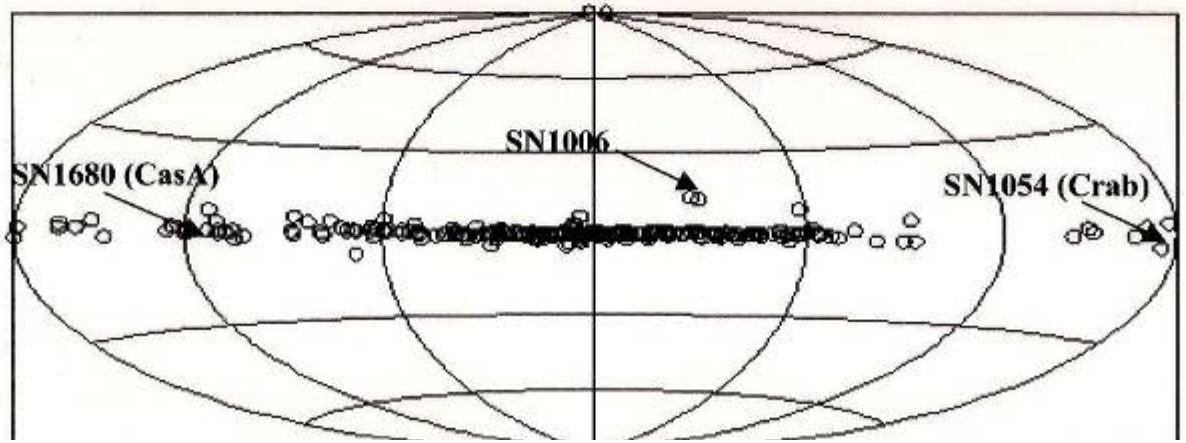

Crab

Kepler

Cas A

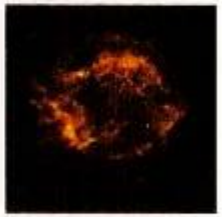

SN1006

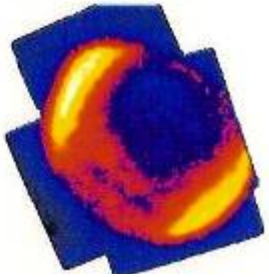

The Crab in Multi-Wavelengths Photons

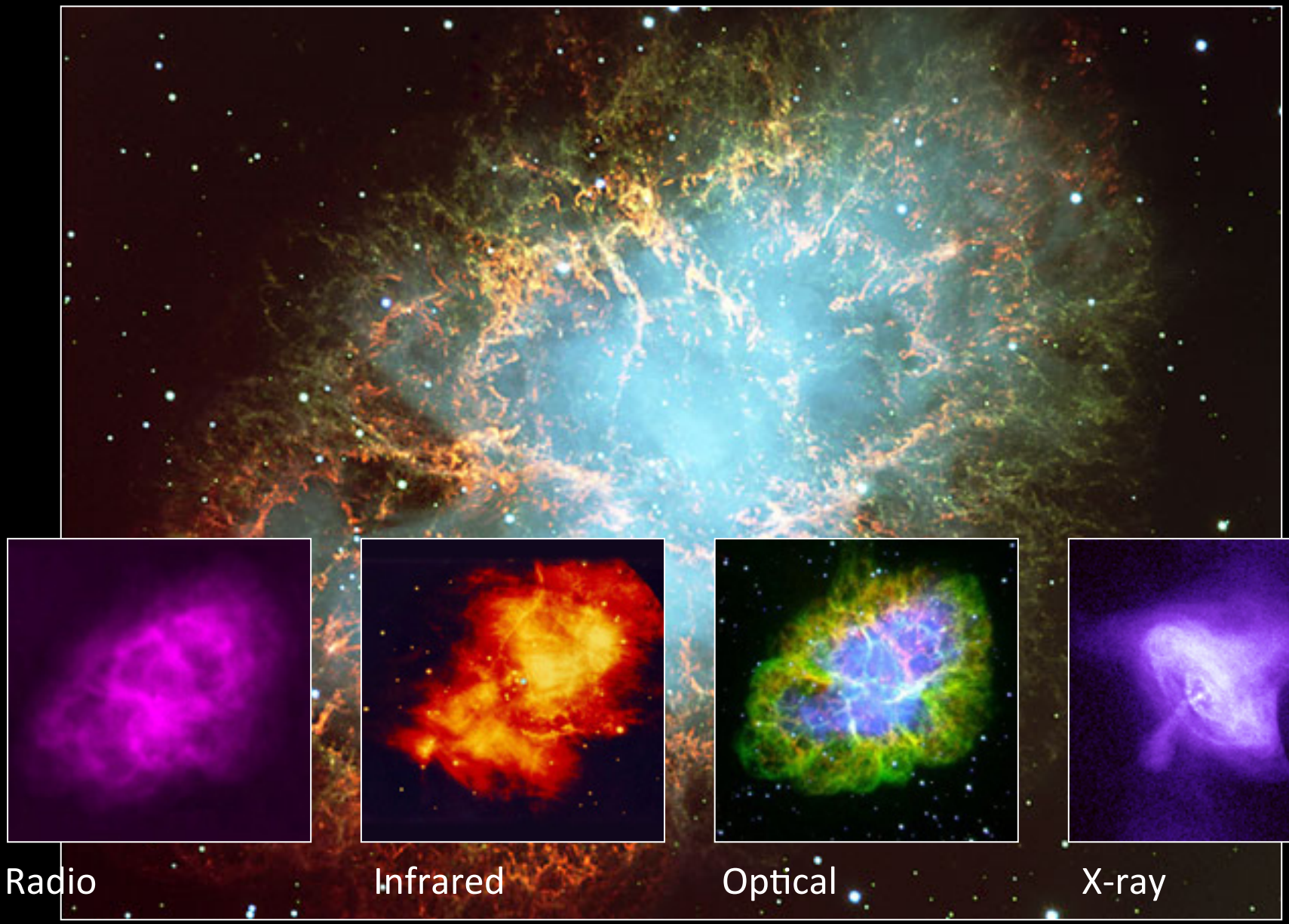

Astrofisica Nucleare e Subnucleare

Solar Neutrinos

The 2002 Nobel Prize for the Solar Neutrino Physics

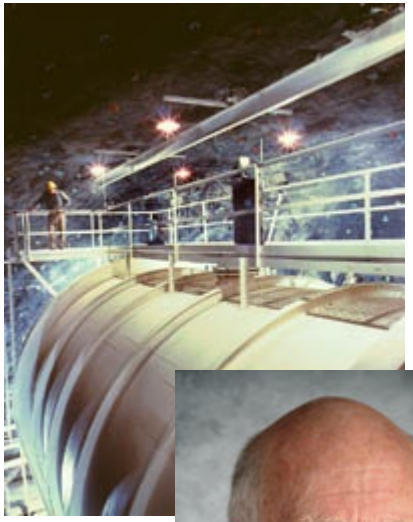

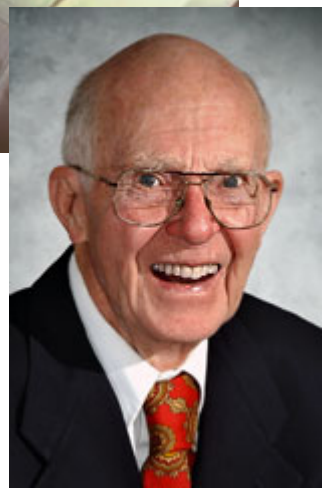

Raymond Davis Jr.

http://nobelprize.org/nobel_prizes/physics/laureates/2002/davis-lecture.pdf

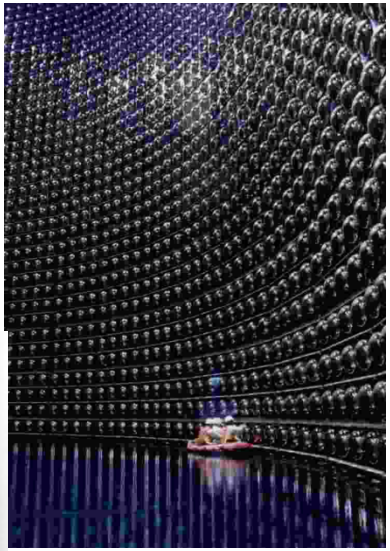

Masatoshi Koshiba

http://nobelprize.org/nobel_prizes/physics/laureates/2002/koshiba-lecture.pdf

The Standard Solar Model

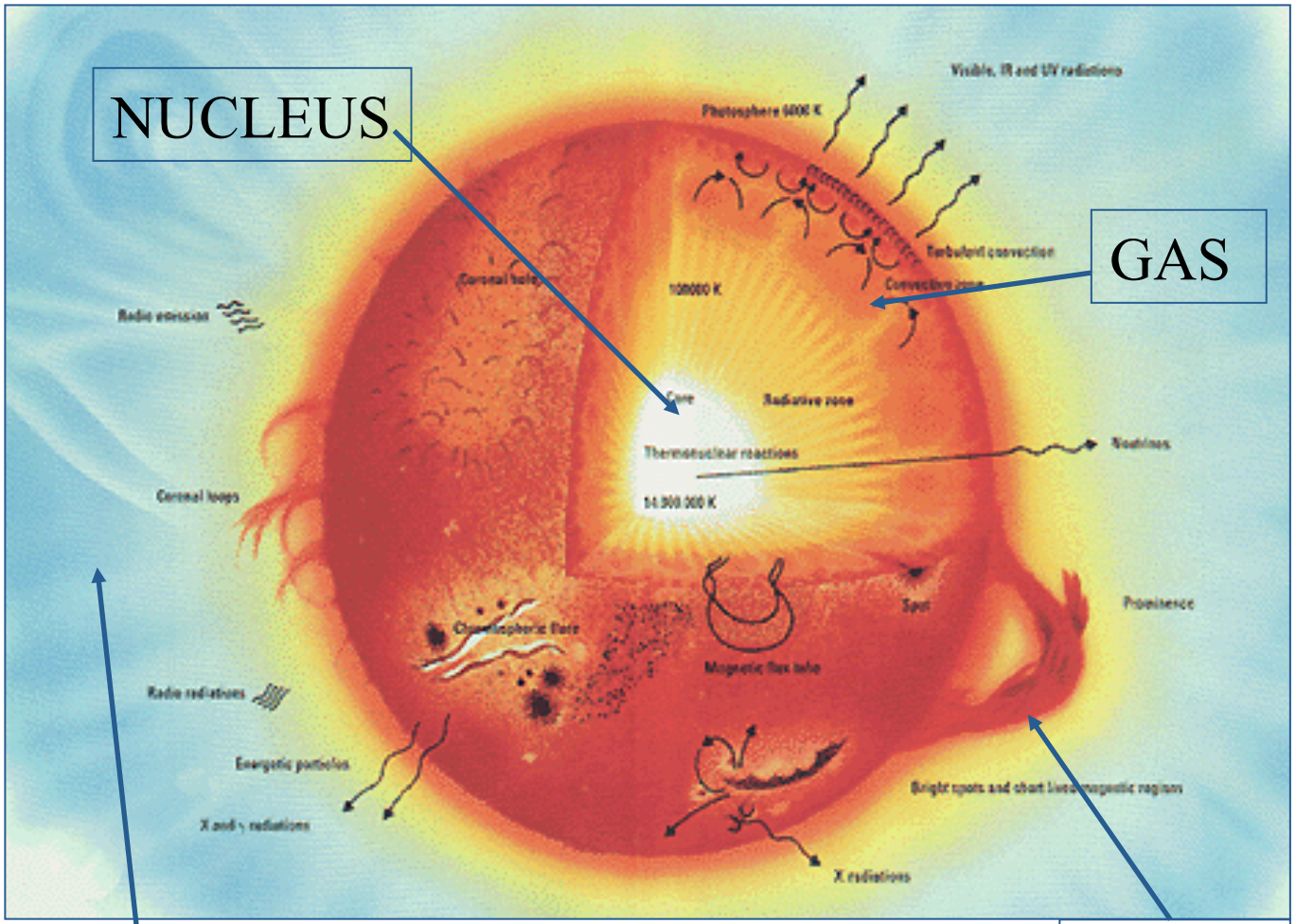

The Standard Solar Model

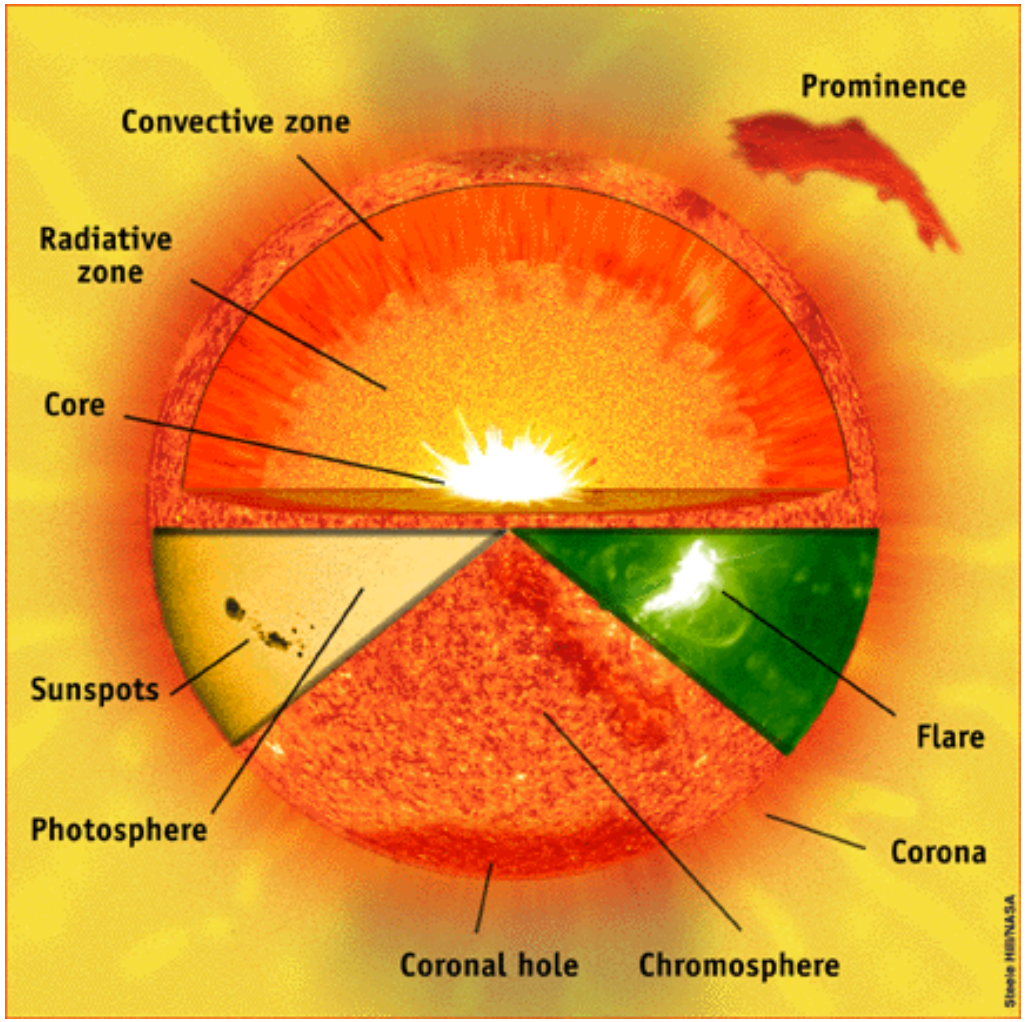

The Standard Solar Model

http://www.sns.ias.edu/~jnb/

- J. Bahcall: The main author of the SSM
- The standard solar model is derived from the conservation laws and energy transport equations of physics, applied to a spherically symmetric gas (plasma) sphere
- Constrained by the luminosity, radius, age and composition of the Sun

- Inputs for the Standard Solar Model
  - –Mass
  - –Age
  - –Luminosity
  - –Radius
- No free parameters
- Tested by helioseismology
- Fusion ⇒ neutrinos

Nota: Leggere l'articolo (tradotto anche in italiano)
http://www.sns.ias.edu/~jnb/Papers/Popular/Nobelmuseum/italianmystery.pdf

The predictions of the SSM

- Most of the neutrinos produced in the sun come from the first step of the pp chain.
- Their energy is so low (<0.425 MeV) → very difficult to detect.
- A rare side branch of the pp chain produces the "boron-8" neutrinos with a maximum energy of roughly 15 MeV
- These are the easiest neutrinos to observe, because the neutrino cross section increases with energy.
- A very rare interaction in the pp chain produces the "hep" neutrinos, the highest energy neutrinos produced in any detectable quantity by our sun.
- All of the interactions described above produce neutrinos with a spectrum of energies. The inverse beta decay of Be^7 produces mono-energetic neutrinos at either roughly 0.9 or 0.4 MeV.

ν from the Sun: the proton cycle

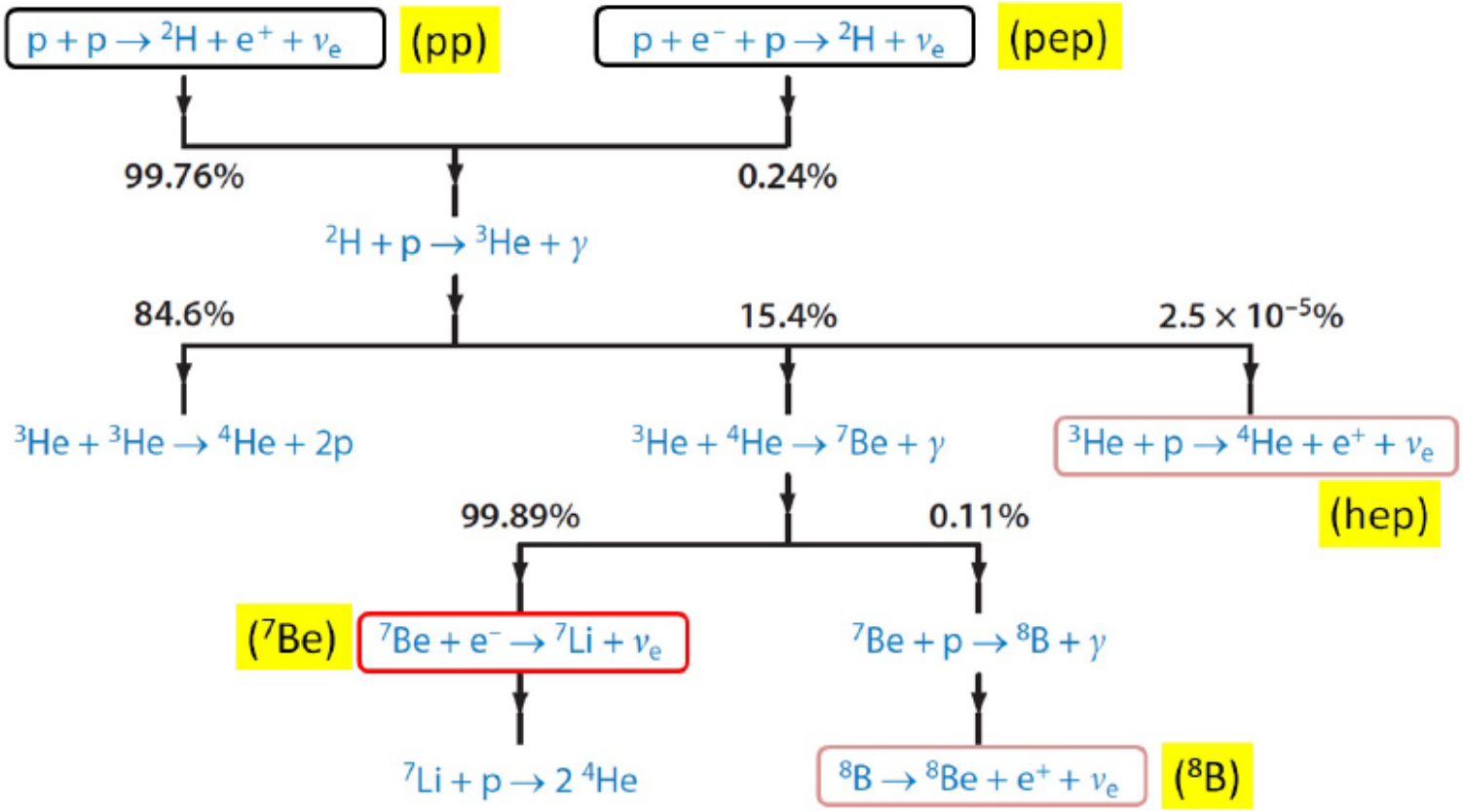

$$4p \rightarrow {}^4\mathrm{He} + 2e^+ + 2\nu_e \qquad Q = 26.73\ \mathrm{MeV} \qquad \langle E_\nu \rangle \simeq 0.3\ \mathrm{MeV}$$

$$\Phi_{\nu_e} \simeq \frac{1}{4\pi D_\odot^2} \frac{2L_\odot}{(Q - \langle E_\nu \rangle)} = 6 \times 10^{10}\ \mathrm{cm}^{-2}\mathrm{s}^{-1}$$

Differential ν_e flux

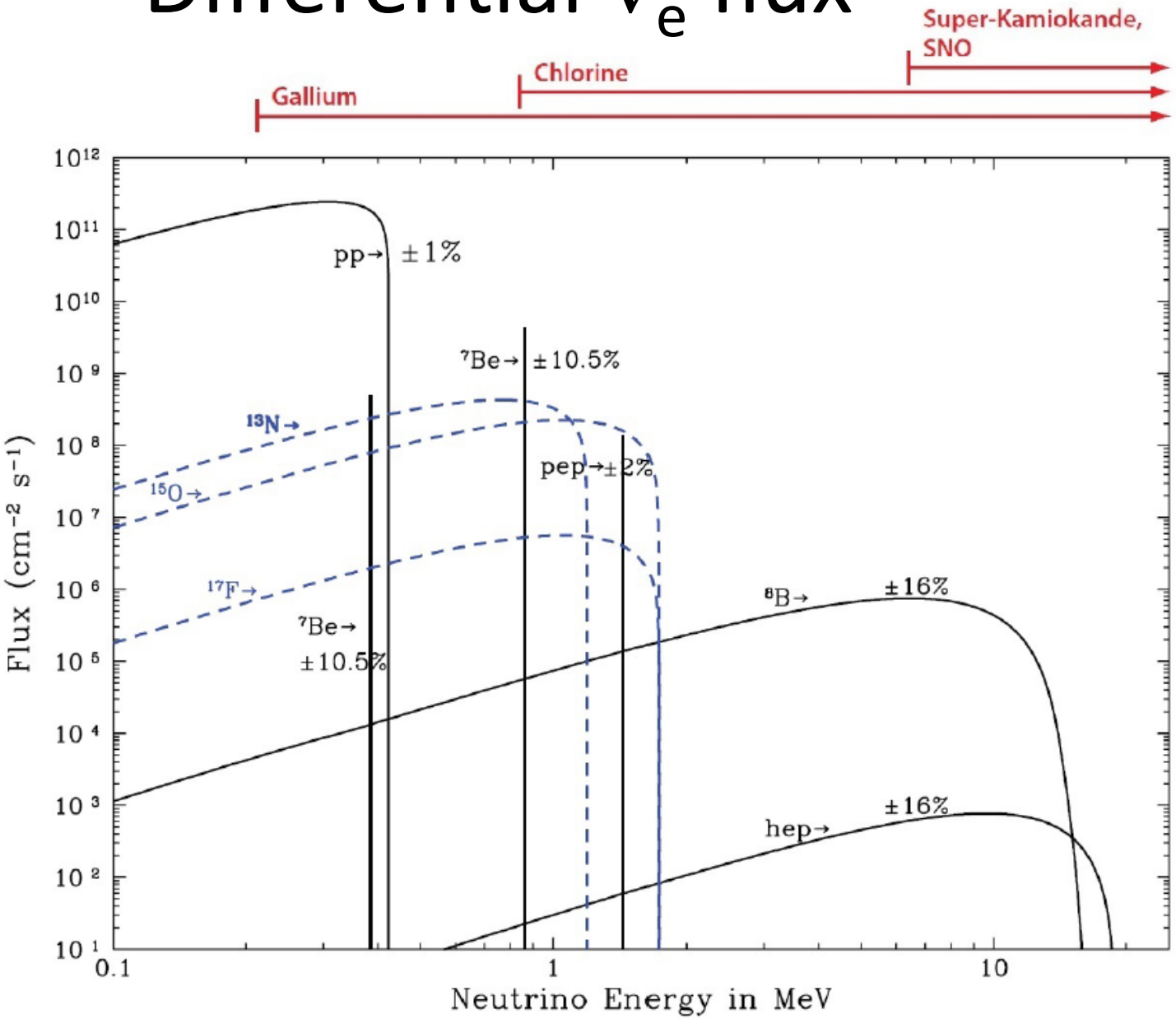

Neutrino Emission

Source r	Reaction	Average Neutrino Energy $\langle E \rangle_r$ (MeV)	Maximum Neutrino Energy (MeV)
pp	$p + p \rightarrow d + e^+ + \nu_e$	0.2668	0.423 ± 0.03
pep	$p + e^- + p \rightarrow d + \nu_e$	1.445	1.445
^{7}Be	$e^- + {}^7\mathrm{Be} \rightarrow {}^7\mathrm{Li} + \nu_e$	0.3855 0.8631	0.3855 0.8631
^{8}B	$^8\mathrm{B} \rightarrow {}^8\mathrm{Be}^* + e^+ + \nu_e$	6.735 ± 0.036	~ 15
hep	$^3\mathrm{He} + p \rightarrow {}^4\mathrm{He} + e^+ + \nu_e$	9.628	18.778
^{13}N	$^{13}\mathrm{N} \rightarrow {}^{13}\mathrm{C} + e^+ + \nu_e$	0.7063	1.1982 ± 0.0003
^{15}O	$^{15}\mathrm{O} \rightarrow {}^{15}\mathrm{N} + e^+ + \nu_e$	0.9964	1.7317 ± 0.0005
^{17}F	$^{17}\mathrm{F} \rightarrow {}^{17}\mathrm{O} + e^+ + \nu_e$	0.9977	1.7364 ± 0.0003

Experimental Techniques

Two detection techniques for the solar neutrinos:

1- elastic scattering

$\nu_e + e \rightarrow \nu_e + e$

SK

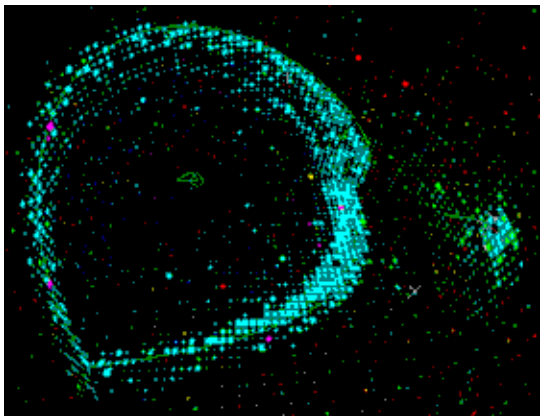

2- Neutron capture $\nu_e + n \rightarrow e + p$

No free neutrons in nature:

$(Z,A) + \nu_e \rightarrow e + (Z+1,A)$

Example: $^{71}Ga + \nu \rightarrow {}^{71}Ge + e$

3- The SNO way:

- $\nu_e + d \rightarrow e + p + p$
- $\nu_x + d \rightarrow \nu_x + n + p$

Solar Neutrino Detectors

- Neutrino Absorption Experiments
  - 37Cl
  - 71Ga
- Neutrino Scattering Experiments
  - SuperKamiokande
- Direct Counting experiments
  - SNO

- ‘Davis’
- GALLEX/GNO < (radiochemical)
- SAGE
- SuperKamiokande (elastic scattering)
- SNO

•The Clorine or ‘Davis’ experiment

$$^{37}\mathrm{Cl} + \nu_e \rightarrow {}^{37}\mathrm{Ar} + e$$

- Pioneering experiment by Ray Davis at Homestake mine began in 1967
- Consisted of a 600 ton chlorine tank
- Experiment was carried out over a 20 year period, in an attempt to measure the flux of neutrinos from the Sun
- **Measured flux was only one third the predicted value !!**

^{37}Cl experiment

- The Clorine or 'Davis' experiment

$$^{37}\mathrm{Cl} + \nu_e \rightarrow {}^{37}\mathrm{Ar} + e$$

- Pioneering experiment by Ray Davis at Homestake mine began in 1967
- Consisted of a 600 ton chlorine tank
- Threshold E = 0.814 MeV
- Experiment was carried out over a 20 year period, in an attempt to measure the flux of neutrinos from the Sun
- Chemical extraction of Argon and direct counting of Argon decays (15 atoms over 130 tons of Cl every month!)
- Measured flux was only one third the predicted value

^{37}Cl experiment

^{37}Cl experiment

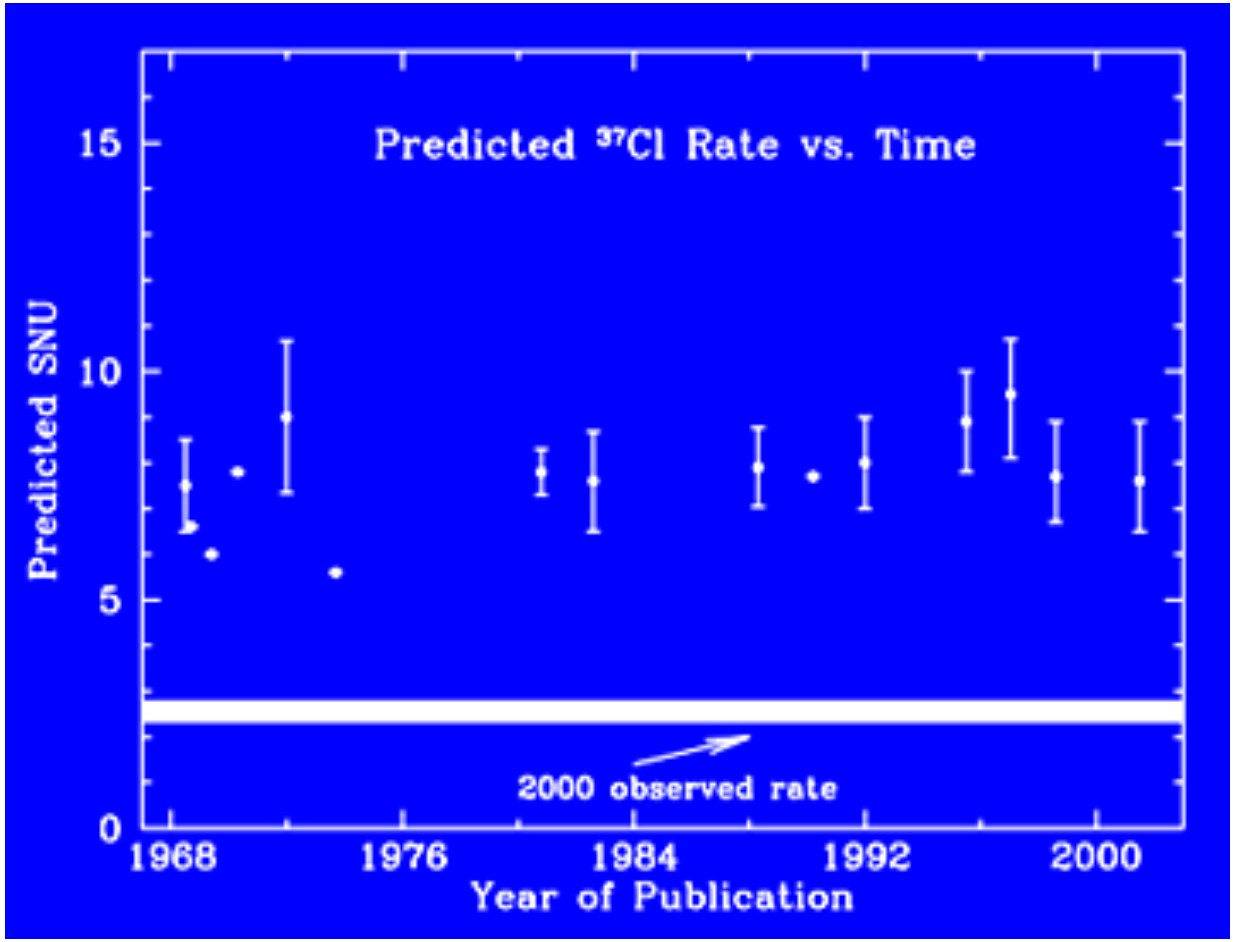

Radiochemical experiments: GALLEX/GNO and SAGE

- The main solar neutrino source is from the p-p reaction:

$$p + p \rightarrow d + e^{+} + \nu_e + 0.42MeV$$

- Solar neutrino experiment based on the reaction:

$$^{71}Ga + \nu_e \rightarrow {}^{71}Ge + e^{-}$$

- Ability to detect the low-energy neutrinos from p-p fusion

- **SAGE:** Located at the Baksan Neutrino Observatory in the northern Caucasus mountains of Russia (1990-2000)

- **GALLEX/GNO:** Located at the Gran Sasso

- Energy threshold: 233.2 ± 0.5 keV, below that of the p-p ν_e (420 keV)

•GALLEX/GNO

• 30.3 tons of gallium in form of a concentrated $GaCl_3$-HCl solution exposed to solar ν's

• Neutrino induced ^{71}Ge forms the volatile compound $GeCl_4$

• Nitrogen gas stream sweeps $GeCl_4$ out of solution

• $GeCl_4$ is absorbed in water $GeCl_4 \rightarrow GeH_4$ and introduced into a proportional counter

•Number of ^{71}Ge atoms evaluated by their radioactive decay

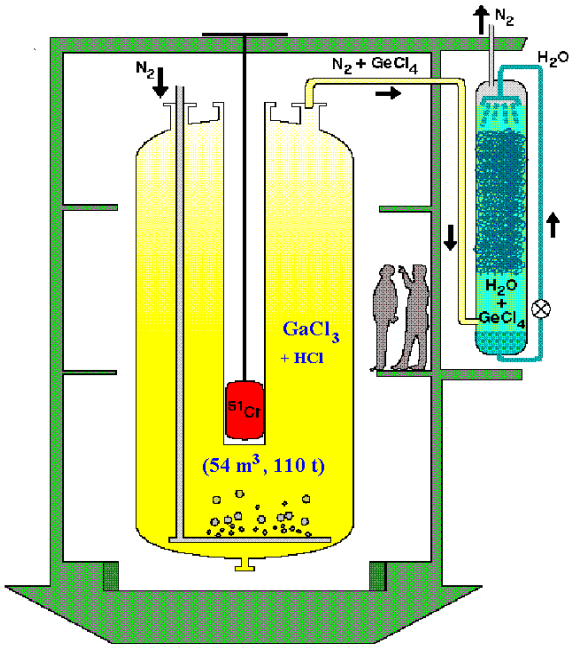

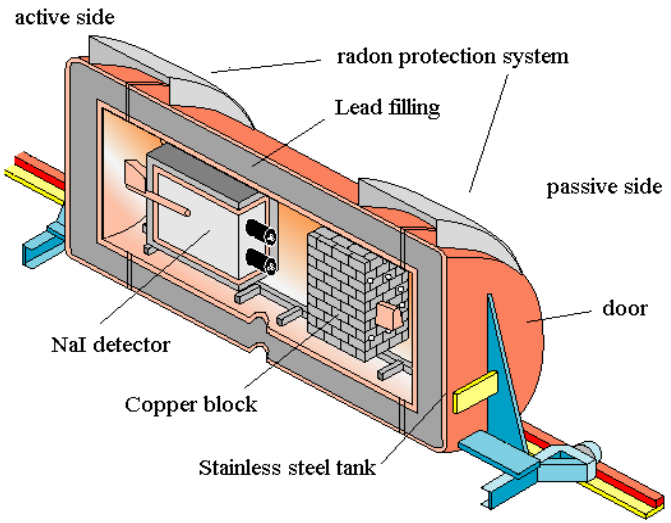

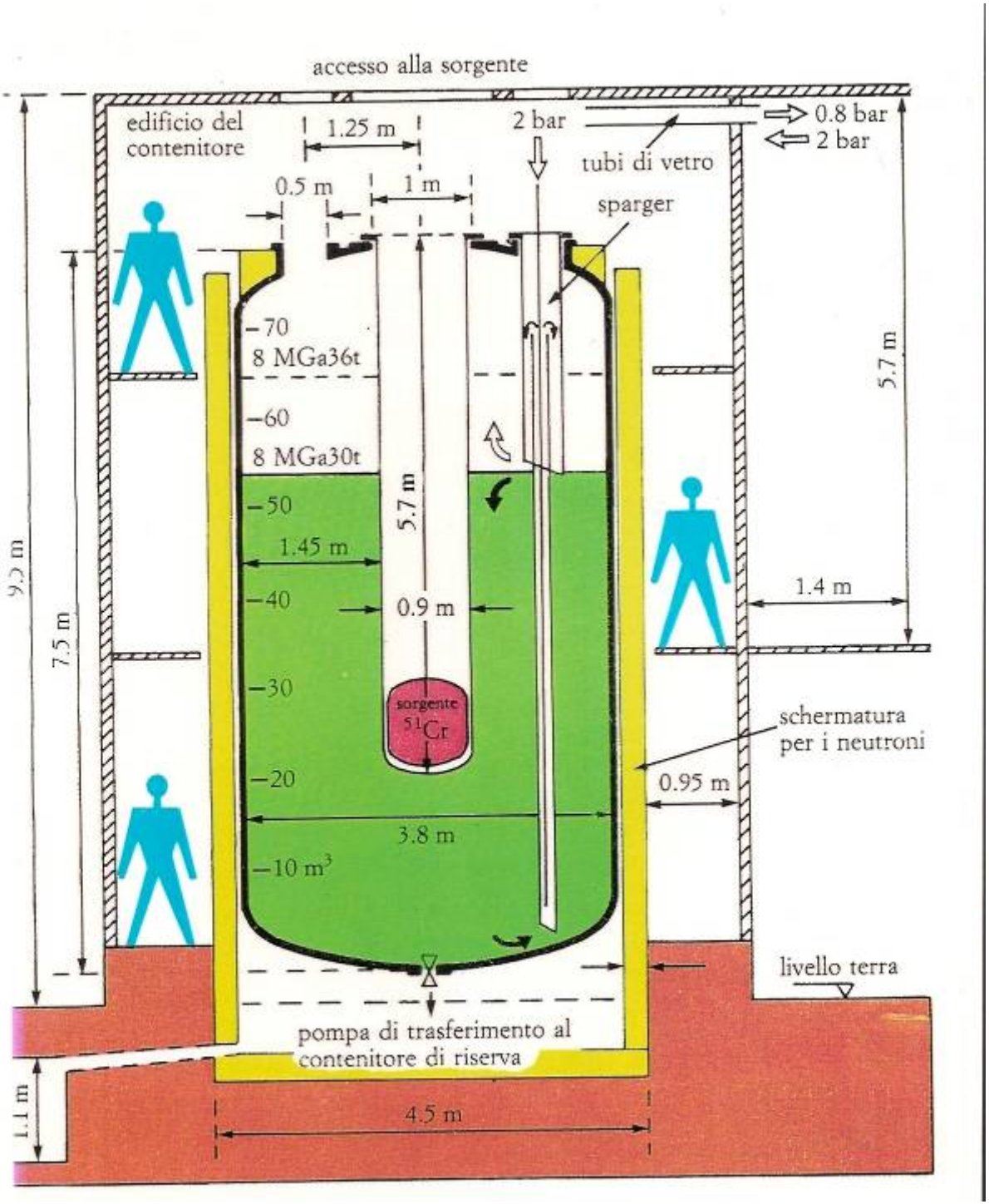
accesso alla sorgente
edificio del contenitore
1.25 m
2 bar
0.8 bar
2 bar
tubi di vetro
0.5 m
1 m
sparger
−70
8 MGa36t
−60
8 MGa30t
−50
1.45 m
5.7 m
−40
0.9 m
−30
sorgente ^{51}Cr
−20
−10 m^3
3.8 m
9.3 m
7.5 m
5.7 m
1.4 m
schermatura per i neutroni
0.95 m
livello terra
pompa di trasferimento al contenitore di riserva
1.1 m
4.5 m

GALLEX

GALLIUM EUROPEAN COLLABORATION

30 TONS OF GALLIUM IN $GaCl_3$ (IN HCl)

12 Tons ^{71}Ga

NEUTRINO FLUX FROM SUN (BACHALL et al.)

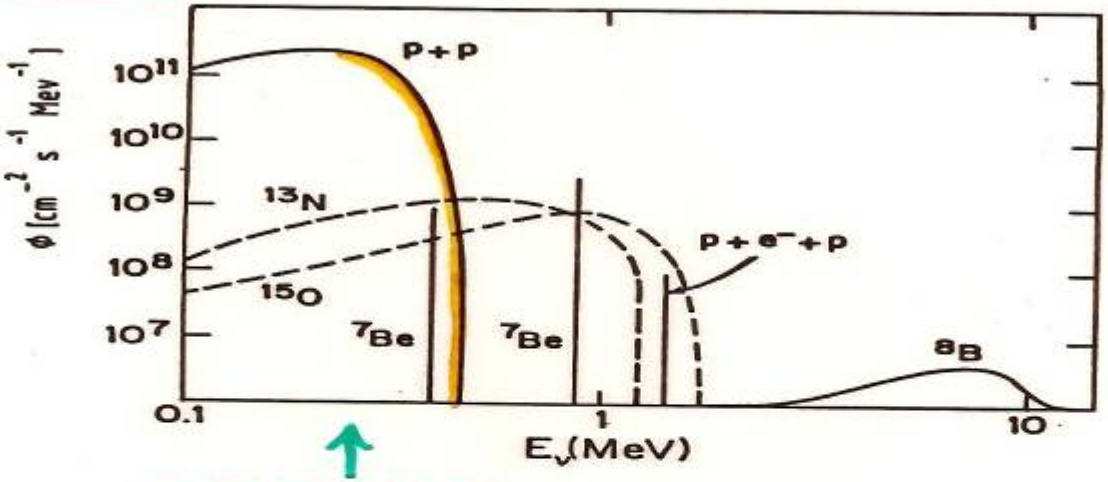

THRESHOLD

E > 233 KeV

$\nu_e + {}^{71}Ga \longrightarrow {}^{71}Ge + e^-$

LIQUIDO $GaCl_3 \Rightarrow GeCl_4$ GASSOSO

$T_{1/2} = 11.43$ d

$^{71}Ge \rightarrow {}^{71}Ga + \gamma$

(1.2 KeV
10.4 KeV)

SAGE – Russian American Gallium Experiment

- **radiochemical Ga experiment at Baksan Neutrino Observatory with 50 tons of metallic gallium**
- **running since 1990-present**

$66.2^{+3.3\ +3.5}_{-3.2\ -3.2}$ SNU

measures *pp* solar flux in agreement with SSM when oscillations are included – the predicted signal is

$67.3^{+3.9}_{-3.5}$ SNU

- latest result from 157 runs (1990-2006)

Figure 12.17. The SAGE experiment in the Baksan underground laboratory in the Caucasus. The 10 so-called reactors can be seen, 8 of which contain a total of 57 tons of metallic gallium (with kind permission of the SAGE collaboration).

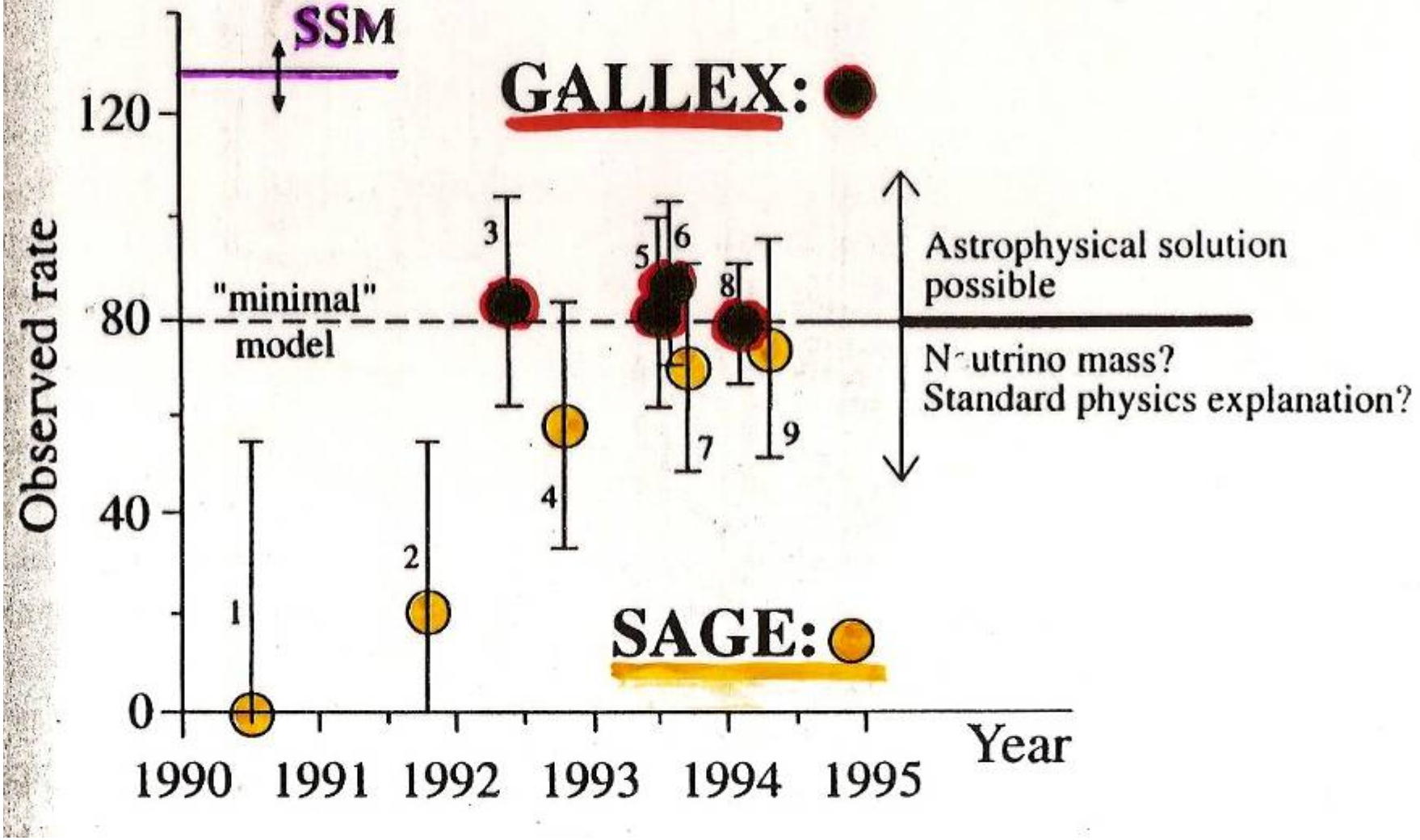

GALLEX-SAGE results

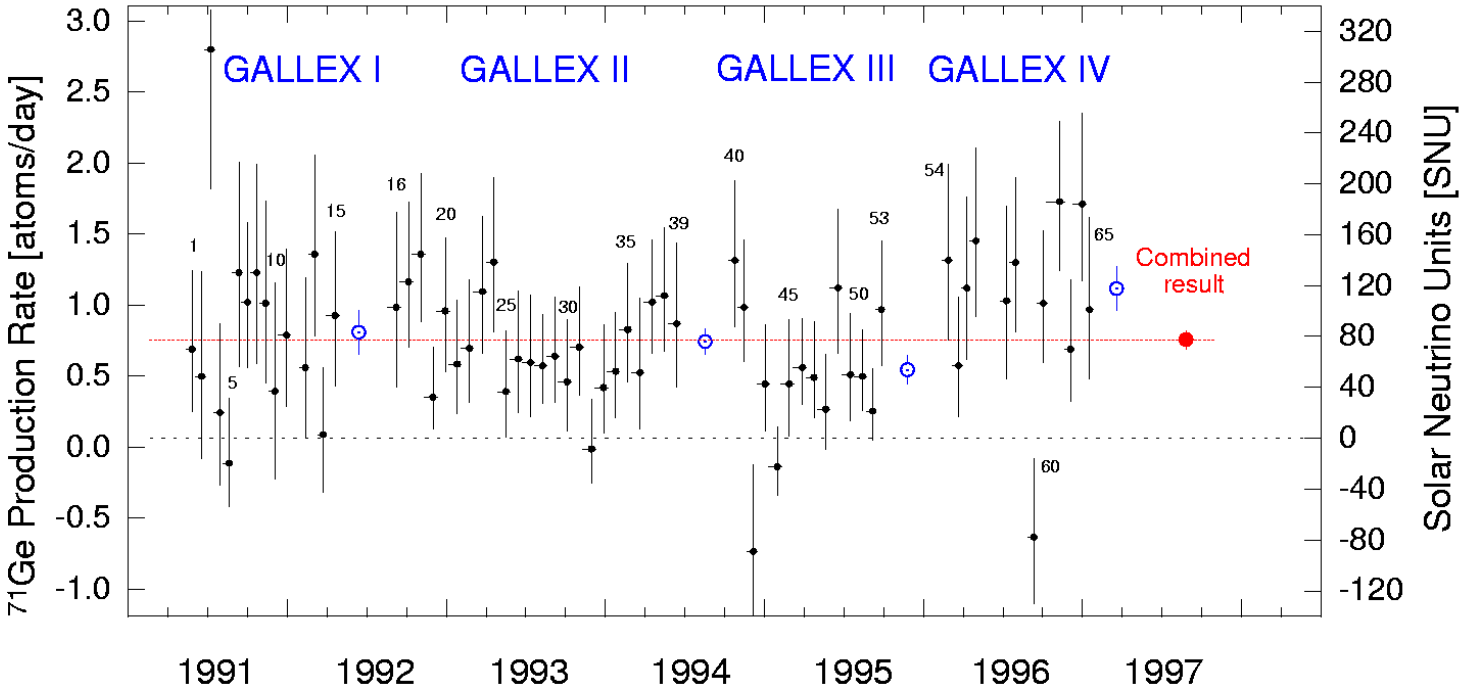

	GALLEX+GNO (SNU)	SAGE (SNU)
Measured	71 ± 5	66 ± 5
Expected	128 ± 8	128 ± 8

SNU= 10^{-36} (interactions/s · nucleus)

Solar Neutrino Problem

Experiment	Result	Theory	$\frac{\text{Result}}{\text{Theory}}$
Homestake [38]	$2.56 \pm 0.16 \pm 0.16$ (2.56 ± 0.23)	$7.7^{+1.2}_{-1.0}$	$0.33^{+0.06}_{-0.05}$
GALLEX [322]	$77.5 \pm 6.2^{+4.3}_{-4.7}$ (78 ± 8)	129^{+8}_{-6}	0.60 ± 0.07
SAGE [323]	$66.6^{+6.8\,+3.8}_{-7.1\,-4.0}$ (67 ± 8)	129^{+8}_{-6}	0.52 ± 0.07
Kamiokande [41]	$2.80 \pm 0.19 \pm 0.33$ (2.80 ± 0.38)	$5.15^{+1.0}_{-0.7}$	0.54 ± 0.07
Super-Kamiokande [48]	$2.44 \pm 0.05^{+0.09}_{-0.07}$ $(2.44^{+0.10}_{-0.09})$	$5.15^{+1.0}_{-0.7}$	$0.47^{+0.07}_{-0.09}$

The Solar Neutrino Problem

How can this deficit be explained?

1. The Sun's reaction mechanisms are not fully understood

   NO! *new measurements (~1998) of the sun resonant cavity frequencies*

2. The experiment is wrong –

   NO! *All the fourthcoming new experiments confirmed the deficit!*

3. Something happens to the neutrino as it travels from the Sun to the Earth

   YES! Oscillations of electron neutrinos!

Solar Neutrino Problem

- Astrophysical solutions?:
  - Low metallicity
  - Burnt out core
  - Rapid Rotation
  - High mass loss rate
  - Pure CNO cycle
  - WIMP
  - Central BH

The SK way- The elastic scattering of neutrinos on electrons

- Real-time detector
- Elastic scattering

$\nu e \rightarrow \nu e$

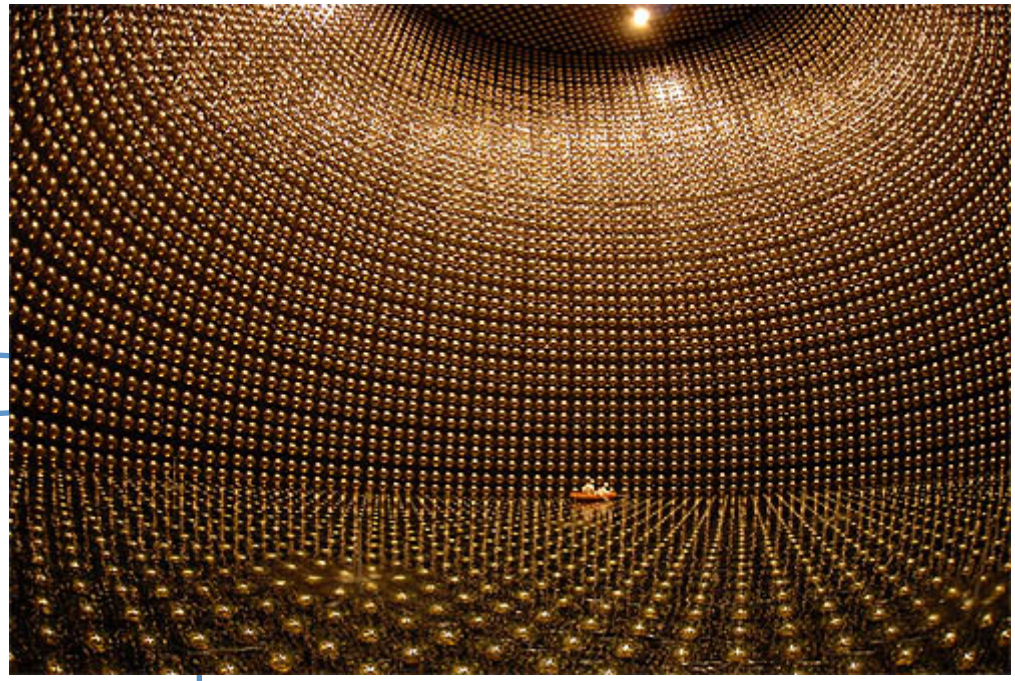

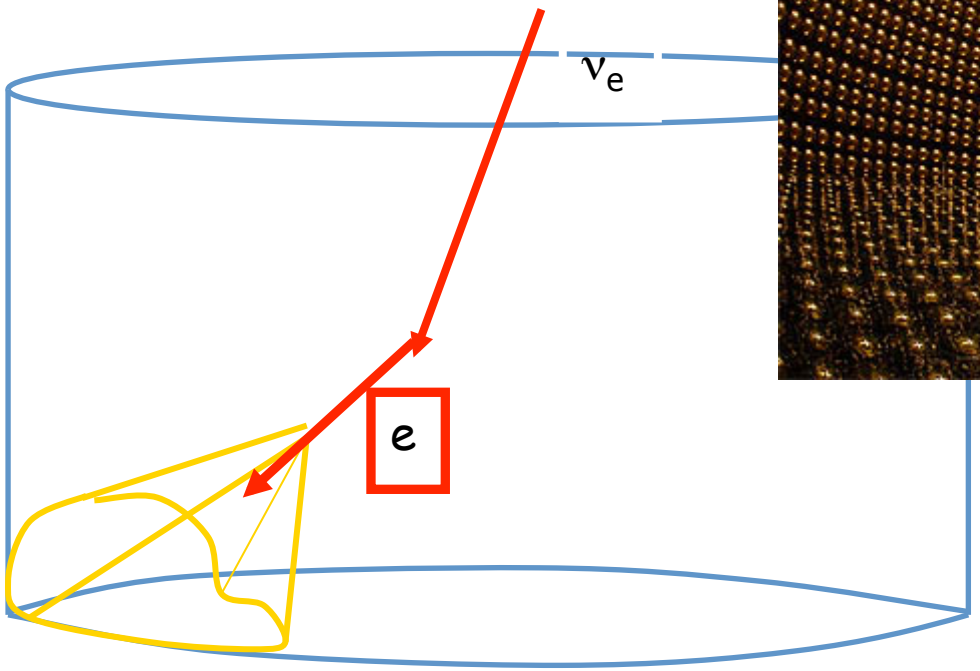

Neutrino Scattering Experiments

Particle	Cherenkov threshold in total Energy
$e^{\pm}$	0.768(MeV)
$\mu^{\pm}$	158.7
$\pi^{\pm}$	209.7

Cherenkov threshold energies of various particles.

$$\cos\theta = \frac{1}{n\beta'}$$

Cherenkov light is emitted in a cone of half angle θ from the direction of the particle track

Neutrino Scattering Experiments

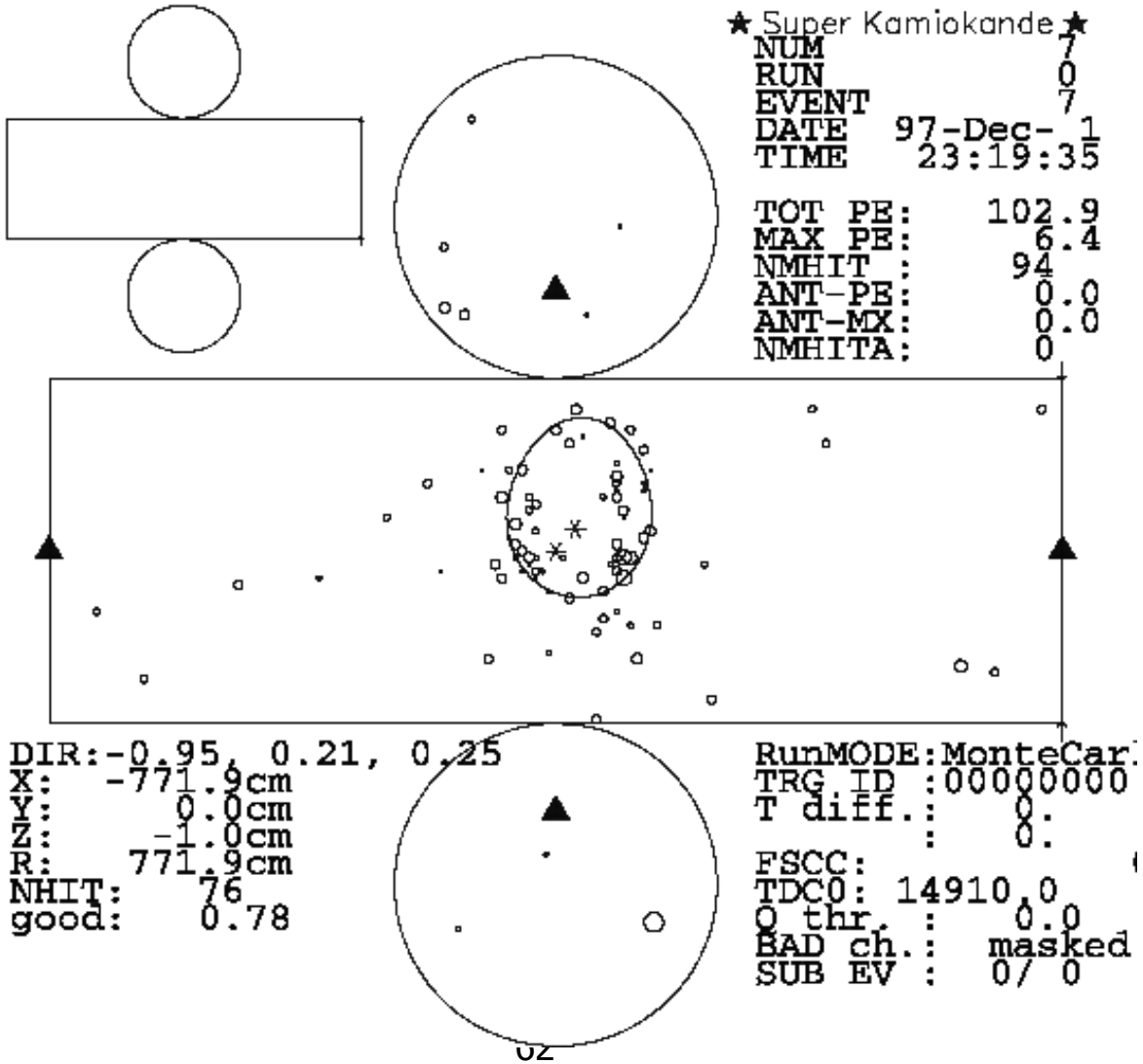

Neutrino Scattering Experiments

Radioactivity Background

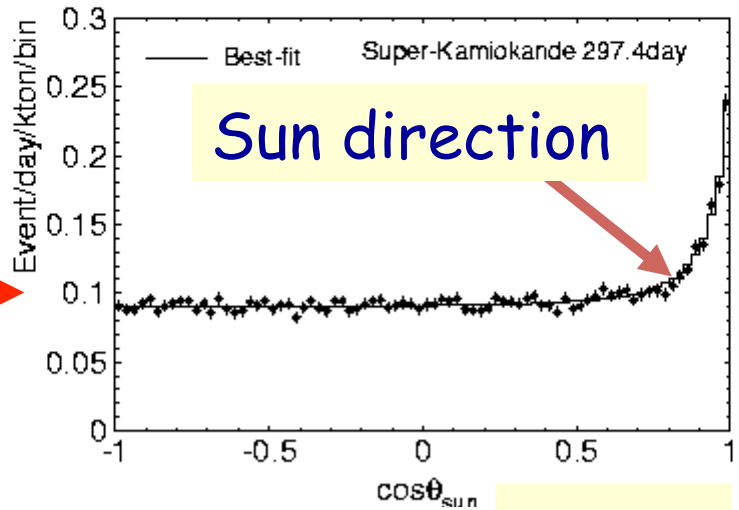

$\cos\theta_{sun}$

Ratio of observed electron energy spectrum and expectation from SSM

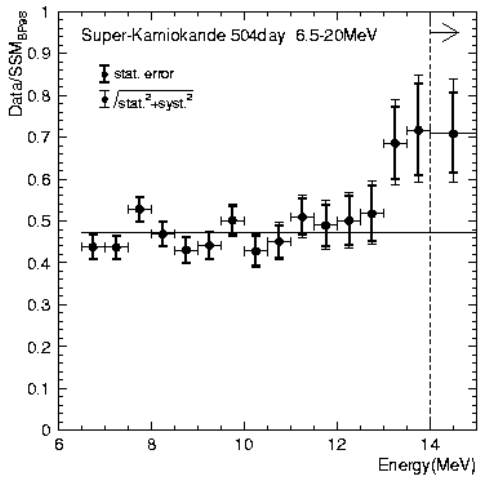

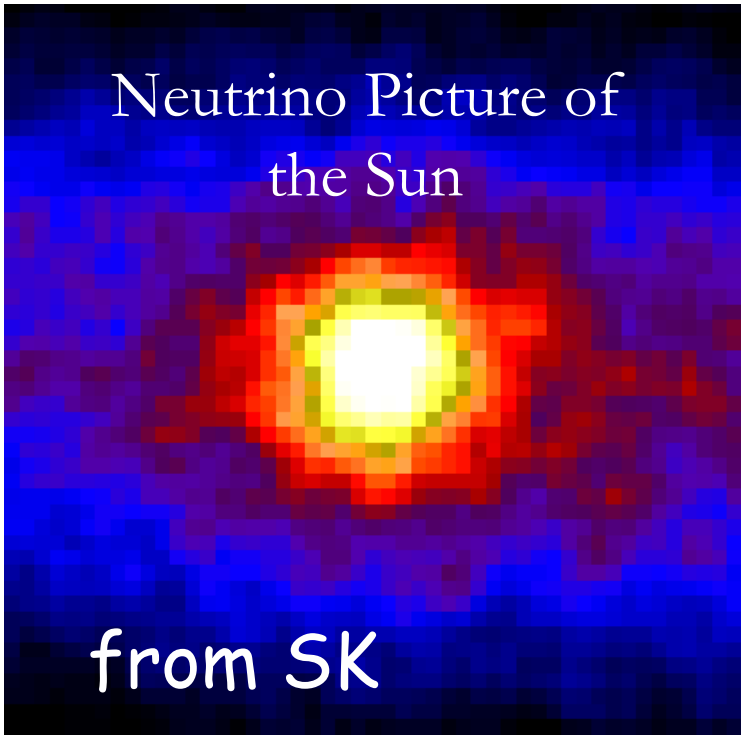

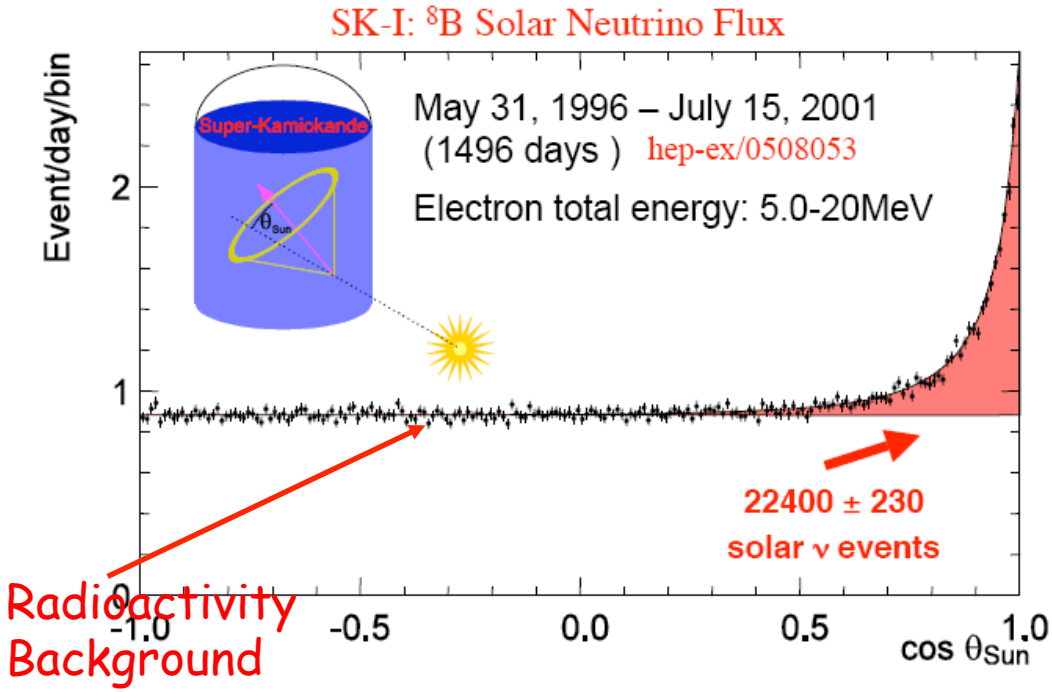

$\phi_{ES} = 2.35 \pm 0.02 \pm 0.08$ [x10^6/cm^2/s]

- SK measured a flux of solar neutrinos with energy > 5 MeV (from B^8) about 40% of that predicted by the SSM
- The reduction is almost constant up to 18 MeV

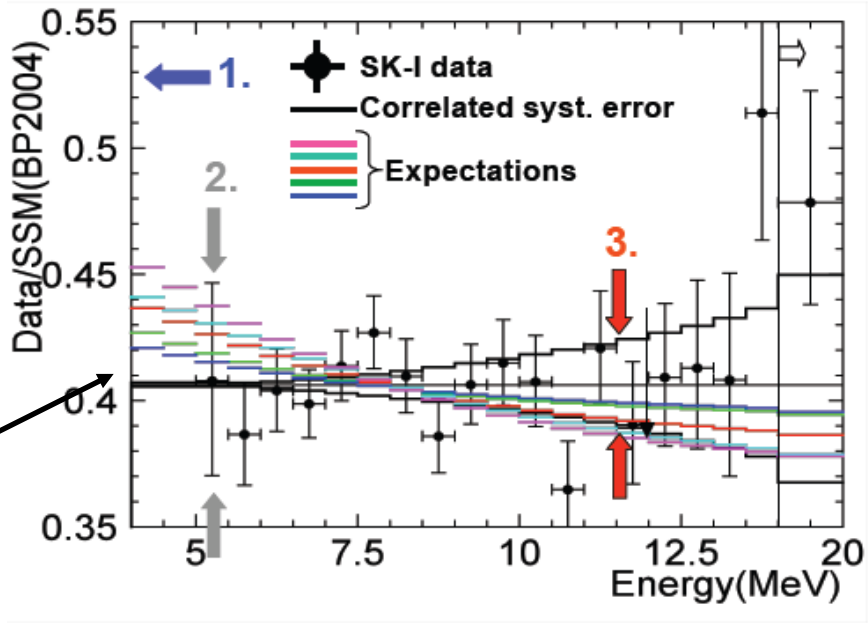

Ratio of observed electron energy spectrum and expectation from SSM

The decisive results: SNO (α: 1999 –Ω:2006)

- 18m sphere, situated underground at about 2.5km underground, in Ontario
- 10,000 photomultiplier tubes (PMT)
- Each PMT collect Cherenkov light photons
- Heavy water (D_2O) inside a transparent acrylic sphere (12m diameter)
- Pure salt is added to increase sensitivity of NC reactions (2002)
- It can measure the flux of all neutrinos '$\Phi(\nu_x)$' and electron neutrinos '$\Phi(\nu_e)$'
- The flux of non-electron neutrinos

$$\Phi(\nu_\mu,\ \nu_\tau) = \Phi(\nu_x) - \Phi(\nu_e)$$

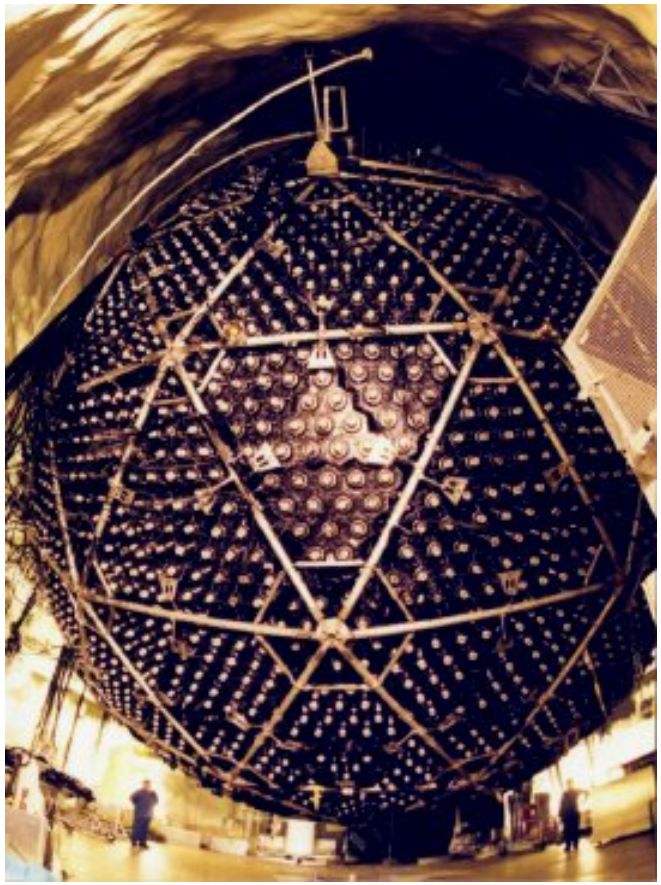

These fluxes can be measured via the 3 different ways in which neutrinos interact with heavy water

Sudbury Neutrino Observatory

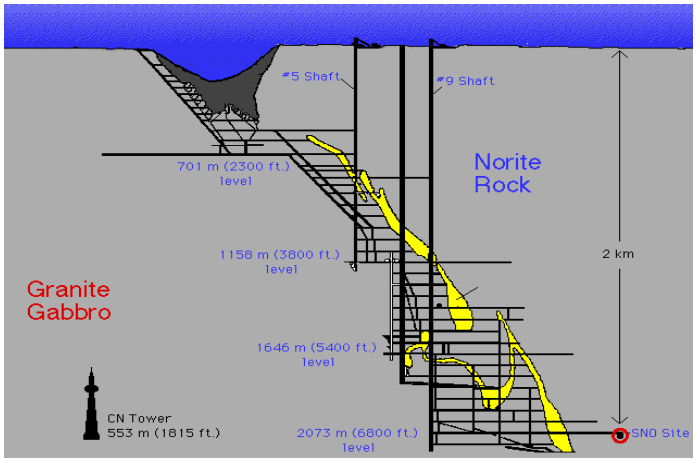

1000 tonnes D_2O

Support Structure for 9500 PMTs, 60% coverage

12 m Diameter Acrylic Vessel

1700 tonnes Inner Shielding H_2O

5300 tonnes Outer Shield H_2O

Urylon Liner and Radon Seal

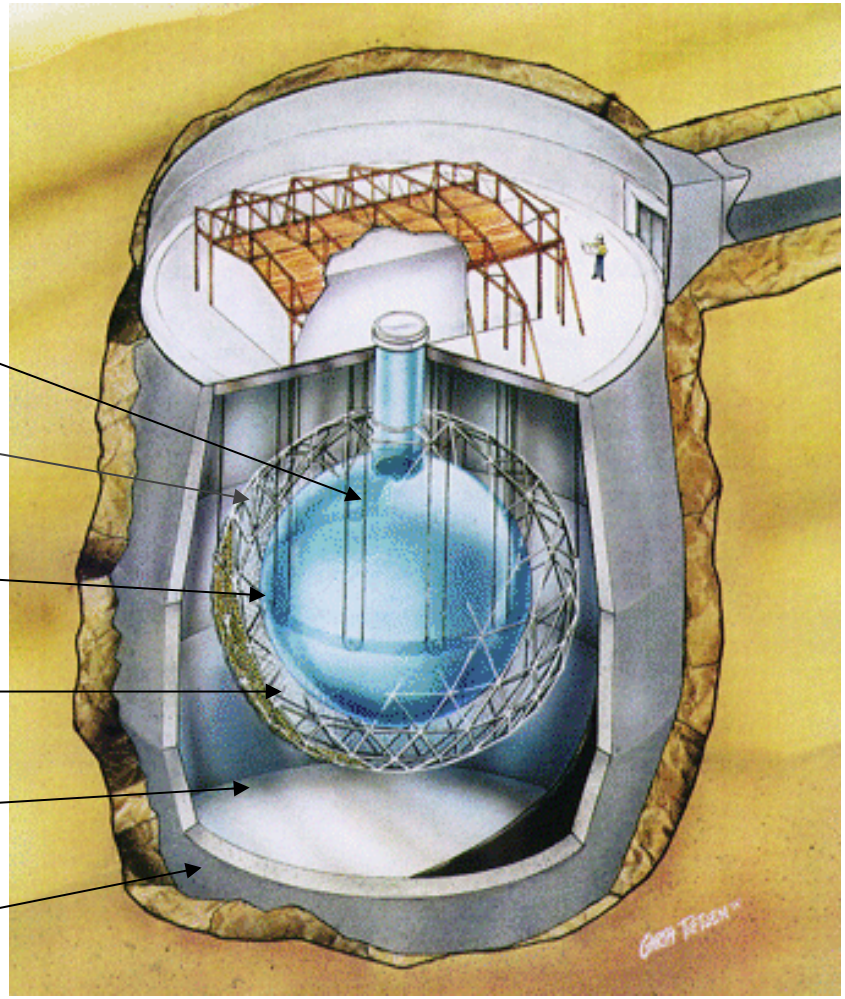

ν Reactions in SNO

CC $\nu_e + d \Rightarrow p + p + e^-$

-Gives ν_e energy spectrum well
-Weak direction sensitivity $\propto$ 1-1/3cos(θ)
- ν_e only.
-SSM: 30 CC events day^{-1}

NC $\nu_x + d \Rightarrow p + n + \nu_x$

- Measure total ^{8}B ν flux from the sun.
- Equal cross section for all ν types
- SSM: 30/day

ES $\nu_x + e^- \Rightarrow \nu_x + e^-$

-Low Statistics (3/day)
-Mainly sensitive to ν_e, some
-sensitivity to ν_μ and ν_τ
-Strong direction sensitivity

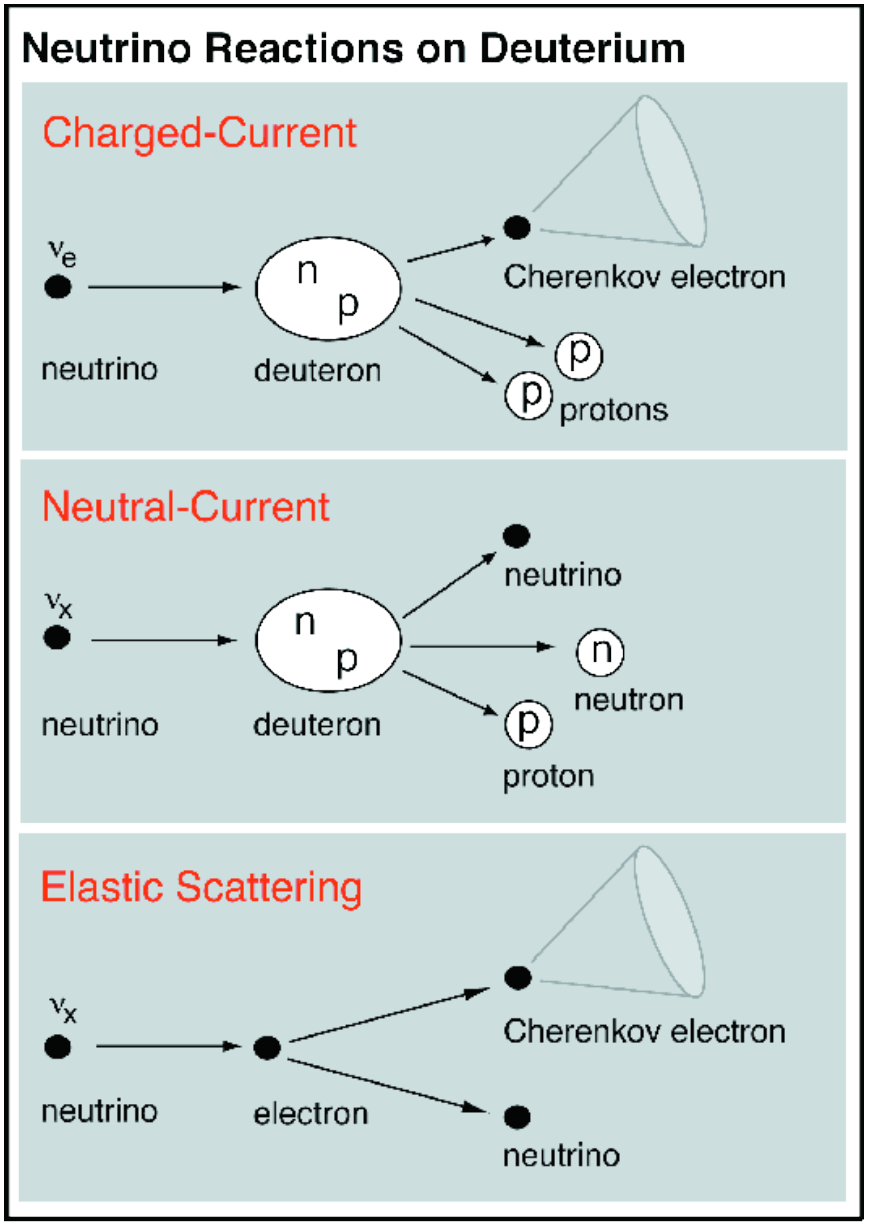

OBSERVABLE REACTIONS IN S.N.O.

Le Reazioni Osservabili in SNO

CHARGED CURRENT

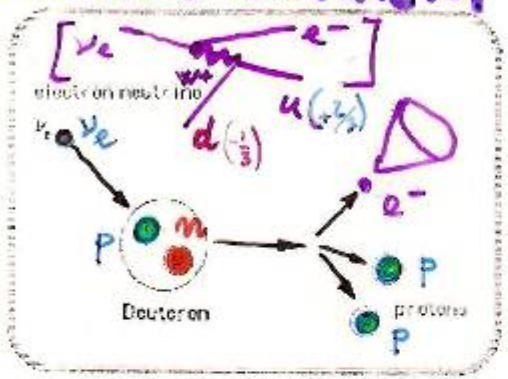

ELASTIC SCATTERING

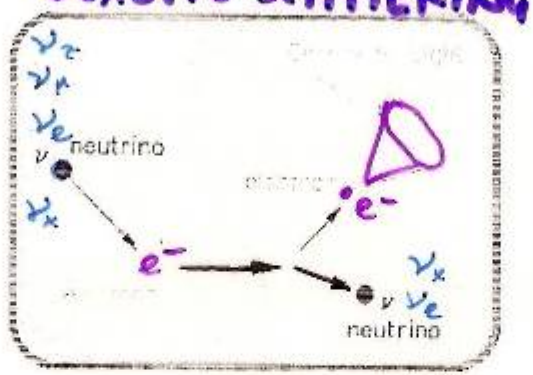

NEUTRAL CURRENT

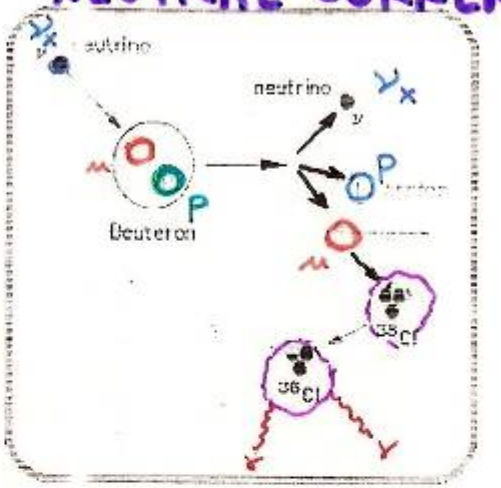

$\nu_e + d \rightarrow p + p + e^-$ (CC)

Solo neutrini elettronici

ν_e ONLY

$\nu_x + e^- \rightarrow \nu_x + e^-$ (ES)

Tutti i neutrini

ν_x = ALL NEUTRINOS

$\nu_x + d \rightarrow n + p + \nu_x$ (NC)

Tutti i neutrini

ν_x = ALL NEUTRINOS

Neutrini prodotti da ^8B (E_ν<15 MeV)

Soglia Rivelatore 6.75 MeV

THRESHOLD @ 6.75 MeV

Può essere separato il contributo dei diversi neutrini

IT IS POSSIBLE TO SEPARATE ν_x CONTRIBUTIONS

⇓

Indipendenza dalle previsioni del modello Solare

INDIPENDENT FROM S. SOLAR MODEL

❑ The 2001 results

❑ The ν_e's flux from ^8B decay is measured by the CC (1) reaction: $\phi^{CC}(\nu_e)$

$= (1.75 \pm 0.24) \times 10^6\ cm^{-2}s^{-1}$

❑ Assuming no oscillations, the total ν flux inferred from the ES (3) reaction rate is:

❑ $\phi^{ES}(\nu_x) = (2.39 \pm 0.50) \times 10^6\ cm^{-2}s^{-1}$ (SNO)

❑ $\phi^{ES}_{SK}(\nu_x) = (2.32 \pm 0.08) \times 10^6\ cm^{-2}s^{-1}$ (SK)

❑ The difference between the ^8B flux deduced from the ES and the CC rate at SNO and SK is:

❑ $\Phi(\nu_\mu, \nu_\tau) = (0.57 \pm 0.17) \times 10^6\ cm^{-2}s^{-1}$ (3.3 σ)

❑ This difference first shows that **there is a non-electron** flavour active neutrino component in the solar flux !

UNITS:
x 10^6 cm^{-2} s^{-1}

$$\phi_{CC}^{SNO} = 1.59^{+0.08}_{-0.07}(stat)^{+0.06}_{-0.08}(syst)$$
$$\phi_{ES}^{SNO} = 2.21^{+0.31}_{-0.26}(stat) \pm 0.10\,(syst)$$
$$\phi_{NC}^{SNO} = 5.21 \pm 0.27\,(stat) \pm 0.38\,(syst)$$

ATTESO: Bahcall et al. – SSM= **5.05±0.8**

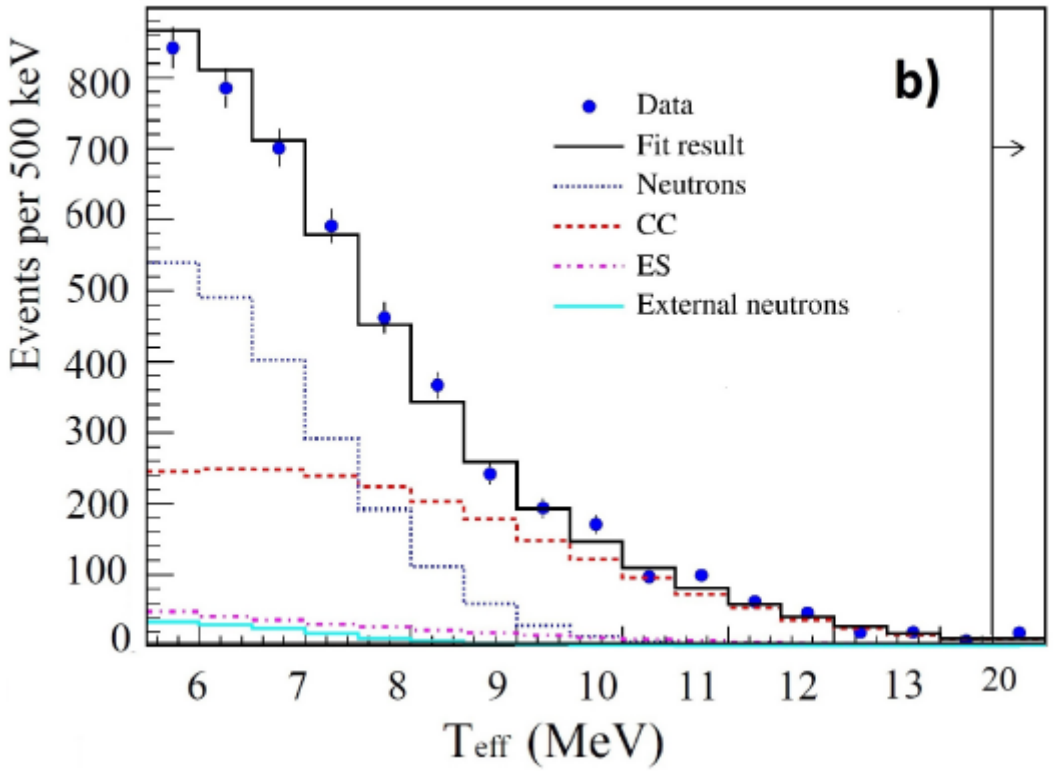

Electron kinetic energy

2003 SNO Energy spectra (Salt data)

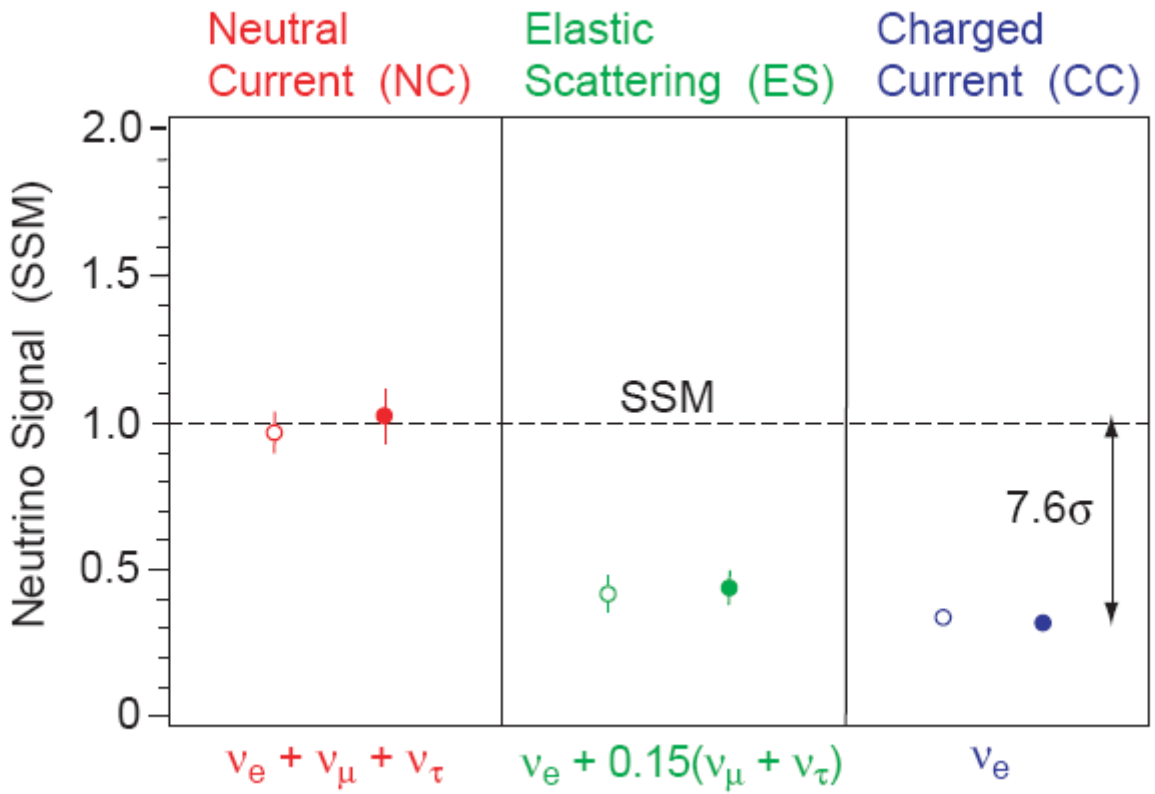

Figure 8: Evidence for neutrino flavor change seen by SNO. The open (filled) circles represent the 2003 SNO flux results, relative to the SSM, under the assumption of an undistorted (unconstrained) ^{8}B neutrino energy spectrum.

Solar Neutrino Problem

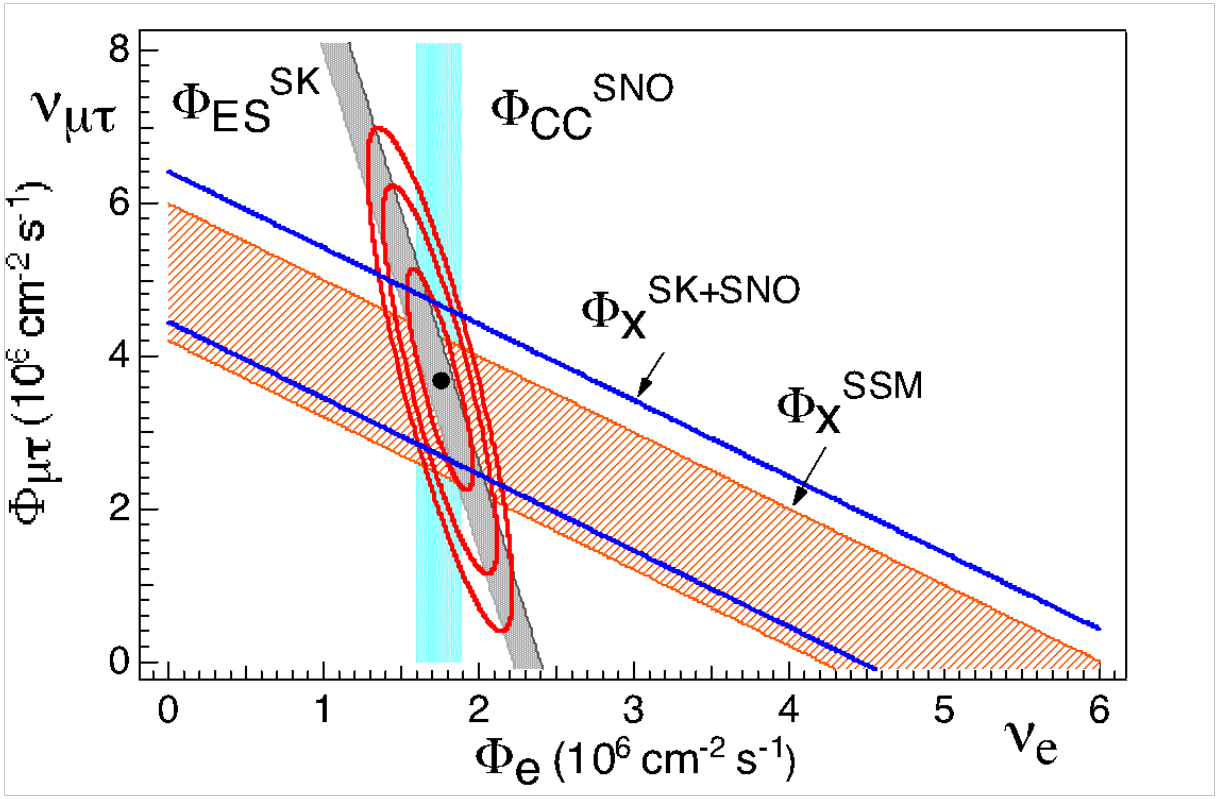

- The total flux of active ^{8}B neutrinos is:

  $(5.44 \pm 0.99) \times 10^6$ cm^{-2}s^{-1} , in agreement with SSM

Solar Neutrino Problem

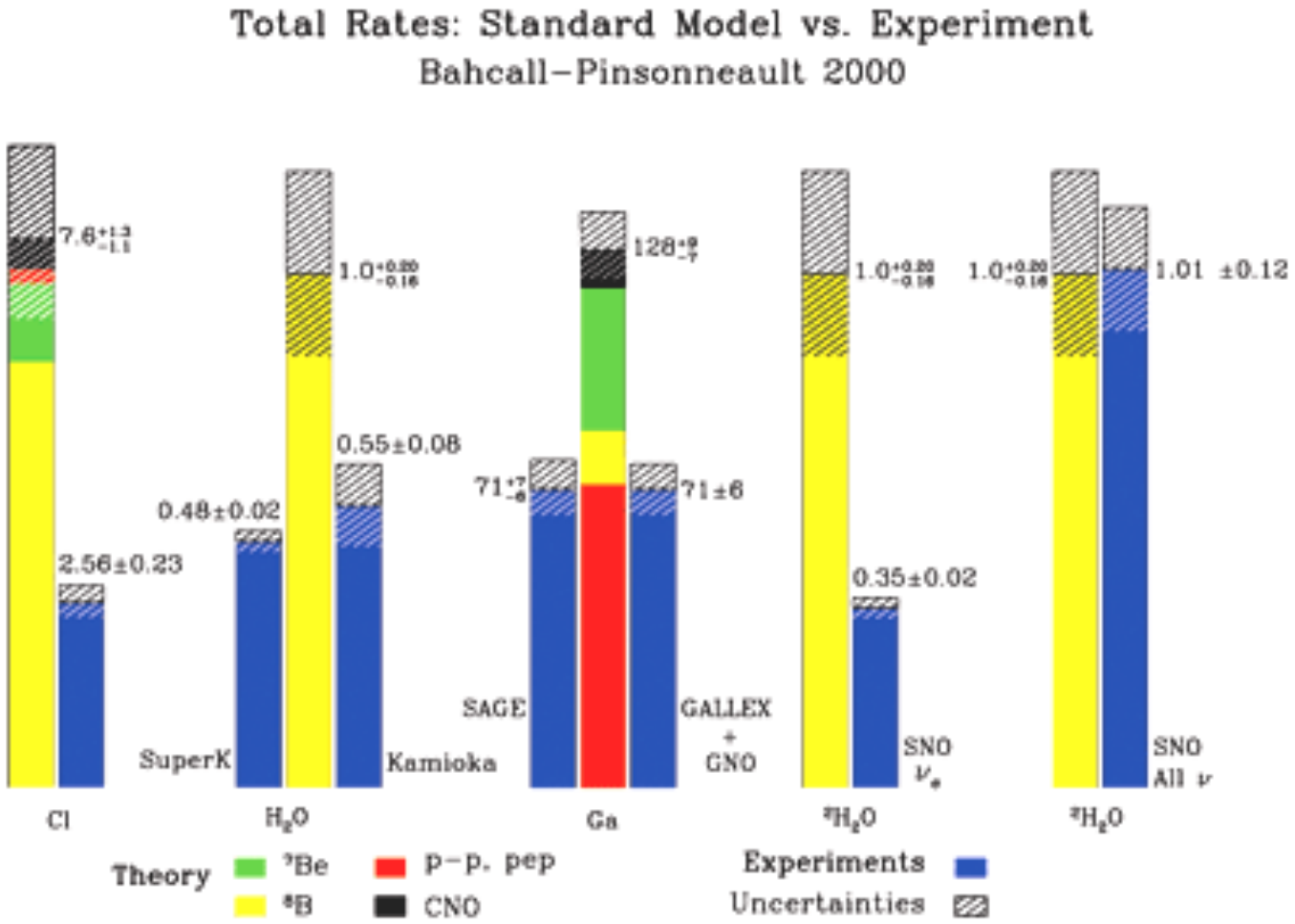

Borexino @LNGS

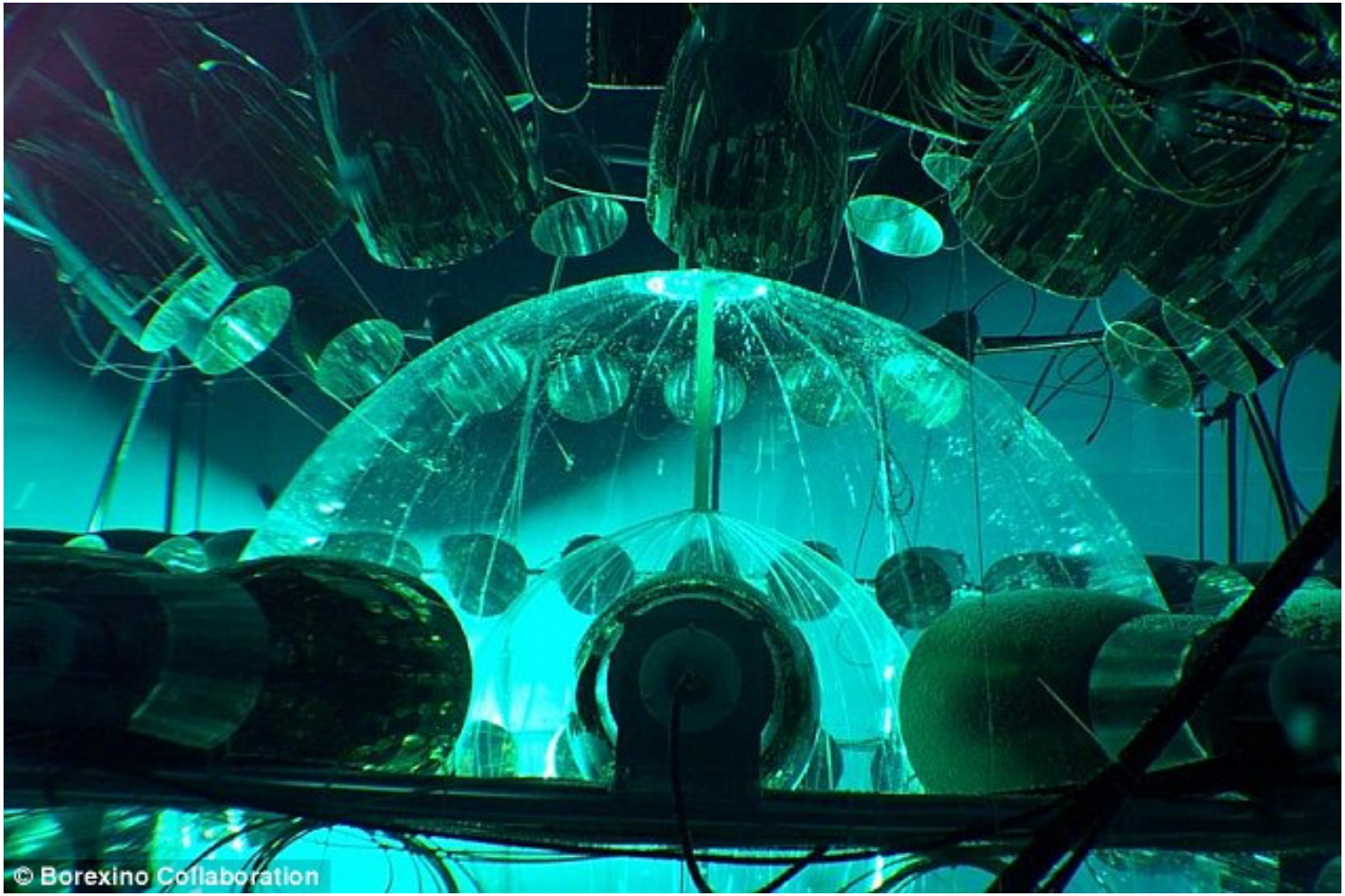

Borexino @LNGS

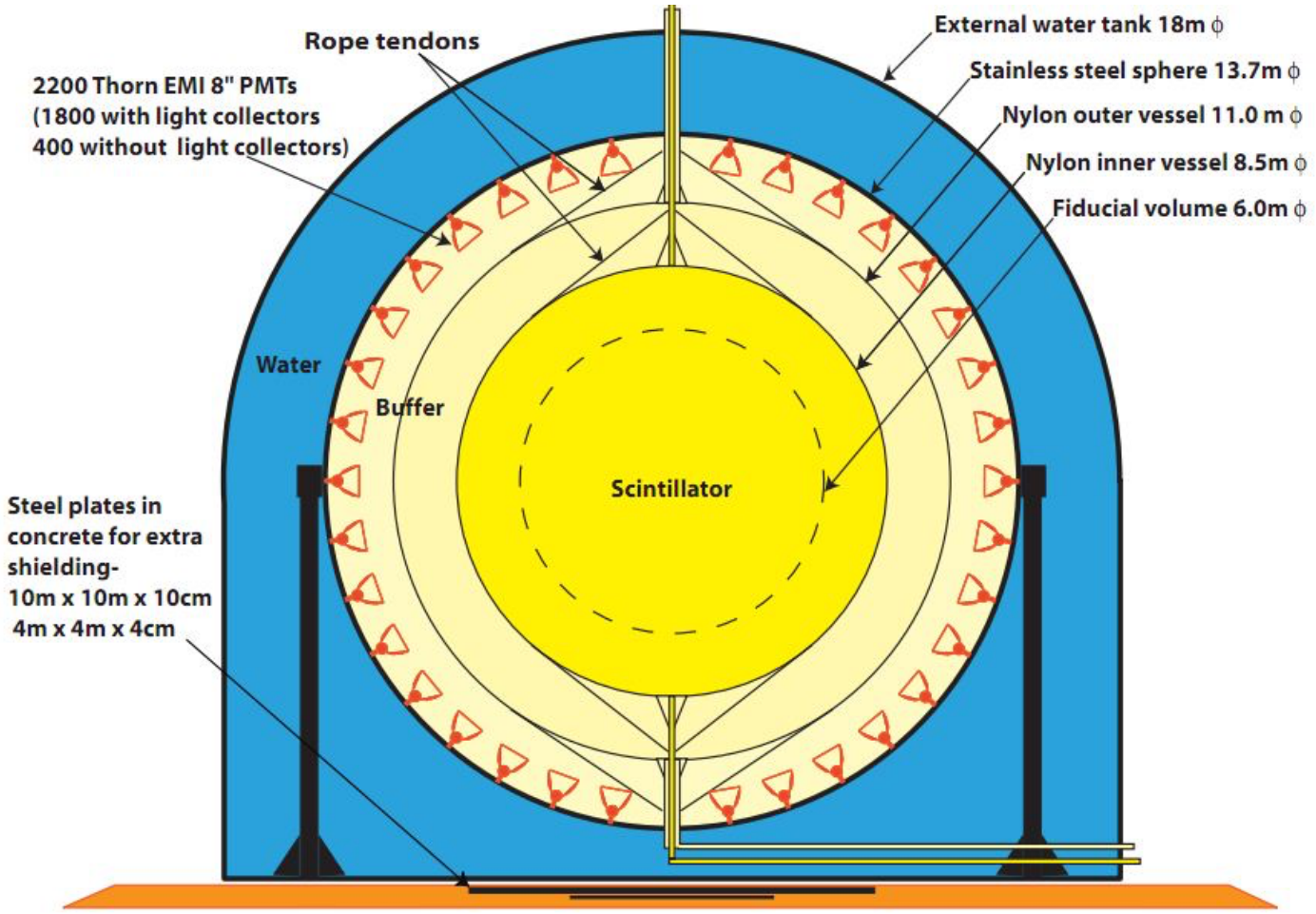

BOREXINO
Recent Solar And Terrestrial Neutrino Results

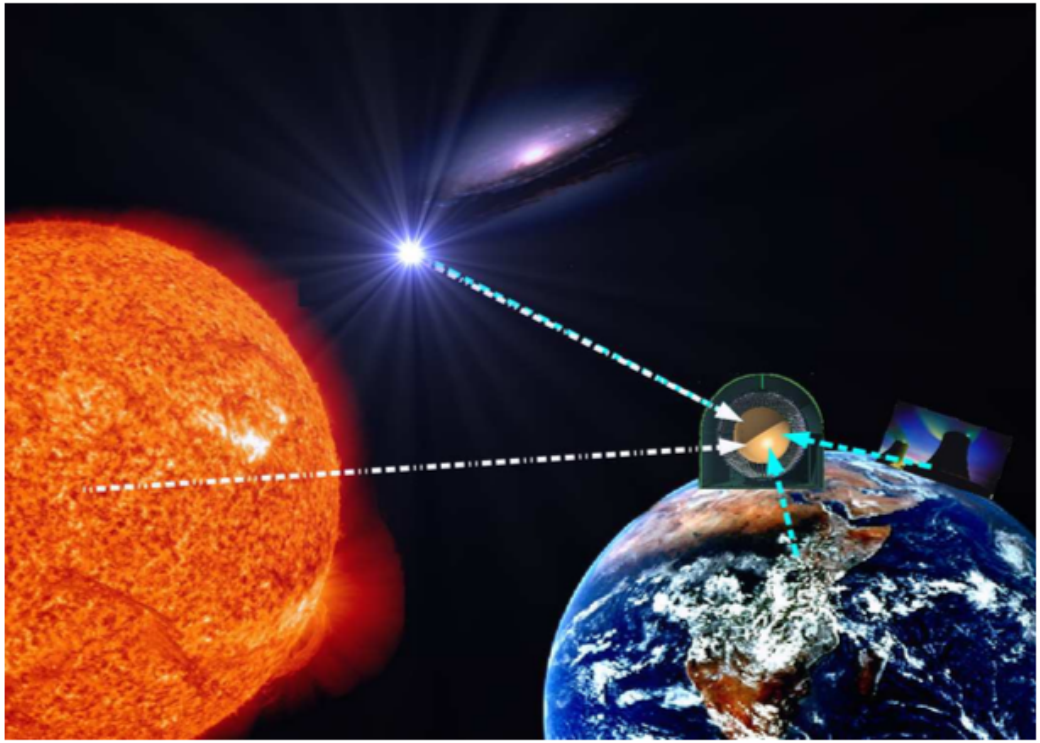

Werner Maneschg
on behalf of the Borexino Collaboration

Borexino: detector properties & design, and physics goals

Main properties:

- Large volume organic liquid scintillator detector:
  - at LNGS (1.4 km overburden)
  - operational since May 2007
- Ultra low background (radiopurest environment ever measured)
- Real-time detection (time stamp and pulse shape for every event)
- Spectroscopy at low energies, typically between 0.1-15 MeV
- 3D position reconstruction

Main physics goals:

- Neutrinos from Sun
- Antineutrinos from Earth & reactors
- Sterile neutrinos (TH 23-07-15:13.5)
- SN-(anti)neutrinos & other exotic particles and processes

Nut shell profile:

1. Water tank (2100 m^3):
   - Absorption of environmental γ rays and neutrons
   - μ Cherenkov detector (208 PMTs)
2. Stainless Steel Sphere:
   - 2212 PMTs, 1350 m^3, R=6.85 m
3. 2 buffer layers: PC+DMP
   - Outer R_2=5.50 m, Inner R_1=4.25 m
   - Shielding from external γ rays
4. Scintillator: 270 tons of PC+PPO

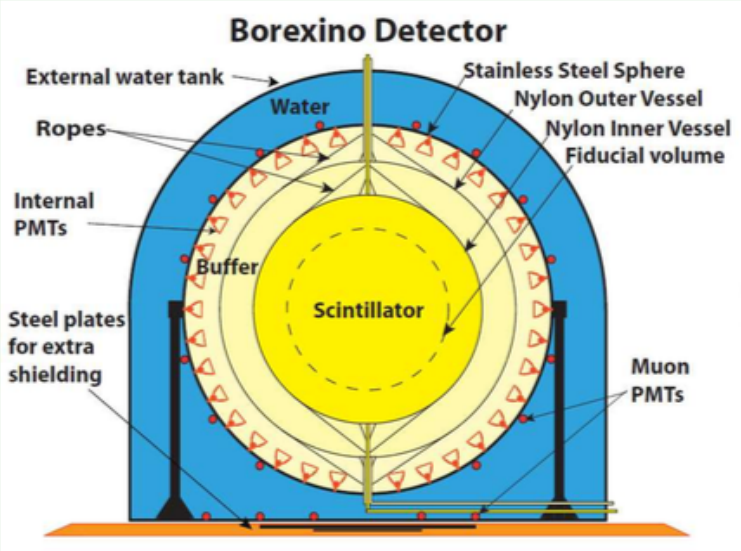

Solar neutrino fluxes (according to Standard Solar Model predictions)

Neutrino fluxes at 1 AU:

from simulations by A. Serenelli et al., Astrophys. J. 743, 24 (2011)

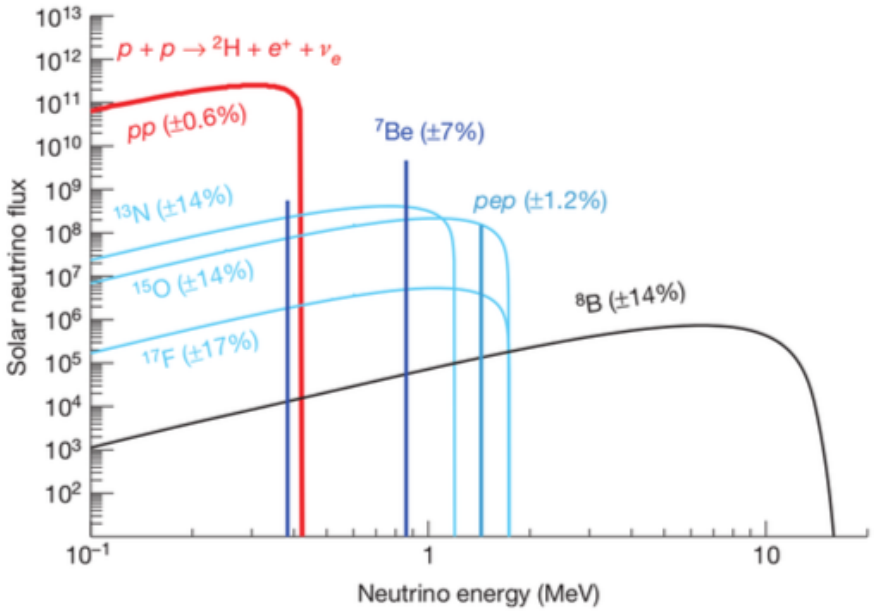

Units: $[\mathrm{cm}^{-2}\mathrm{s}^{-1}\mathrm{MeV}^{-1}]$ for continuum neutrino sources, $[\mathrm{cm}^{-2}\mathrm{s}^{-1}]$ for mono-energetic neutrino sources.

ν flux	GS98	AGSS09
pp	5.98(1±0.006)	6.03(1±0.006)
^{7}Be	5.00(1±0.07)	4.56(1±0.07)
pep	1.44(1±0.012)	1.47(1±0.012)
^{13}N	2.96(1±0.14)	2.17(1±0.14)
^{15}O	2.23(1±0.15)	1.56(1±0.15)
^{17}F	5.52(1±0.17)	3.40(1±0.16)
^{8}B	5.58(1±0.14)	4.59(1±0.14)

Factors: 10^{10} (pp), 10^{9} (^{7}Be), 10^{8} (pep, ^{13}N, ^{15}O), 10^{6} (^{8}B, ^{17}F);
Units: $\mathrm{cm}^{-2}\mathrm{s}^{-1}$.

Solar neutrino measurements:
different obstacles: diff. background, detector response, energy threshold
sensitivity for different phenomena: neutrino osc. (incl. matter effects (MSW)), SSM metallicity scenarios

Solar ^{7}Be neutrino rate measurement

Averaged ^{7}Be-ν rate fitted with MC (ROI: 0.2-0.7 MeV)

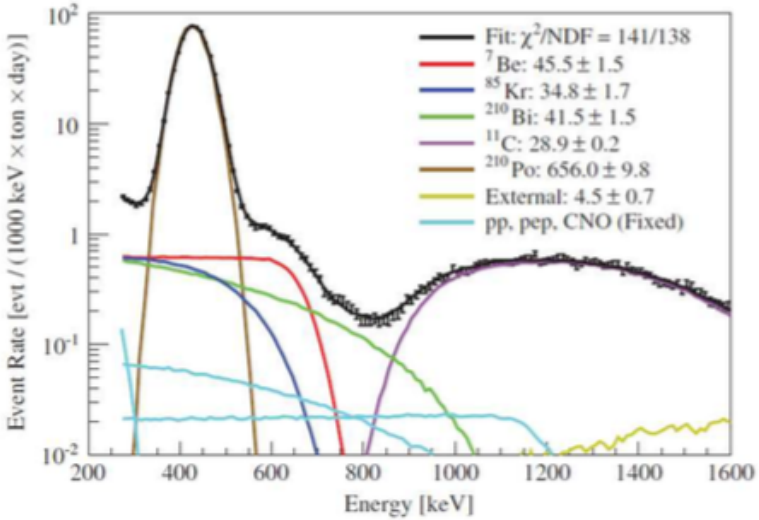

Results and remarks:

- Averaged rate: R=(46±1.5(stat)$^{+1.5}_{-1.6}$(sys)) c/d/100 ton (uncertainty ±5%)
  Comparison to SSM predictions:
  - Without osc.: (74±5) c/d/100 ton (5σ exclusion)
  - With osc.: 44 (High-met.) and 48 (Low-met.) c/d/100 ton
- Day-Night asymmetry: (N-D)/((N+D)/2) = 0.001±0.012(stat)±0.007(sys)
  (8.5 σ exclusion of LOW osc. solution)
- 7% Annual modulation: according to rate-vs-time analysis: T=(1.01±0.07) yr;
  ϵ=0.0398±0.0102 → expected value within 2 σ

Solar ^{8}B neutrino rate measurement

Data vs. MC of ^{8}B recoil energy spectrum (ROI: 3-15 MeV)

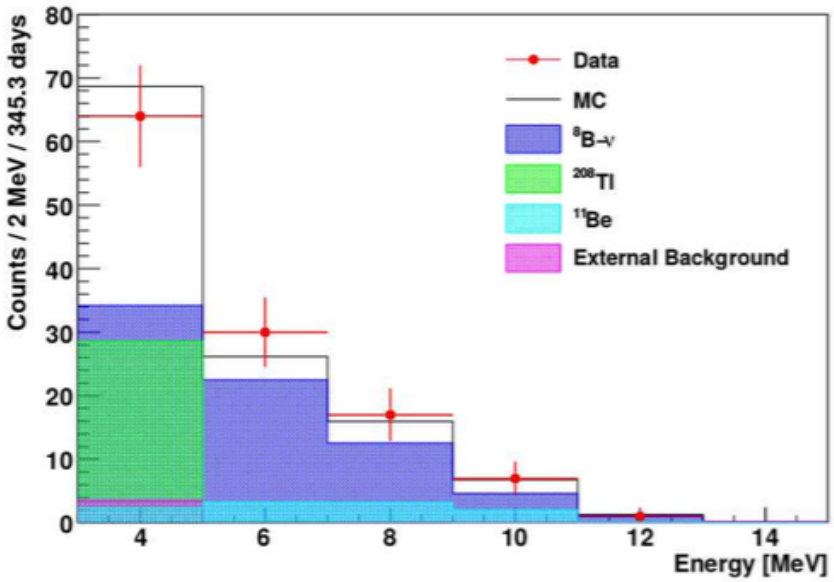

Results and remarks:

- Challenging: low neutrino rate, many small background components
- Rate above 3 MeV: $0.217 \pm 0.038(\text{stat}) \pm 0.008(\text{syst})$ c/d/100ton
- Flux at 1 AU: $(2.7 \pm 0.4 \pm 0.1) \times 10^6$ cm^{-2} s^{-1}
  → good agreement with SuperKamiokaNDE and SNO
  → confirmation of MSW-LMA solution for oscillation in vacuum/matter
- Data set: used 488 d; new analysis with multiple statistics ongoing

Towards the detection of solar pp neutrinos

pp recoil energy spectrum (ROI: 0.05-0.27 MeV)

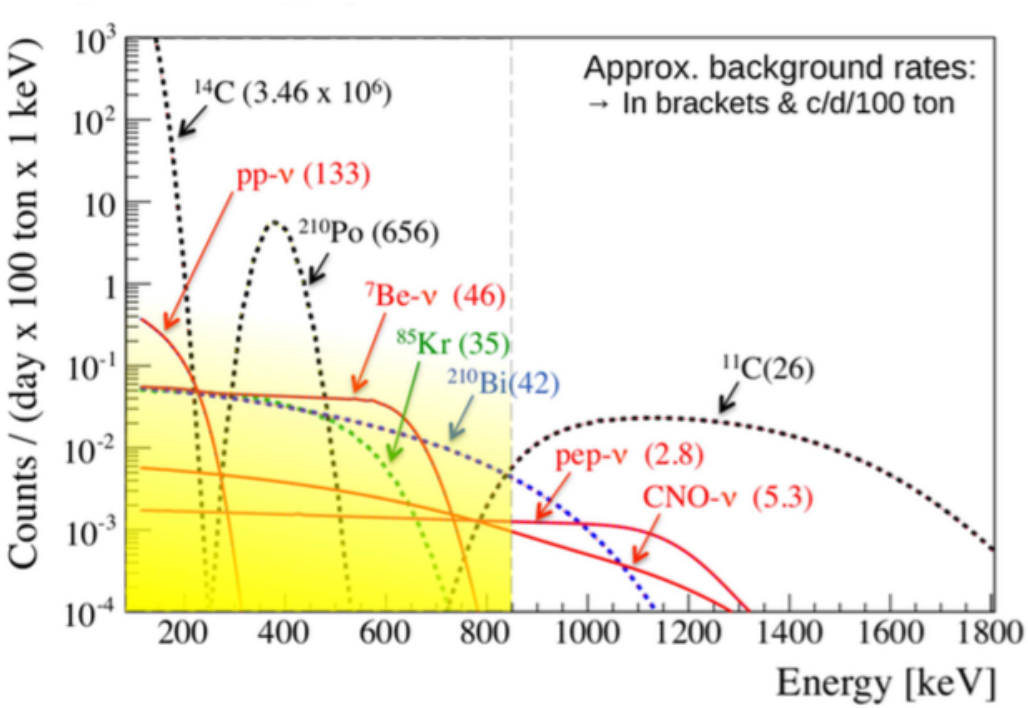

pp neutrinos:

Endpoint energy E_{mx}:
$0 < E_{mx} < 420$ keV
$\rightarrow E_{rec} < 264$ keV
Energy threshold E_{th}:
Borexino: $E_{th} \sim 50$ keV
Radiochem. experiments:
$E_{th} \sim 233$ keV

Main obstacles:

- Above ~240 keV: decays of ^{85}Kr, ^{210}Bi (^{210}Pb daughter)
- Below ~240 keV: decays of ^{14}C, ^{14}C pile-ups

Solar pp neutrino rate measurement (August 2014)

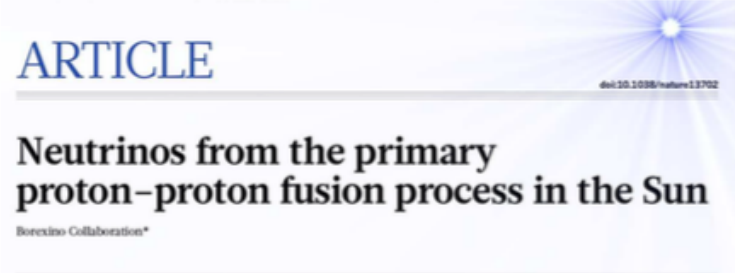
ARTICLE

Neutrinos from the primary proton–proton fusion process in the Sun

Borexino Collaboration*

Nature, Vol. 512, August 28, 2014

Results and remarks:

- Rate:
  144±13(stat)±10(sys) c/d/100 ton
  (10σ exclusion of pp ν absence)
- Robustness of analysis:

Parameter	Systematics:
energy estimator fit energy range data selection pile-up evaluation	±7%
fiducial mass	±2%

- Check of residual background

Measured recoil energy spectrum

Fit in (165-590) keV

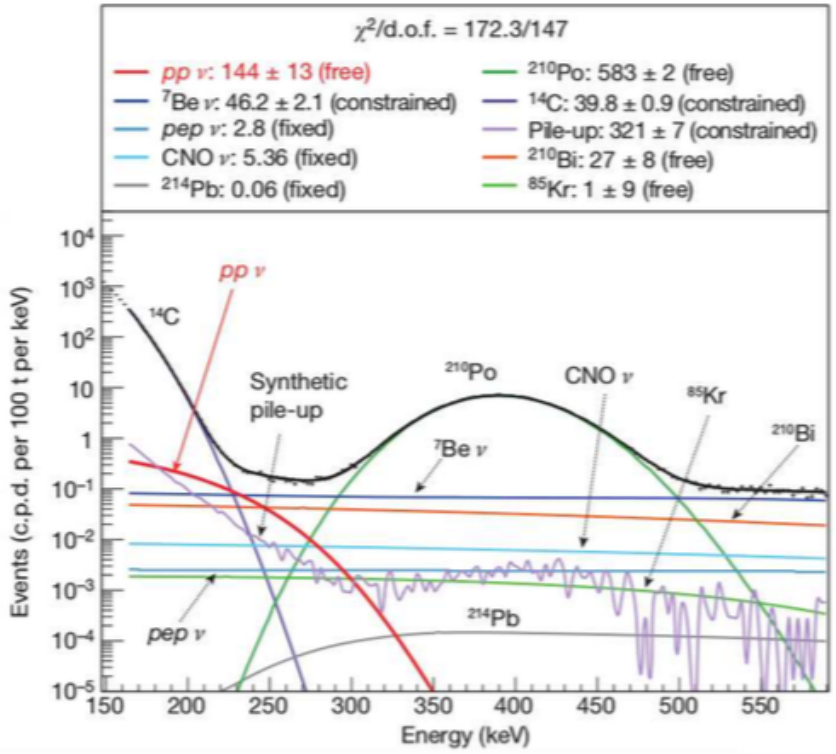

Rates in [c/d/100 ton], except for ^{14}C [c/s/100 ton]

Astrofisica Nucleare e Subnucleare

Neutrino Oscillations

Scoperta graduale

1964. Homestake + Modello Solare di J. Bahcall

flusso di ν_e dal sole ≈1/3 dell'aspettato ha colpa il sole, la fisica nucleare, il neutrino?

1997. GALLEX + LUNA

il colpevole è il neutrino

1998. SuperKAMIOKANDE

scoperta oscillazioni: scomparsa nei ν_μ da atmosfera

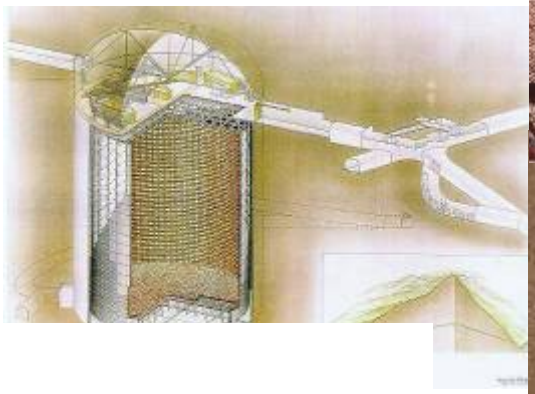

2002. SNO

osservazione di comparsa di ν_μ e ν_τ dal sole, tanti quanti sono i ν_e scomparsi

2002. KamLAND

osservazione dell'oscillazione "solare" su≠ ν_e nel vuoto

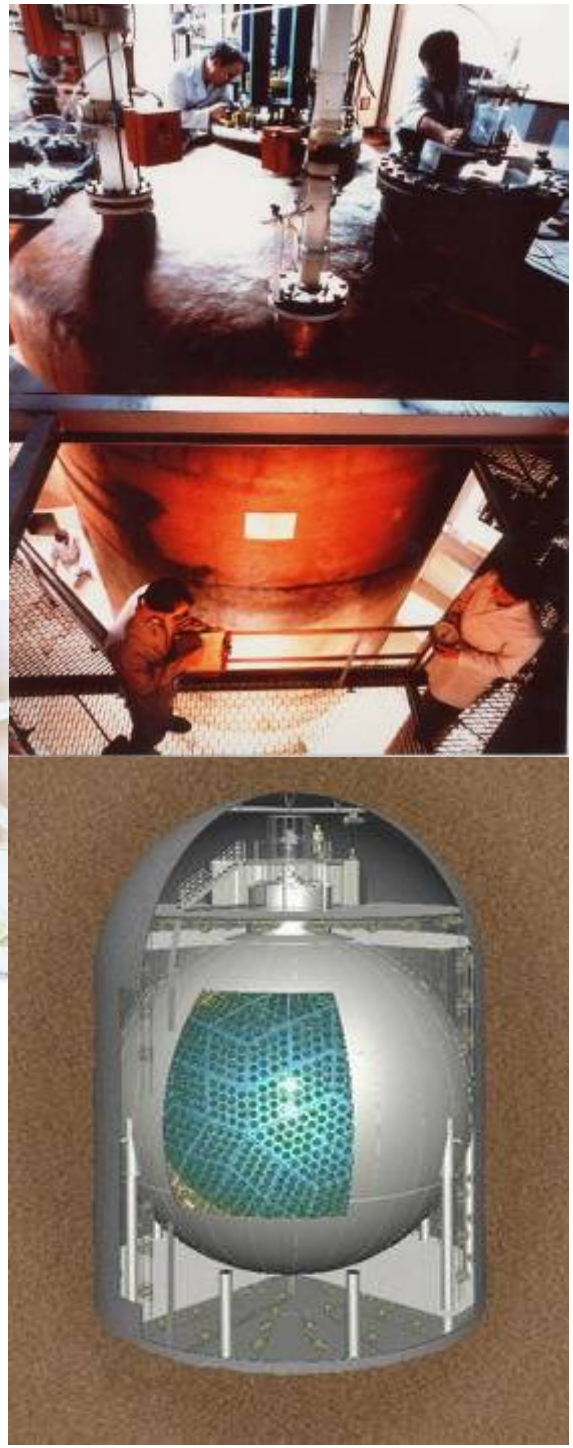

Comparsa/Appearance

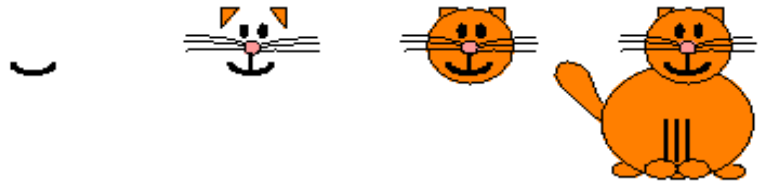

"Appearance Experiments"
see the new neutrino type
in the detector

A *"Disappearance Experiment"* observes
fewer

than expected

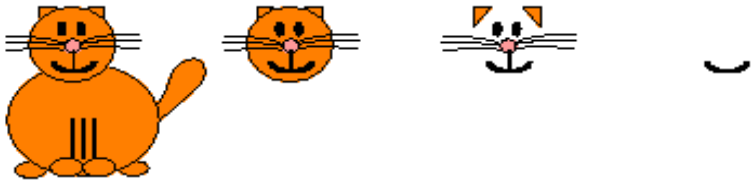

Scomparsa/Desappearance

Oscillazioni dei Neutrini

- Idea della massa dei neutrini suggerita per la prima volta da Bruno Pontecorvo

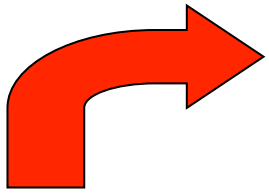

I Neutrini Interagiscono (Produzione o Rivelazione) come Autostati dell'Interazione Debole

$|\nu_e\rangle$, $|\nu_\mu\rangle$, $|\nu_\tau\rangle$ =Autostati dell' Interazione Debole

$|\nu_1\rangle$, $|\nu_2\rangle$, $|\nu_3\rangle$ =Autostati di Massa (H → Evoluzione t)

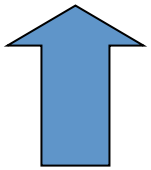

- I Neutrini si propagano (evolvono) come sovrapposizione di autostati di **massa: MESCOLAMENTO**

Mescolamento tra neutrini: p.es. due famiglie

$$|\nu_e\rangle = \cos\theta\,|\nu_1\rangle + \sin\theta\,|\nu_2\rangle$$

$$|\nu_\mu\rangle = -\sin\theta\,|\nu_1\rangle + \cos\theta\,|\nu_2\rangle$$

θ = mixing angle
Angolo di mescolamento

$$P_{\nu_\mu\nu_\mu} = 1 - \sin^2 2\theta \cdot \sin^2\left[1.27\frac{\Delta m^2 \cdot L}{E_\nu}\right]$$

- Distanza percorsa **L=ct (Km)**
- Differenza di massa quadra **$\Delta m^2 = m_2^2 - m_1^2$ (eV^2)**
- Energia del neutrino **Eν (GeV)**

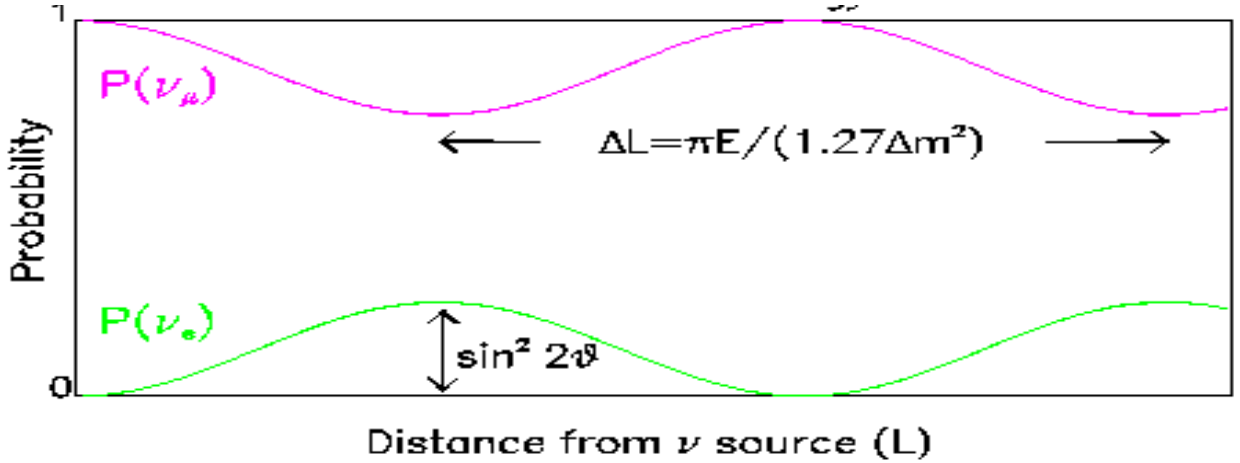

Vacuum flavor oscillations: mass and weak eigenstates

flavor states

$$|\nu_e> \quad \leftrightarrow \quad |\nu_L> \quad m_L$$
$$|\nu_\mu> \qquad\quad |\nu_H> \quad m_H$$

mass states

Noncoincident bases ⇒ oscillations down stream:

$$|v_e> = \cos\theta|\nu_L> + \sin\theta|\nu_H>$$
$$|v_\mu> = -\sin\theta|\nu_L> + \cos\theta|\nu_H>$$

vacuum mixing angle

$$|\nu_e^k> = |\nu^k(x=0,t=0)> \qquad E^2 = k^2 + m_i^2$$
$$|\nu^k(x\sim ct,t)> = e^{ikx}\left[e^{-iE_Lt}\cos\theta|\nu_L> + e^{-iE_Ht}\sin\theta|\nu_H>\right]$$
$$|<\nu_\mu|\nu^k(t)>|^2 = \sin^2 2\theta \sin^2\left(\frac{\delta m^2}{4E}t\right), \qquad \delta m^2 = m_H^2 - m_L^2$$

ν_μ appearance downstream ⇔ vacuum oscillations

Can slightly generalize this

$$|\nu(0)\rangle \;\rightarrow\; a_e(0)|\nu_e\rangle + a_\mu(0)|\nu_\mu\rangle$$

with the subsequent evolution downstream governed by

$$i\frac{d}{dx}\begin{pmatrix} a_e(x) \\ a_\mu(x) \end{pmatrix} = \frac{1}{4E}\begin{pmatrix} -\delta m^2\cos 2\theta & \delta m^2 \sin 2\theta \\ \delta m^2 \sin 2\theta & \delta m^2 \cos 2\theta \end{pmatrix}\begin{pmatrix} a_e(x) \\ a_\mu(x) \end{pmatrix}$$

vacuum m_ν^2 matrix

This problem familiar from hadronic physics: the Cabibbo angle and CKM matrix.

solar matter generates a flavor asymmetry

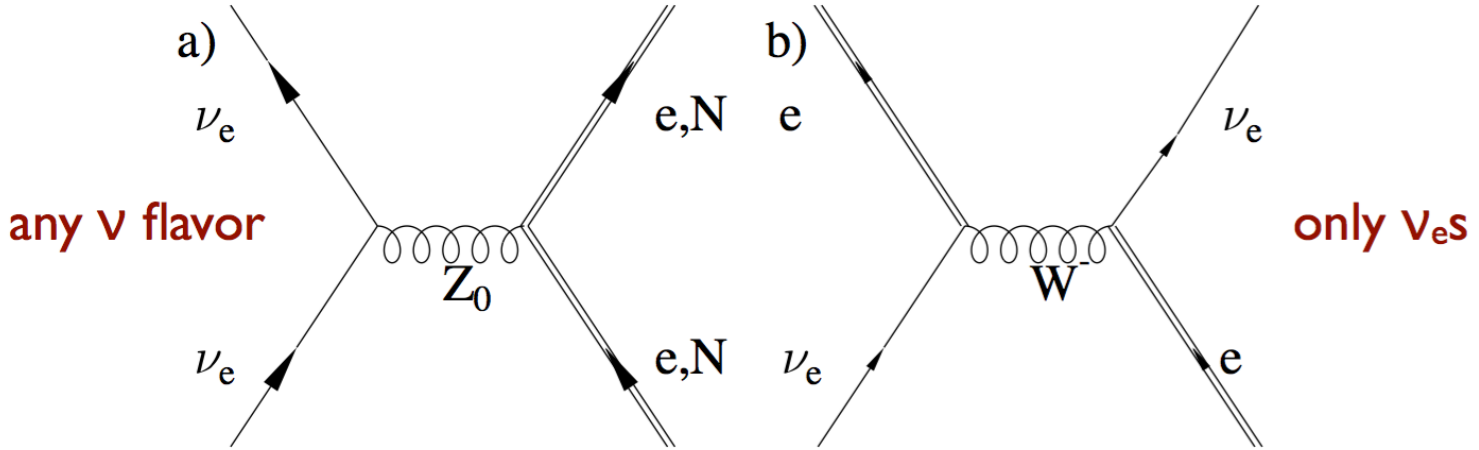

- modifies forward scattering amplitude: flavor-dependent index of refraction
- the affect is proportional to the (changing) solar electron density
- makes the electron neutrino heavier at high density

$$m^2_{\nu_e} = 4E\sqrt{2}G_F\ \rho_e(x)$$

from Art McDonald

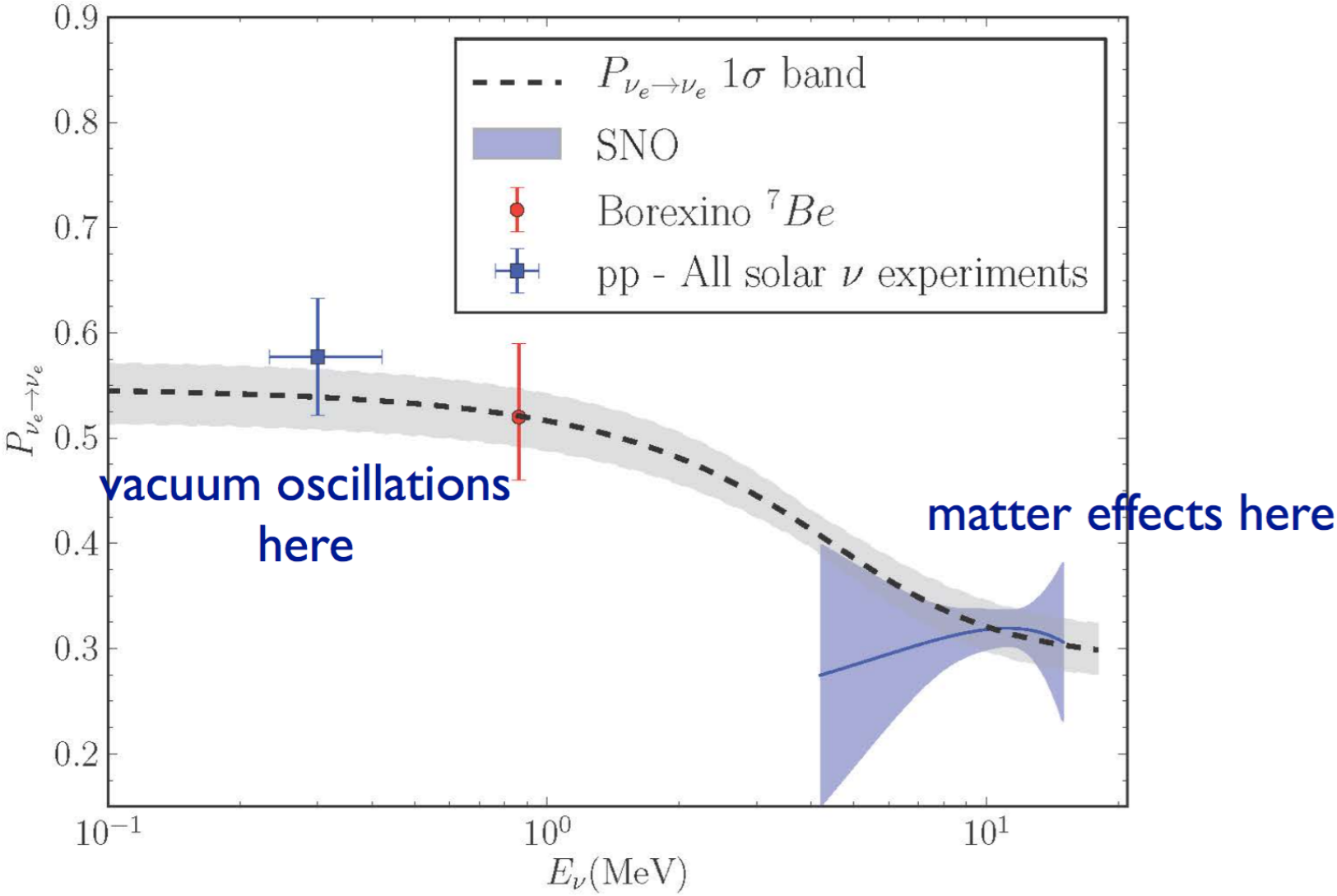

Matter effects produce a characteristic energy-dependence in the ν_e survival probability, in accord with experiments

Neutrino oscillations and the Sun

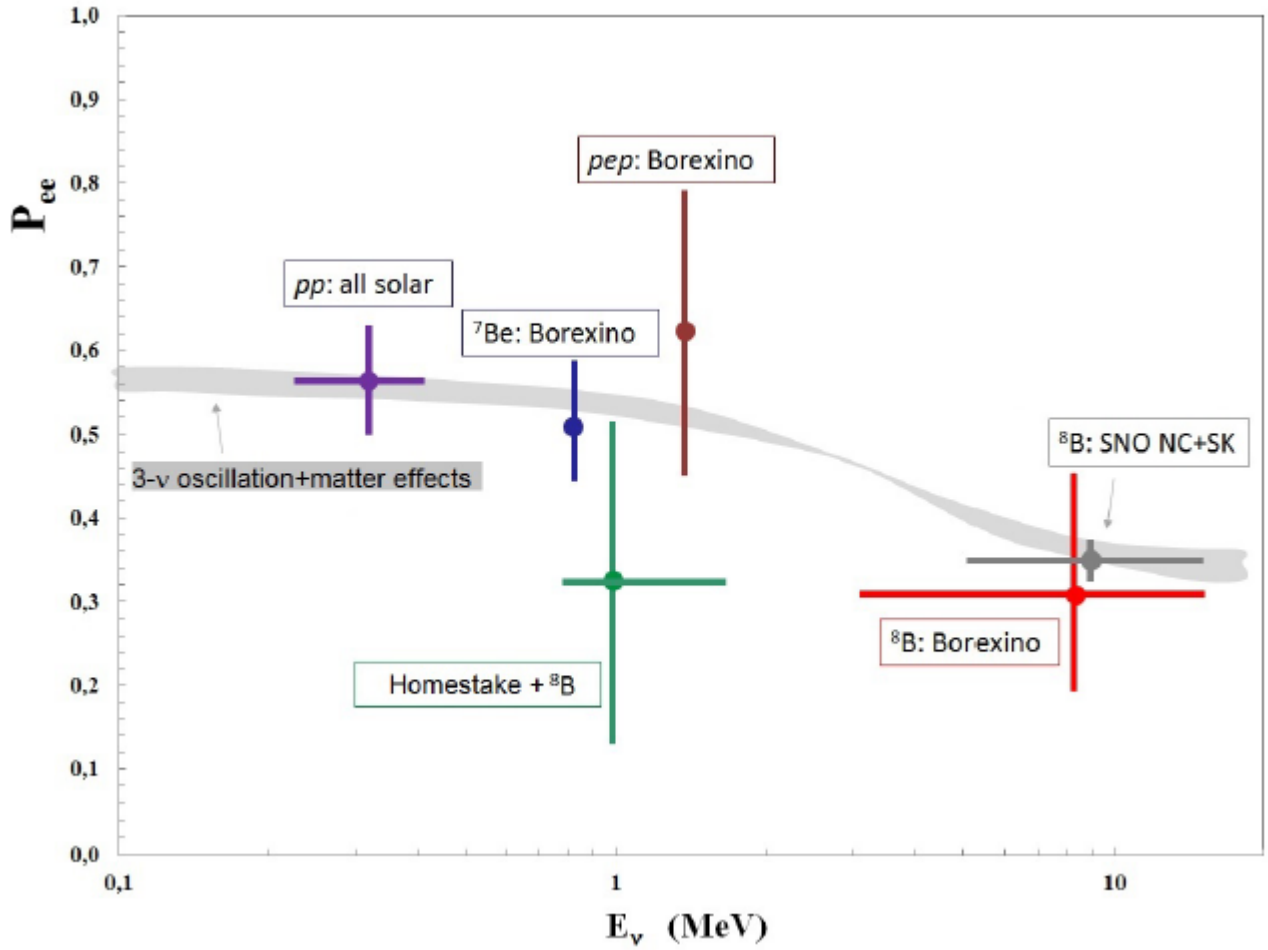

Neutrino parameters

Parameter	best-fit value ($\pm 1\sigma$)
$\Delta m^2_{\odot}$	$(7.58^{+0.22}_{-0.26}) \times 10^{-5}$ eV^2
Δm^2_{atm}	$(2.35^{+0.12}_{-0.09}) \times 10^{-3}$ eV^2
$\sin^2\theta_{12}$	$0.306^{+0.018}_{-0.015}$
$\sin^2\theta_{23}$	$0.42^{+0.08}_{-0.03}$
$\sin^2\theta_{13}$	0.0251 ± 0.0034

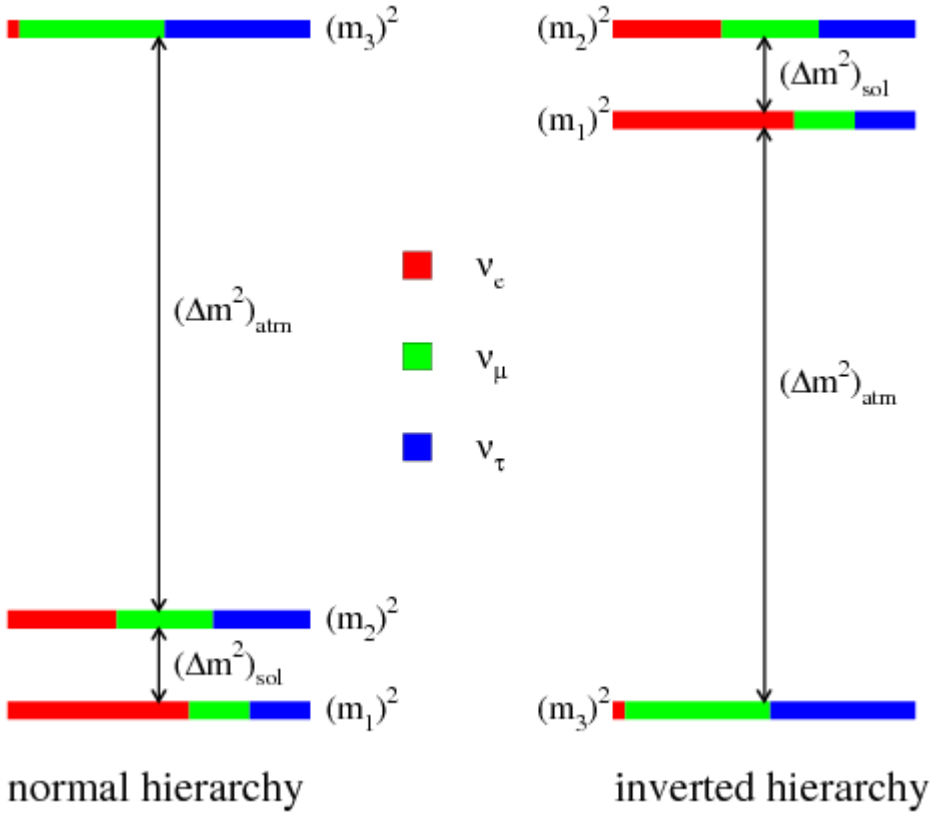

Astrofisica Nucleare e Subnucleare

The Sun in Gamma-rays

Solar Flares in Gamma-rays

Solar γ-Ray Physics Comes of Age

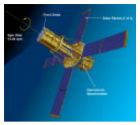

The High Energy Solar Spectroscopic Imager

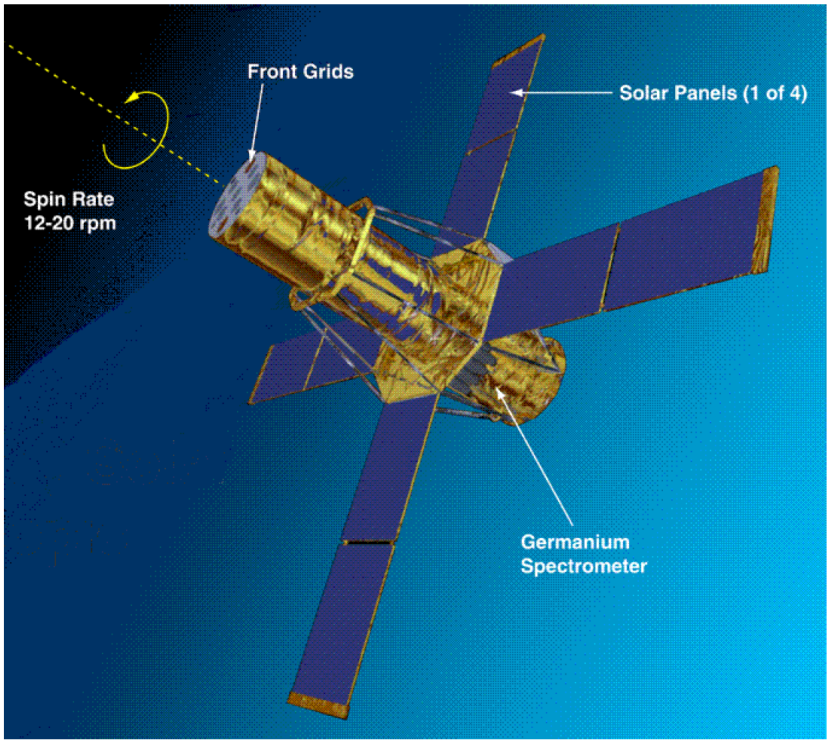

Share 2001

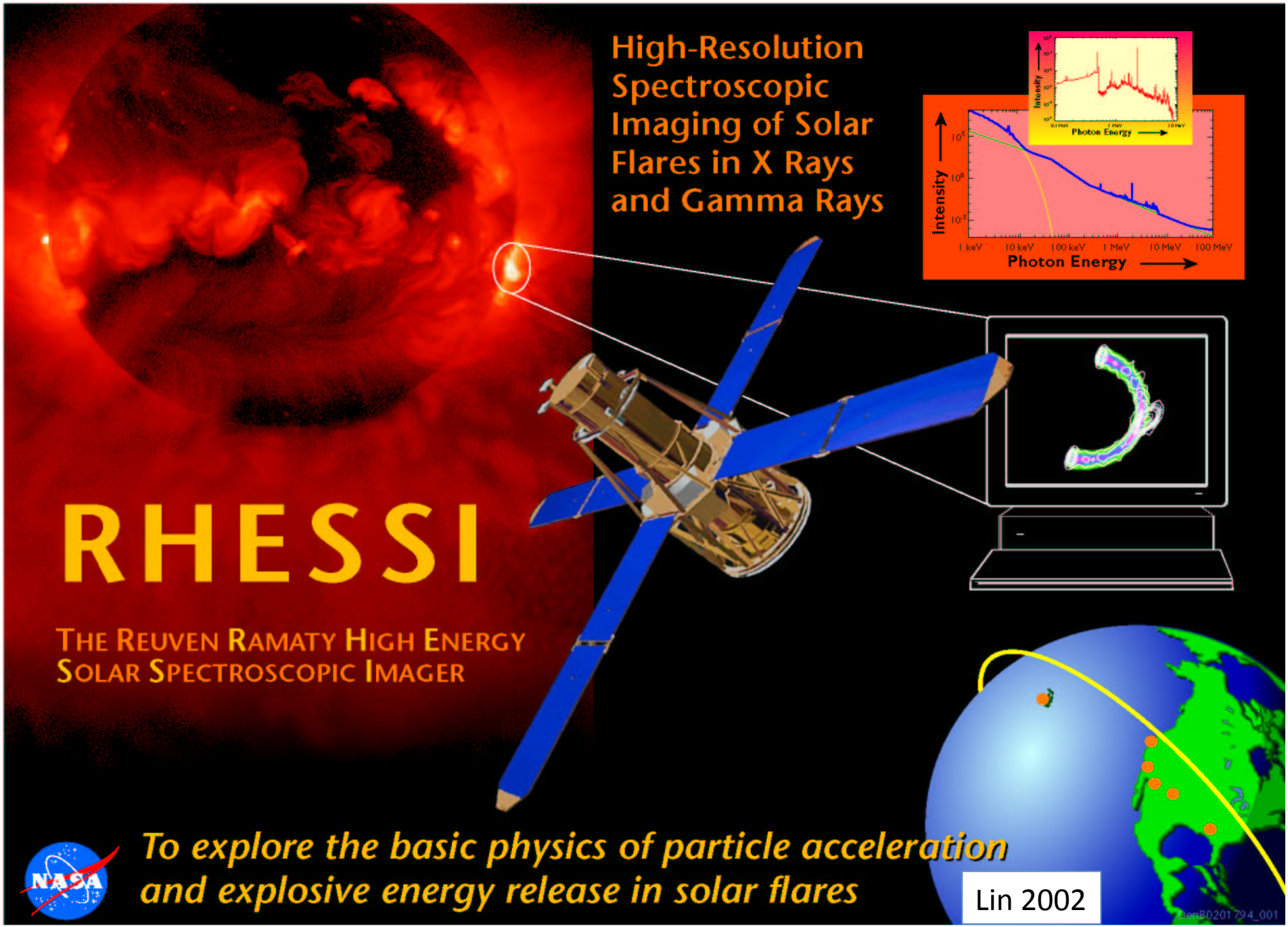
High-Resolution
Spectroscopic
Imaging of Solar
Flares in X Rays
and Gamma Rays
Intensity
Photon Energy
1 keV
10 keV
100 keV
1 MeV
10 MeV
100 MeV
RHESSI
THE REUVEN RAMATY HIGH ENERGY
SOLAR SPECTROSCOPIC IMAGER
To explore the basic physics of particle acceleration
and explosive energy release in solar flares
NASA
Lin 2002

HESSI Science Objective

To explore the basic physics of particle acceleration and explosive energy release in solar flares

- Impulsive Energy Release in the Corona
- Acceleration of Electrons, Protons, and Ions
- Plasma Heating to Tens of Millions of degrees
- Energy and Particle Transport and Dissipation

Lin 2002

A1309.03

HESSI Primary Observations

- Hard X-ray Images
  - Angular resolution as fine as 2 arcseconds
  - Temporal resolution as fine as 10 ms
  - Energy resolution of <1 keV to ~3 keV (FWHM)
- High Resolution X-ray and Gamma-ray Spectra
  - ~keV energy resolution
  - To energies as high as 15 MeV

Lin 2002

A1309.05

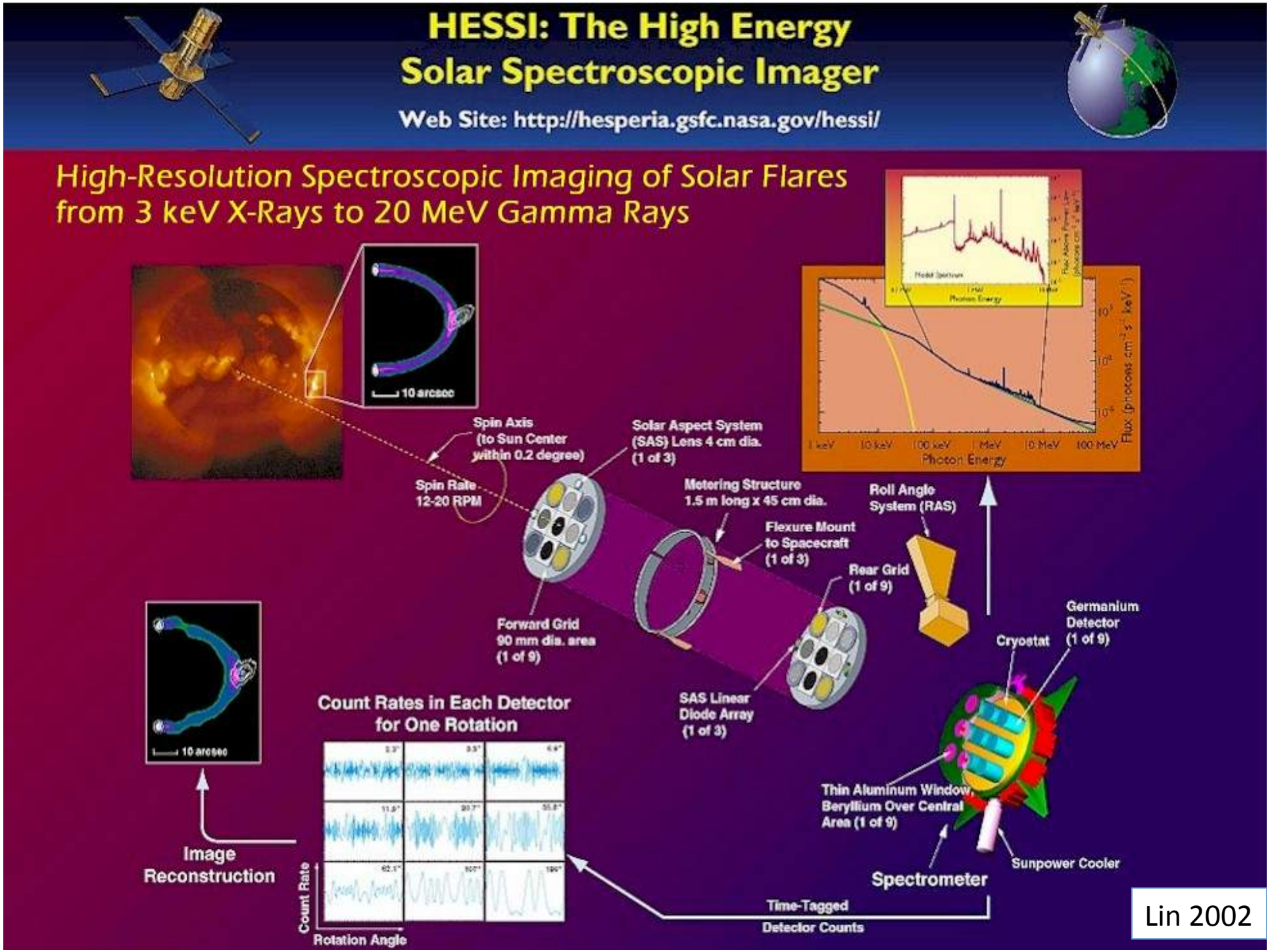
HESSI: The High Energy
Solar Spectroscopic Imager
Web Site: http://hesperia.gsfc.nasa.gov/hessi/
High-Resolution Spectroscopic Imaging of Solar Flares
from 3 keV X-Rays to 20 MeV Gamma Rays
10 arcsec
Spin Axis
(to Sun Center
within 0.2 degree)
Solar Aspect System
(SAS) Lens 4 cm dia.
(1 of 3)
Spin Rate
12-20 RPM
Metering Structure
1.5 m long x 45 cm dia.
Flexure Mount
to Spacecraft
(1 of 3)
Roll Angle
System (RAS)
Rear Grid
(1 of 9)
Forward Grid
90 mm dia. area
(1 of 9)
SAS Linear
Diode Array
(1 of 3)
Germanium
Detector
(1 of 9)
Cryostat
Thin Aluminum Window
Beryllium Over Central
Area (1 of 9)
Sunpower Cooler
Spectrometer
Photon Energy
Flux (photons cm⁻² s⁻¹ keV⁻¹)
1 keV
10 keV
100 keV
1 MeV
10 MeV
100 MeV
Count Rates in Each Detector
for One Rotation
Count Rate
Rotation Angle
Image
Reconstruction
Time-Tagged
Detector Counts

Lin 2002

Solar Flares in Gamma-rays

Solar γ-Ray Physics Comes of Age

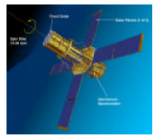

HESSI IMAGING SYSTEM

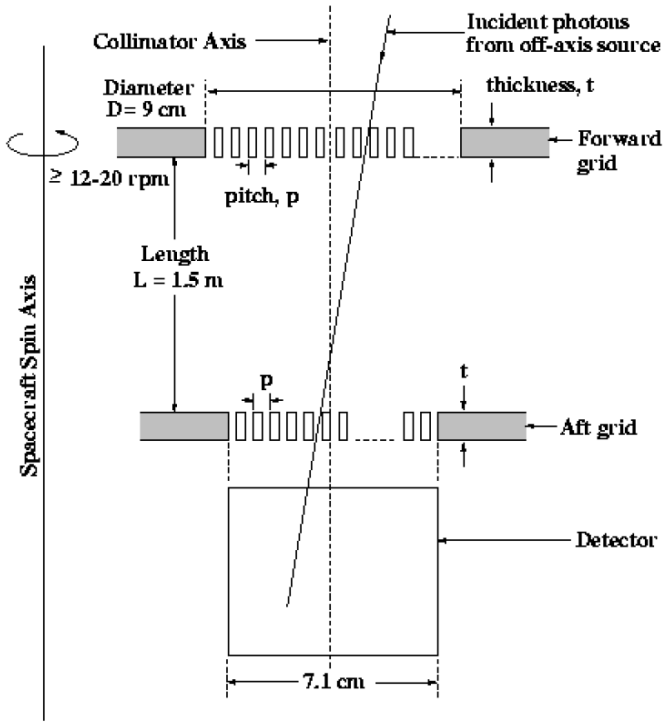

Share 2001

RHESSI

THE RHESSI SPECTROMETER

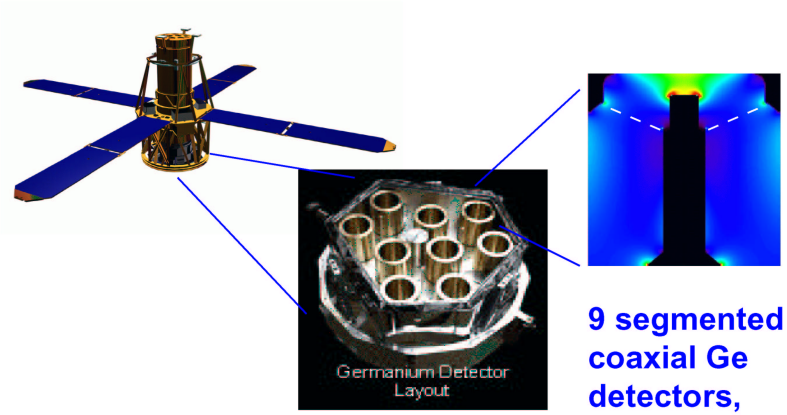

9 segmented coaxial Ge detectors, 7cm x 8.5cm

Energy range:	**Front segments: 3 keV - 2.8 MeV** **Rear segments: 20 keV - 17 MeV**
Resolution:	**Front segments: 1 keV @ 100 keV** **Rear segments: 2.9 keV @ 1 MeV**
Throughput:	**25,000+ counts/segment/second**
Shielding:	**NONE (4mm Al sides, 2cm Al rear)**

Other important subsystems:

Sunpower Stirling-cycle cryocooler, keeps detectors at 75K with 52W of power:

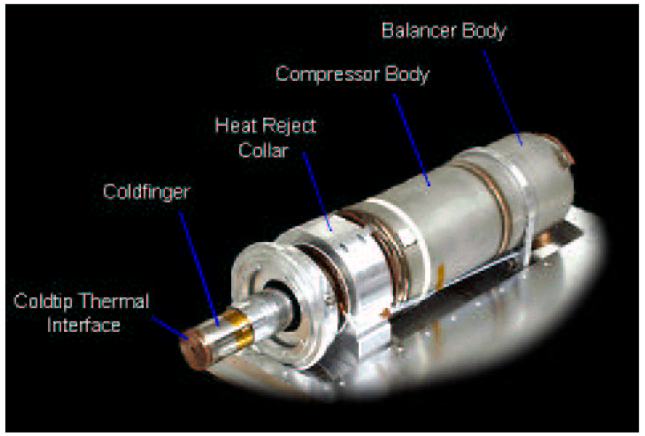

Attenuators: two sets of aluminum disks (thick and thin) that can be manually or automatically moved in front of the detectors to reduce the count rates from large flares.

Lin 2002

Solar Flares in Gamma-rays

Solar γ-Ray Physics Comes of Age

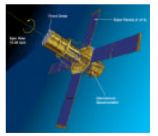

HESSI Germanium Detector Array

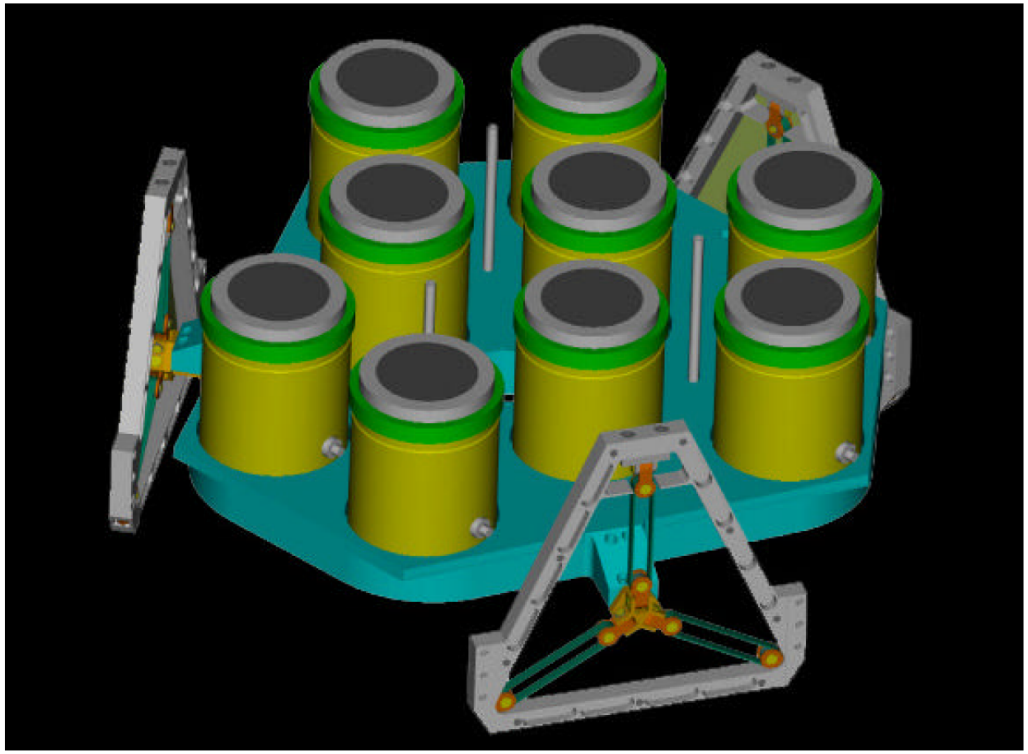

Share 2001

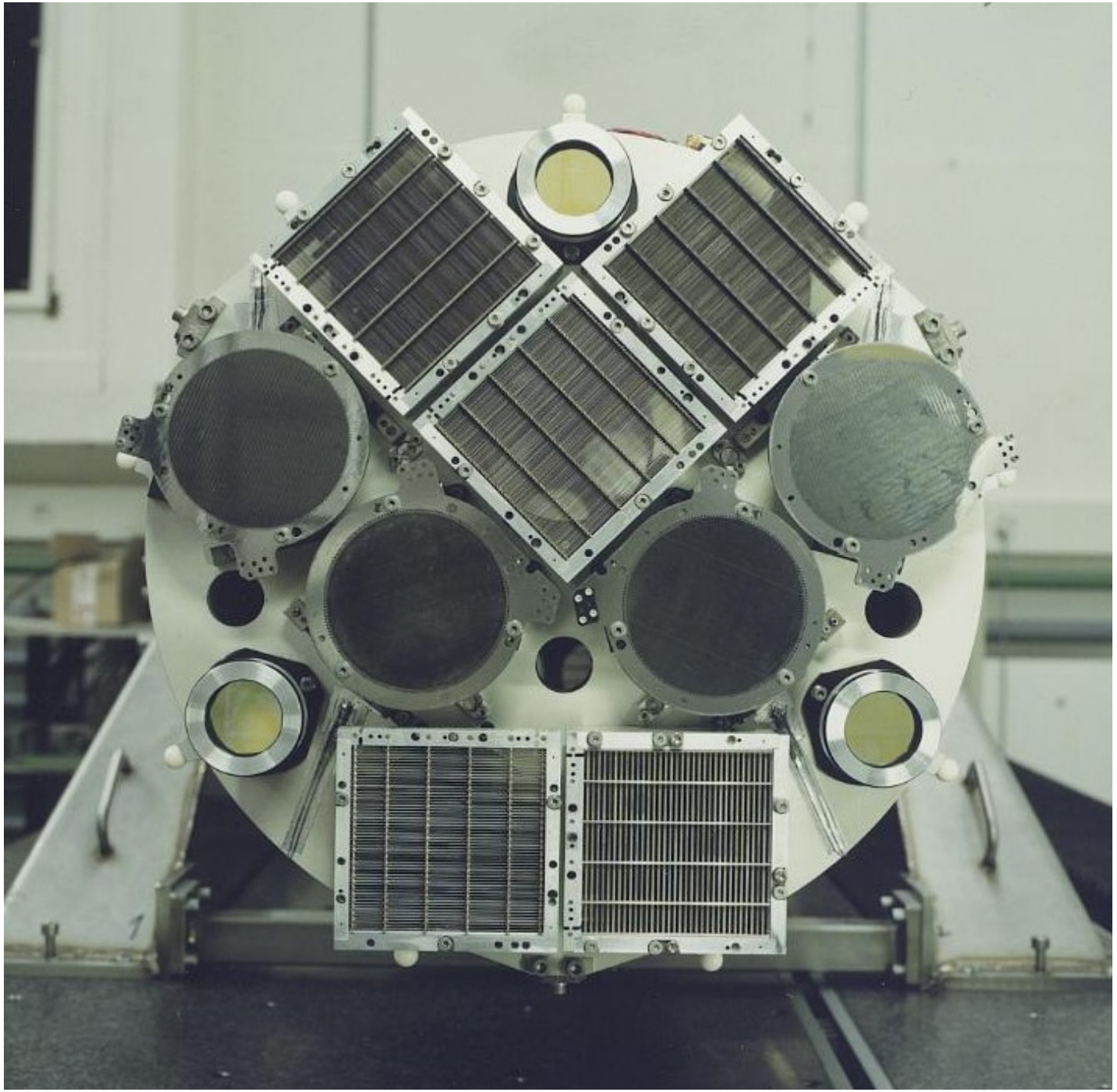

Lin 2002

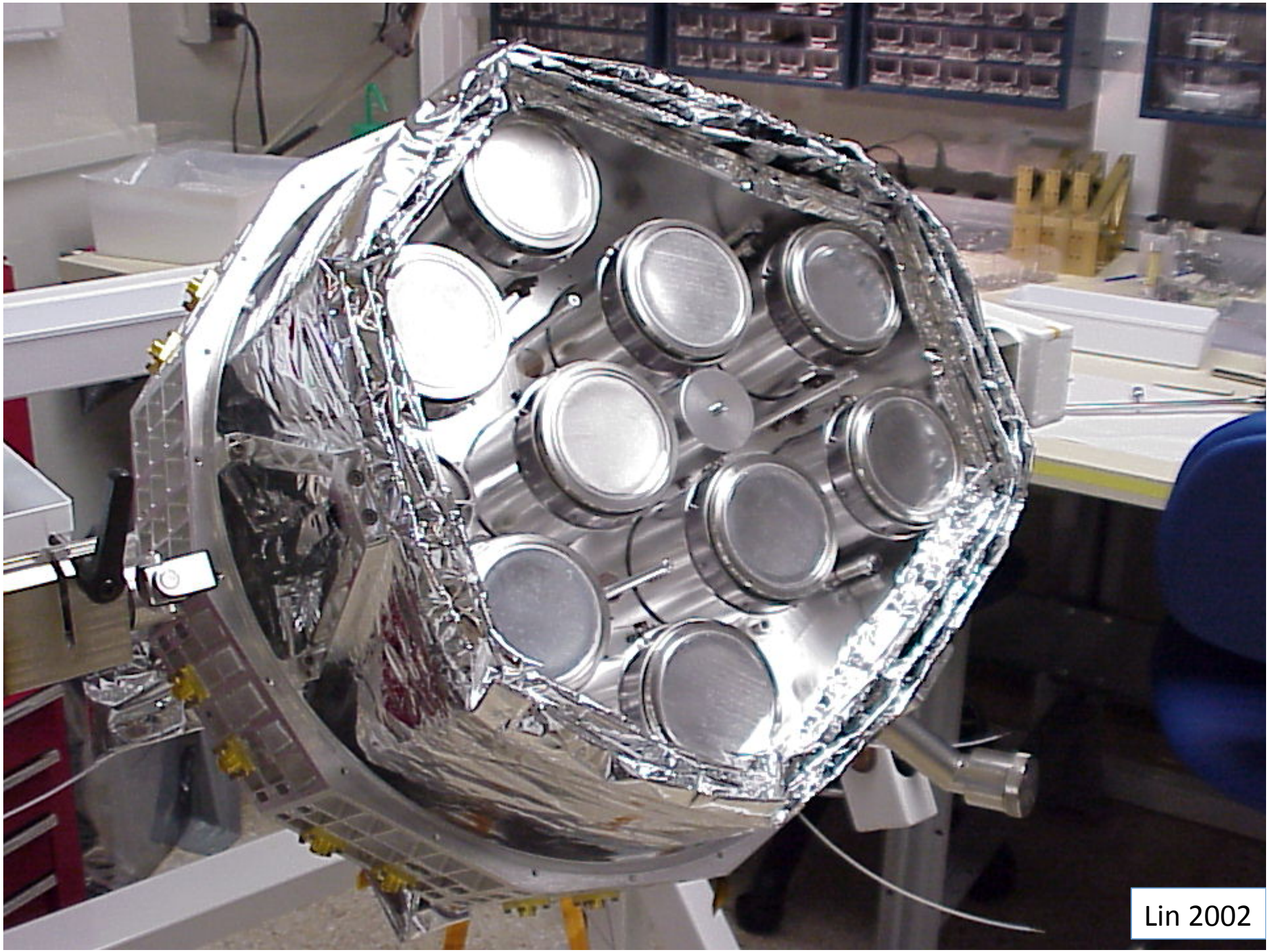
Lin 2002

HESSI Observational Characteristics

• Energy Range	3 keV to 15 MeV
• Energy Resolution (FWHM)	<1 keV FWHM at 3 keV increasing to 5 keV at 15 MeV
• Angular Resolution	2 arcseconds to 100 keV 7 arcseconds to 400 keV 36 arcseconds to 15 MeV
• Temporal Resolution	Tens of ms for basic image 2 s for detailed image
• Field of View	Full Sun
• Effective Area - cm^2 (with attenuators out)	10^{-3} at 3 keV, 50 at 10 keV 60 at 100 keV, 20 at 10 MeV
• Numbers of flares	~1000 imaged to >100 keV. ~100 with spectroscopy to ~10 MeV

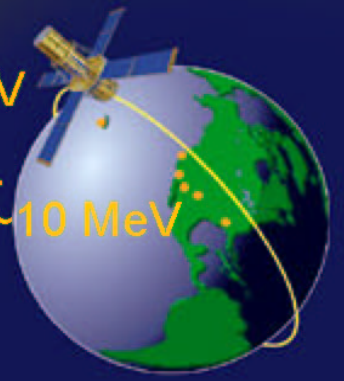

Lin 2002

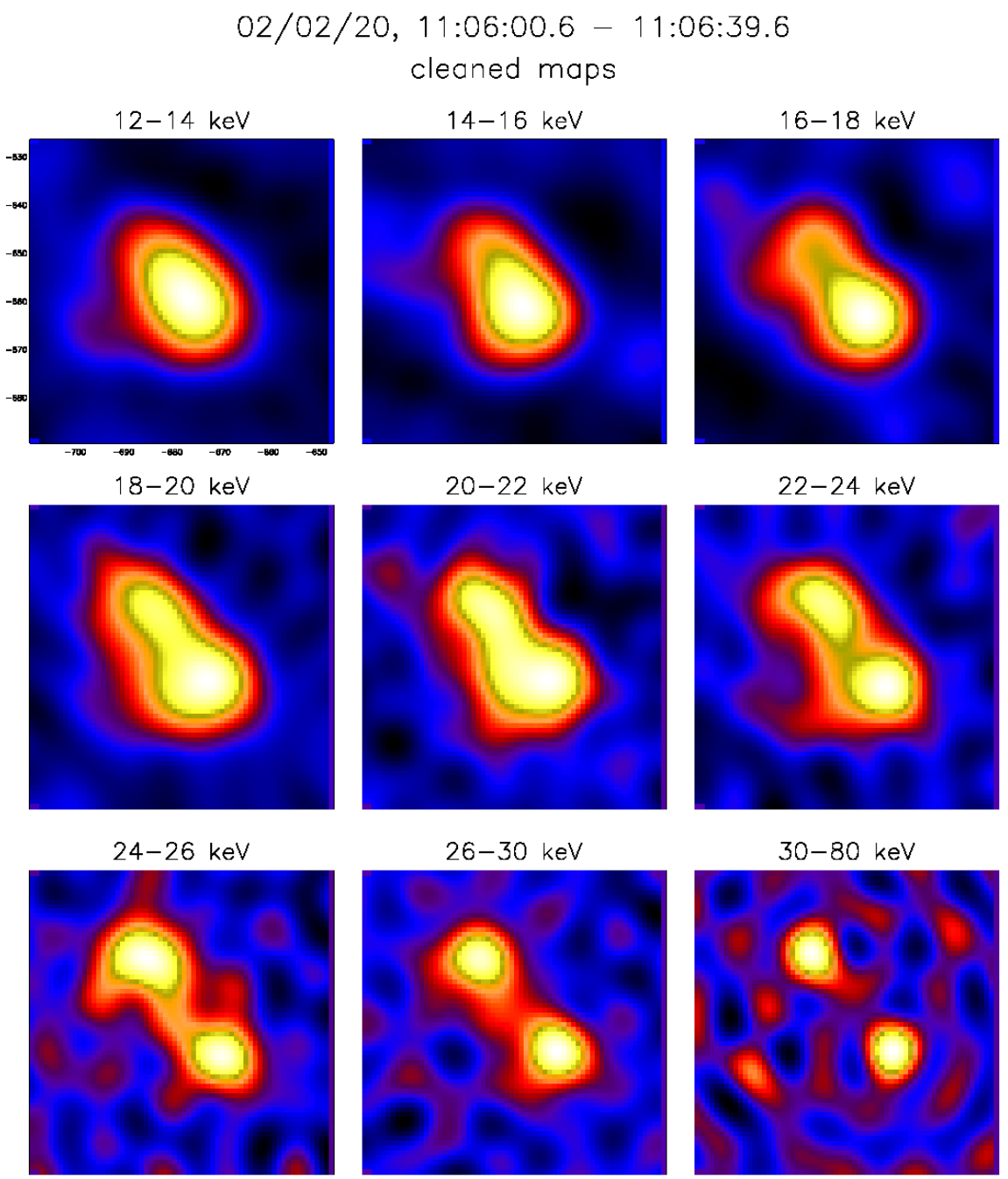
02/02/20, 11:06:00.6 – 11:06:39.6
cleaned maps
12–14 keV
14–16 keV
16–18 keV
18–20 keV
20–22 keV
22–24 keV
24–26 keV
26–30 keV
30–80 keV

Lin 2002

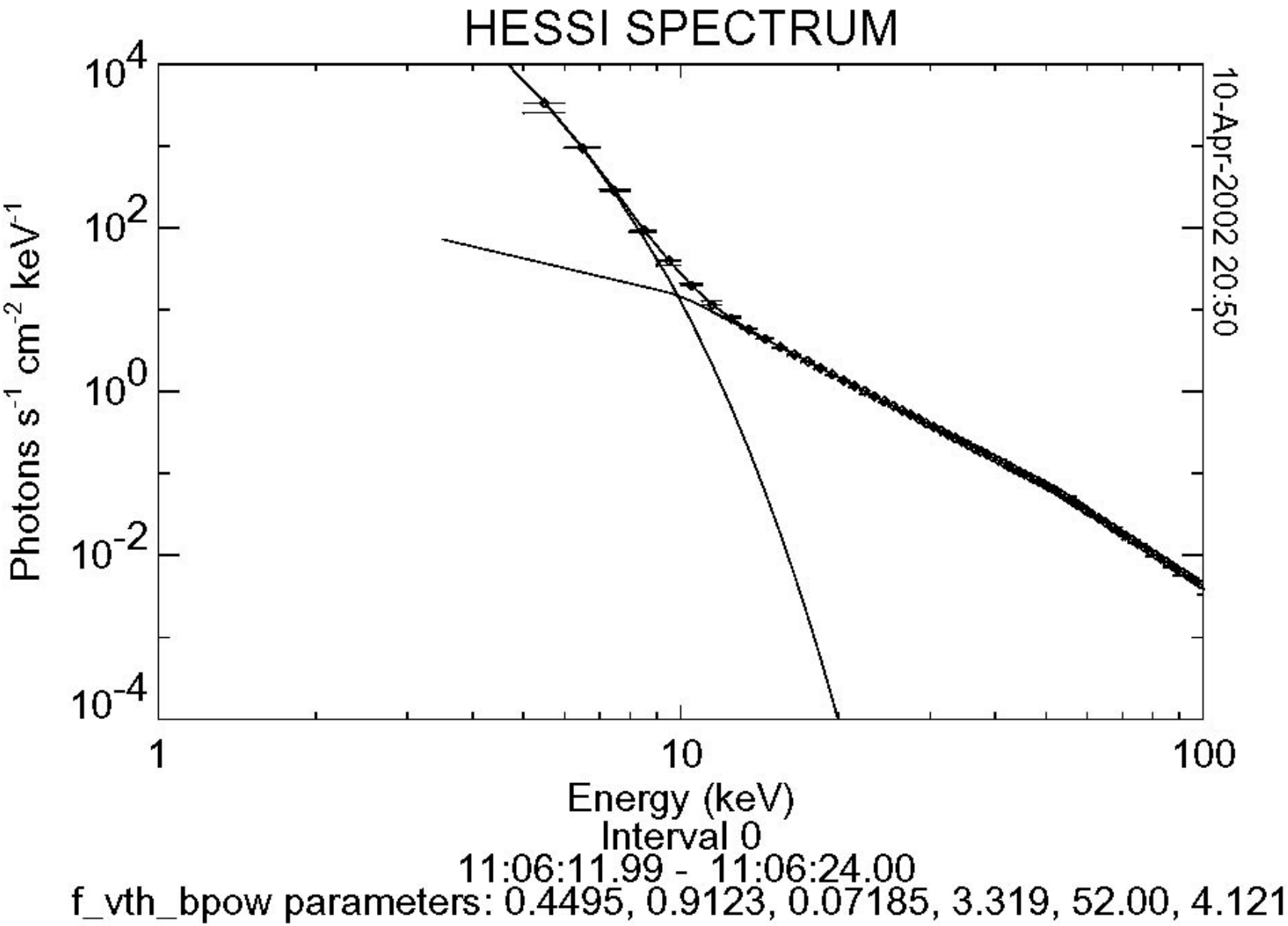
HESSI SPECTRUM
10-Apr-2002 20:50
Photons s-1 cm-2 keV-1
10^4
10^2
10^0
10^-2
10^-4
1
10
100
Energy (keV)
Interval 0
11:06:11.99 - 11:06:24.00
f_vth_bpow parameters: 0.4495, 0.9123, 0.07185, 3.319, 52.00, 4.121

Lin 2002

RHESSI DATA ANALYSIS

Documentation and details at

RHESSI SOFTWARE AND DATA ANALYSIS CENTER

http://hesperia.gsfc.nasa.gov/rhessidatacenter/

Lin 2002

Status of the RHESSI Mission Archive

Target 2020

7-July-2020

R. A. Schwartz A. K. Tolbert

Contributing: B Dennis, A Shih, A Inglis, M Fivian, D Smith, M. Abdallaoui

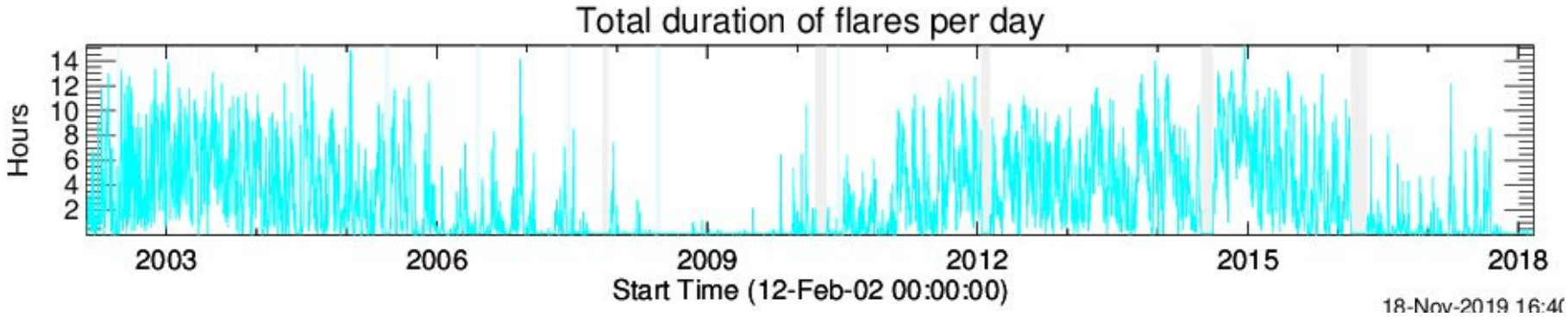

Schartz 2020

Overview of the Archive

- Mission Archive Web Page:
  https://hesperia.gsfc.nasa.gov/rhessi3/mission-archive/index.html
- Image Archive – so much information
- Visibility Archive – coarse and fine
- Energy Spectra – ready for stand-alone spectroscopy
- Detector Health – you have wanted this
- Calibrated SAS data – a select few
- GRB & TGF – in progress
- Calibration and Roll Aspect Databases – in progress
- Ancillary missions – MESSENGER, FERMI, GOES, SMM, AIA

Schartz 2020

Flare Image Archive

RHESSI Image Archive Strategy Guide to RHESSI Image Archive

2002 ▾ February ▾ Load

RHESSI Flare Images February 2002

12-Feb-2002 21:30:00 - 21:41:00	6tx2e	Browser	Aspect Plot	Profile Plot	Panels	Image Movies:	-	6-12	12-25	-	-	-
12-Feb-2002 21:44:00 - 21:48:00	-	Browser	Aspect Plot	-	-	-	-	-	-	-	-	-
13-Feb-2002 00:53:00 - 00:57:00	-	Browser	Aspect Plot	-	-	-	-	-	-	-	-	-
13-Feb-2002 04:22:00 - 04:26:00	1tx1e	Browser	Aspect Plot	Profile Plot	Panels	Image Movies:	-	6-12	-	-	-	-
13-Feb-2002 07:03:00 - 07:30:00	18tx2e	Browser	Aspect Plot	Profile Plot	Panels	Image Movies:	-	6-12	12-25	-	-	-

Flare 20820140, 20-Aug-2002 08:21:52 - 08:36:08 Peak: 08:26:22 Duration: 856 s Peak: 1424 c/s Total Counts: 2876159
Highest Energy: 100-300 keV Flare Position: 569,-264 asec AR: 69

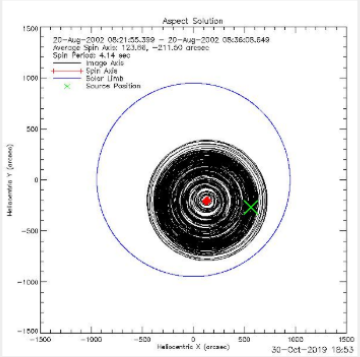

Movie of Aspect Solution in Image Time Bins

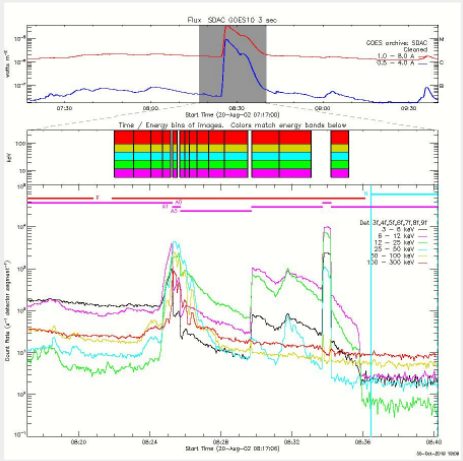

BACK_PROJECTION Images
CLEAN Images
CLEAN_59 Images
MEM_GE Images
VIS_CS Images
VIS_FWDFIT Images

RHESSI Browser
~~AIA movies~~
Direct Link to Plot Folder

Download files:

BACK_PROJECTION Image Cube FITS
CLEAN Image Cube FITS
CLEAN_59 Image Cube FITS
MEM_GE Image Cube FITS
VIS_CS Image Cube FITS
VIS_FWDFIT Image Cube FITS

Visibility FITS
Eventlist FITS

Image Creation Scripts:

BACK_PROJECTION non-default params all params
CLEAN non-default params all params
CLEAN_59 non-default params all params
MEM_GE non-default params all params
VIS_CS non-default params all params
VIS_FWDFIT non-default params all params

Schartz 2020

Solar Flares in Gamma-rays

Solar γ-Ray Physics Comes of Age

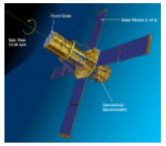

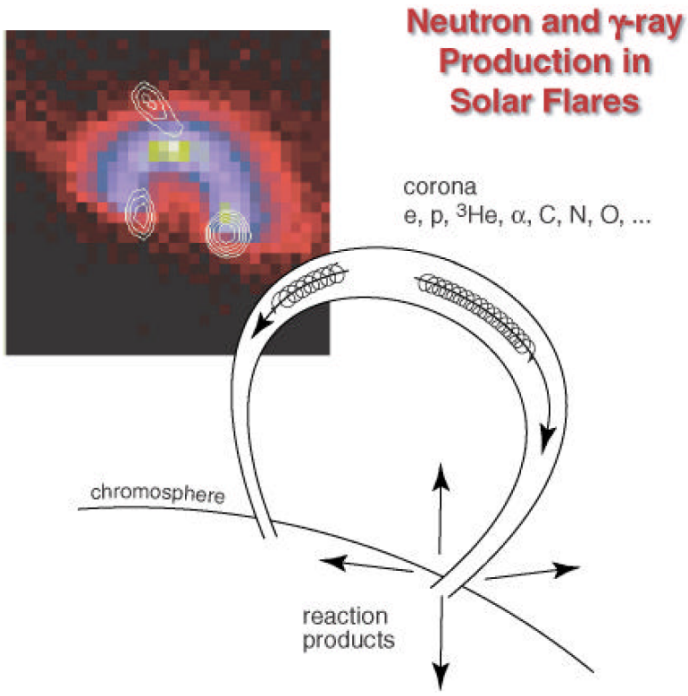

Share 2001

Solar Flares in Gamma-rays

Solar γ-Ray Physics Comes of Age

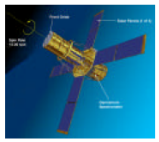

The Physics of Flares Revealed by γ-Ray Spectroscopy

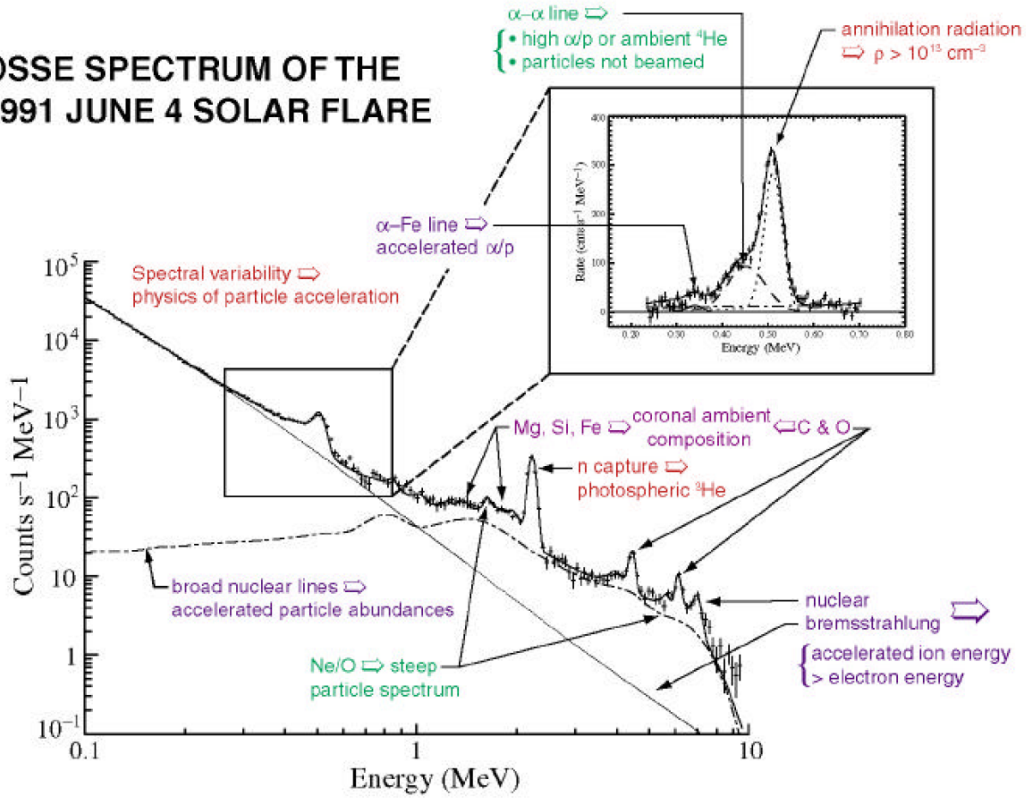

Share 2001

Solar Flares in Gamma-rays

Solar γ-Ray Physics Comes of Age

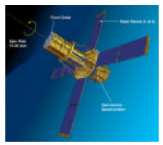

Shape of Bremsstrahlung Continuum >100 keV

Yohkoh

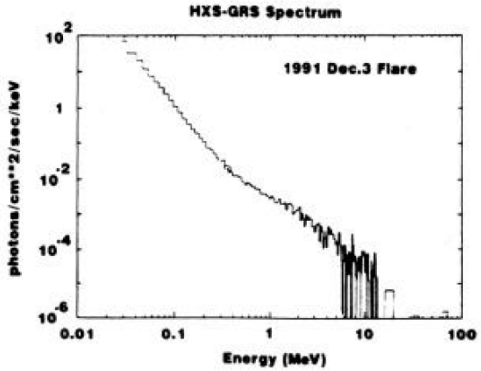

OSSE

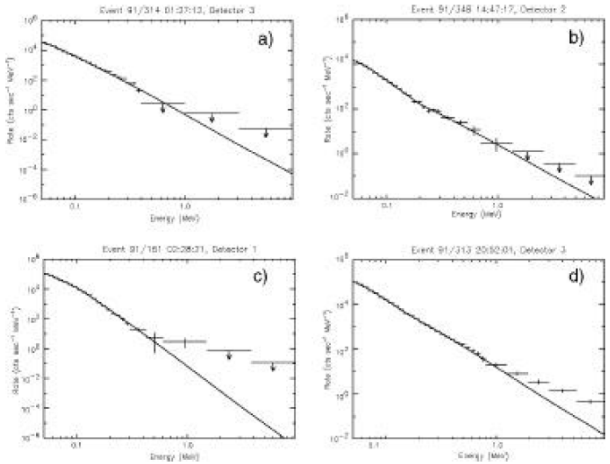

Hardening found in spectra >100 keV by combined analysis of *SMM* GRS/HXRBS spectra.

Similar hardening observed in combined spectrum from *Yohkoh* HRS/GRS.

Important for measurements to be made with the same instrument.

Best instruments BATSE, OSSE, and HESSI.

OSSE continuum spectra exhibit: single power laws, broken power laws with hardening and softening between ~100 and 200 keV, and additional hardening above ~1 MeV.

Share 2001

Solar Flares in Gamma-rays

Solar γ-Ray Physics Comes of Age

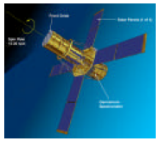

Theoretical Nuclear Line Spectrum

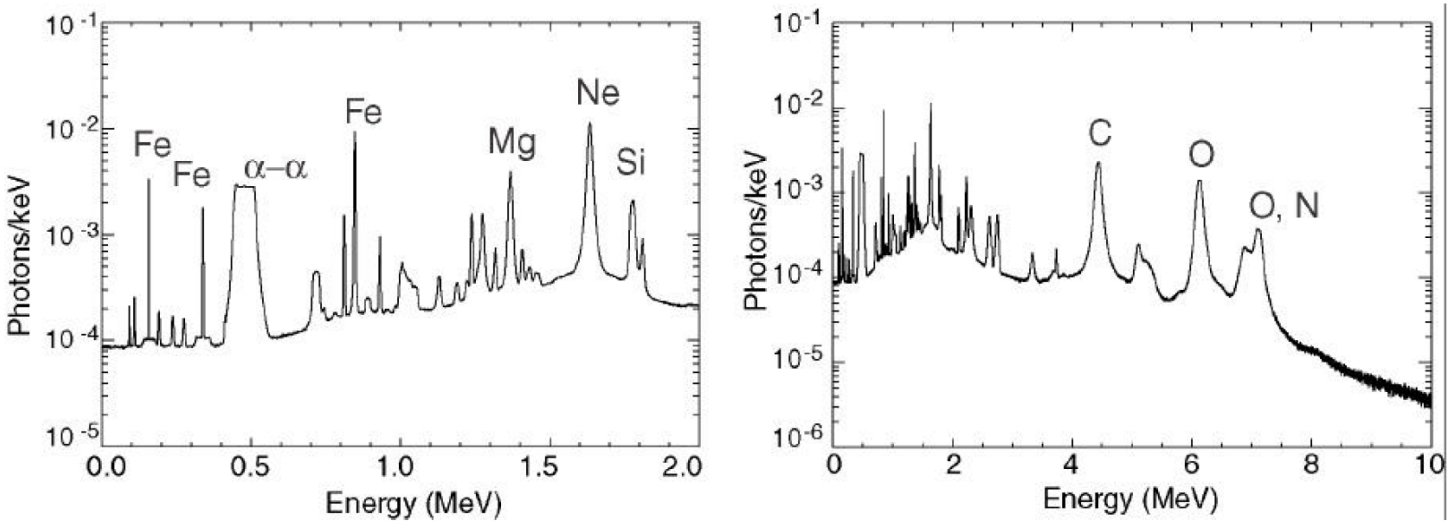

Ramaty, Kozlovsky, Lingenfelter, and Murphy

Share 2001

Solar Flares in Gamma-rays

Solar γ-Ray Physics Comes of Age

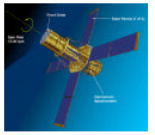

Narrow γ-Ray Lines Observed in Flare Spectra

Produced by p and α interactions with ambient material.

At least 30% of flares with emission >0.3 MeV exhibit γ-ray line features. *HESSI* will make more definitive measurement.

At least 19 de-excitation lines have been identified in fits to flare spectra.

Widths of de-excitation lines measured to be ~2-4% in the summed spectrum. This exceeds theory in some cases suggesting presence of blended lines (e.g. ^{14}N near ^{20}Ne) or different Doppler shifts in the flares (see later discussion).

HESSI can resolve these lines and determine intrinsic widths.

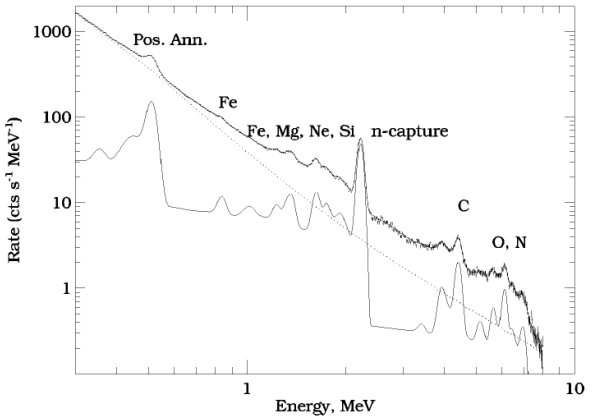

Share 2001

Solar Flares in Gamma-rays

Solar γ-Ray Physics Comes of Age

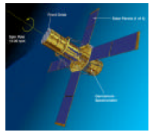

Narrow γ-Ray Lines in Solar-Flare Spectra

Sum of 19 SMM Flares

Energy, MeV	Width (% FWHM)	Identification
0.357 ± 0.002	3.7 ± 3.1	^{59}Ni (0.339 MeV)
0.454	--	^{7}Be, ^{7}Li (0.429, 0.478 MeV)
0.513 ± 0.001	< 2	e^{+}- e^{-} annihilation (0.511 MeV)
0.841 ± 0.003	--	^{56}Fe (0.847 MeV)
0.937	--	^{18}F (0.937 MeV)
~1.020	--	^{18}F, ^{58}Co, ^{58}Ni, ^{59}Ni (1.00/4/5/8)
1.234	3.3 ± 3.9	^{56}Fe (1.238 MeV)
1.317	--	^{55}Fe (1.317 MeV)
1.366 ± 0.003	3.0 ± 1.1	^{24}Mg (1.369 MeV)
1.631 ± 0.002	2.9 ± 0.6	^{20}Ne (1.633 MeV)
1.785	4.3 ± 1.5	^{28}Si (1.779 MeV)
2.226 ± 0.001	< 1.5	n-capture on H (2.223 MeV)
3.332 ± 0.030	--	^{20}Ne (3.334 MeV)
4.429 ± 0.004	3.3 ± 0.3	^{12}C (4.439 MeV)
5.200	--	^{14}N, ^{15}N, ^{15}O
6.132 ± 0.005	2.6 ± 0.3	^{16}O (6.130 MeV)
6.43	--	^{11}C (6.337, 6.476 MeV)
6.983 ± 0.015	4.0 ± 0.5	^{14}N, ^{16}O (7.028, 6919 MeV)

Share 2001

Solar Flares in Gamma-rays

Solar γ-Ray Physics Comes of Age

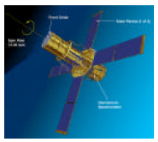

Revealing the Spectrum from Accelerated Heavy Ions

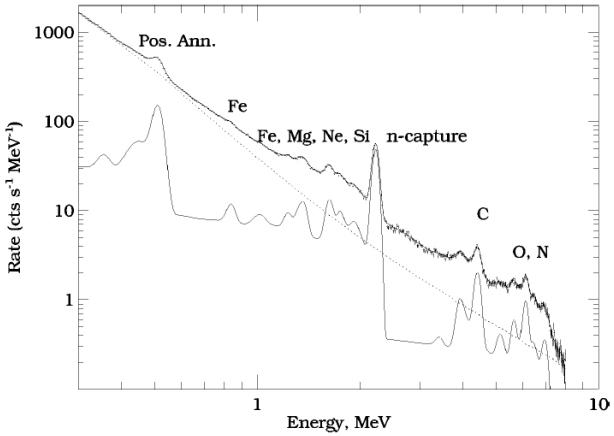

Accelerated heavy ions are excited by interaction with ambient H.

De-excitation lines from these ions are expected to be Doppler broadened by ~25%.

Broad line spectrum is revealed by subtracting best fitting narrow-line and bremsstrahlung components shown for sum of 19 flares observed by the *SMM*/GRS.

Share 2001

Solar Flares in Gamma-rays

Solar γ-Ray Physics Comes of Age

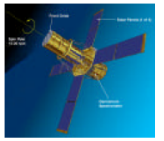

Gamma-Ray Spectrum from Accelerated Heavy Ions

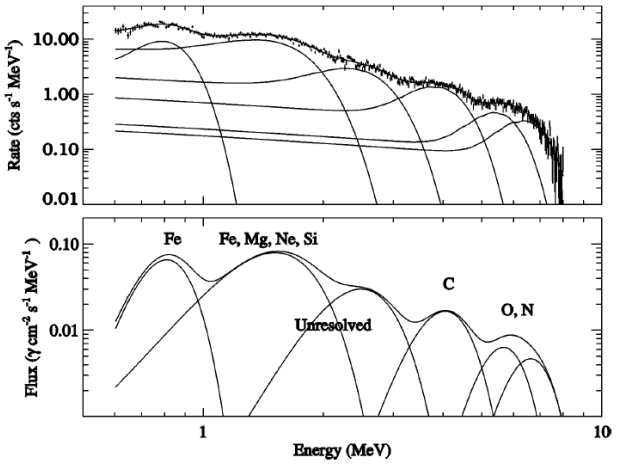

Residual spectrum after subtracting contributions from bremsstrahlung and narrow lines reveals broadened lines from accelerated ions.

Best fit to spectrum contains six Gaussian features that can be identified with different ions.

Fe and C are resolved. The Fe, Mg, Ne, and Si lines between 1 - 2 MeV cannot be resolved.

Major uncertainty is the shape of the 'unresolved line' component that is expected to peak in the 1 - 3 MeV region.

Share 2001

Solar Flares in Gamma-rays

Solar γ-Ray Physics Comes of Age

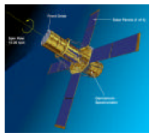

Broadened Lines Identified in γ-Ray Spectra

Energy, MeV	Width, MeV	Identification	Enhancement	
			γ-Rays	SEP's
0.81 ± 0.01	0.25 ± 0.02	^{56}Fe	7.8 ± 1.9	6.7 ± 0.8
1.52 ± 0.02	0.78 ± 0.05	Unresolved, ^{56}Fe, ^{24}Mg, ^{20}Ne, ^{28}Si	2.4 ± 0.4	
		^{24}Mg, ^{20}Ne, ^{28}Si		~2.7
2.49 ± 0.07	1.05 ± 0.17	Unresolved lines		
4.04 ± 0.05	1.26 ± 0.15	^{12}C	1	1
5.67 ± 0.19	1.5	^{16}O	0.9 ±0.2	1.1 ±0.1
6.63 ± 0.16	1.7	^{14}N, ^{16}O	1.3 ± 0.4	

Lines appear to be red-shifted by ~5 - 9 %.

Lines are broadened by ~30%.

Some shift and broadening may be due to summing of 19 spectra.

Enhancement (γ-ray) = $(Fe_{brd}/Fe_{nar})/(C_{brd}/C_{nar)} * Z^2/A$.

O and Fe enhancements in good agreement with SEPs.

Mg, Si, Ne enhancement is upper limit due to unknown contribution from unresolved lines. This suggests higher temperatures than inferred from SEP's.

Share 2001

Solar Flares in Gamma-rays

Solar γ-Ray Physics Comes of Age

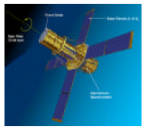

γ Rays and Neutrons Observed from the 1 & 4 June 1991 Flares

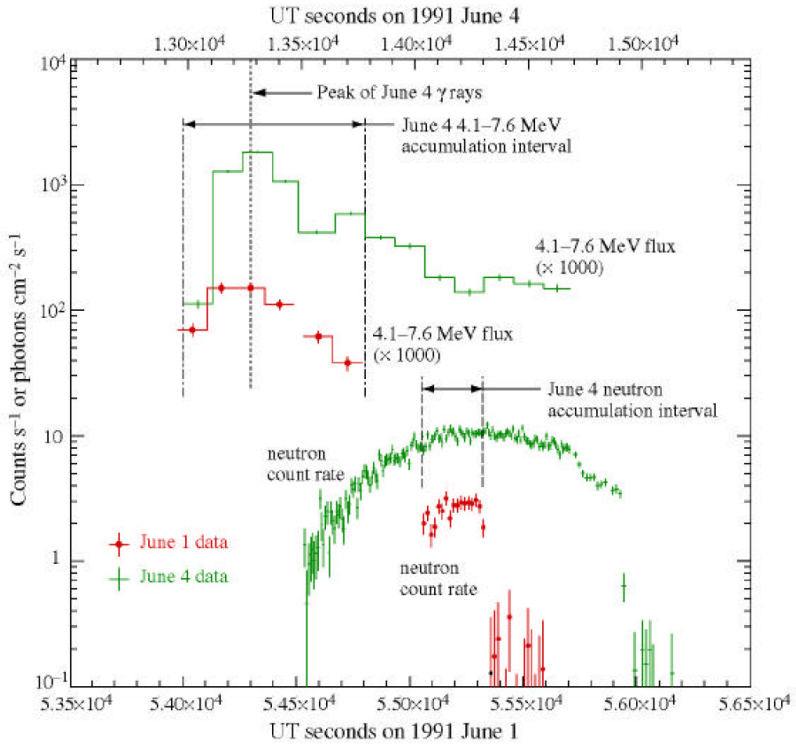

OSSE and GRANAT

Share 2001

Solar Flares in Gamma-rays

Surprises though!
Active regions in January 2005 and December 2006 produced
intense X-Class Flares

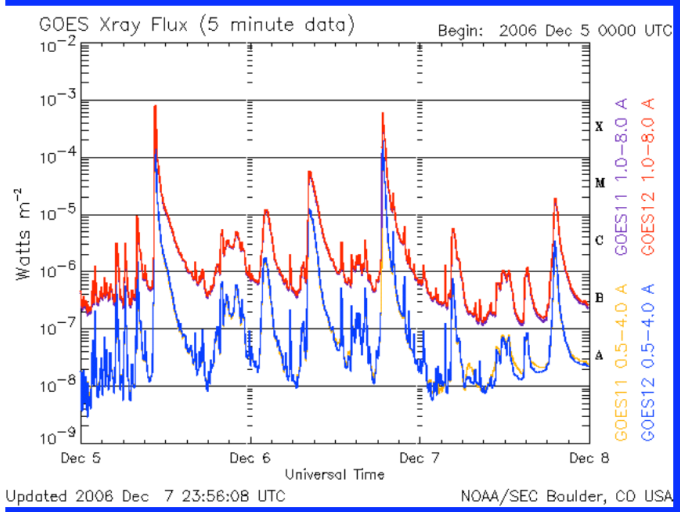

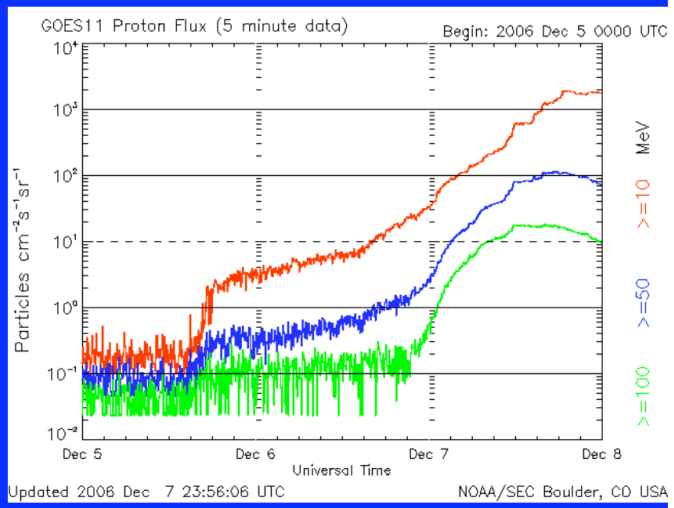

Share 2007

Solar Flares in Gamma-rays

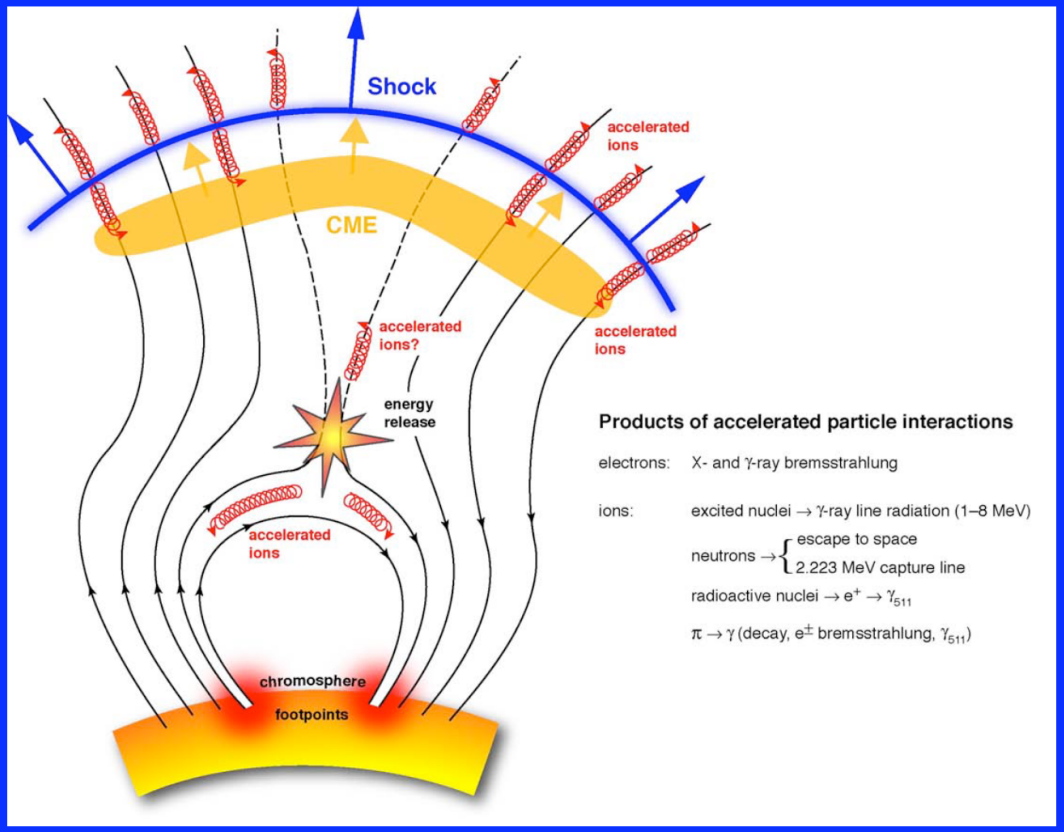

Study how particles are accelerated at the Sun and their relationship to Solar Energetic Particles (SEP) and Ground Level Events (GLE).

Share 2007

Solar Flares in Gamma-rays

Measure the spectrum of flare-accelerated ions and electrons to energies > 1 GeV/nuc

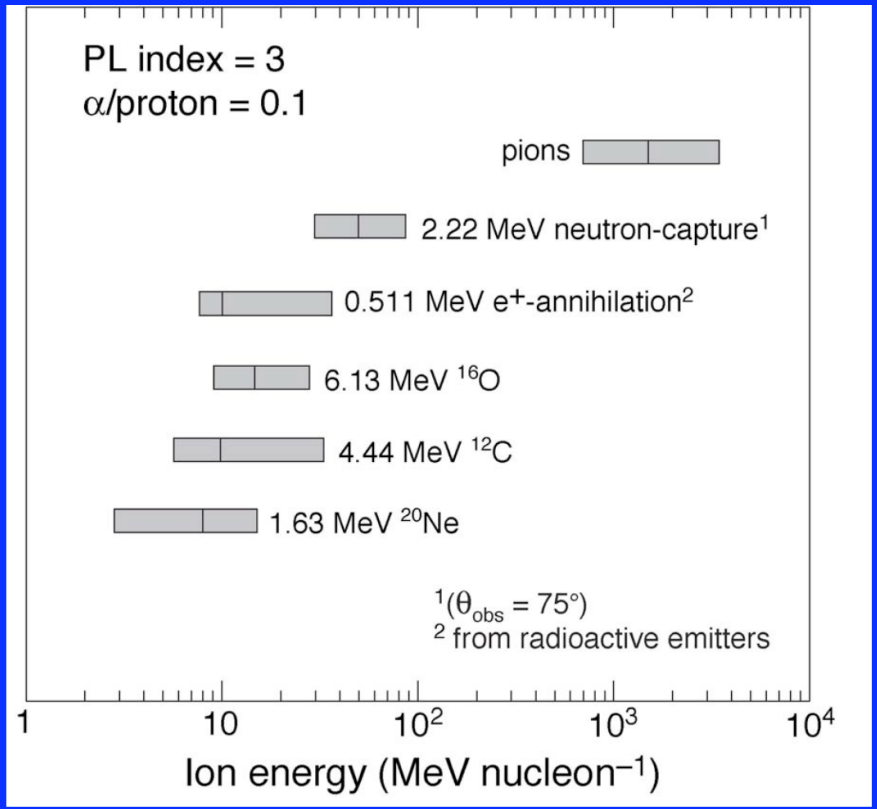

Share 2007

Solar Flares in Gamma-rays

Calculated Pion-decay Photon Spectra (cont.)

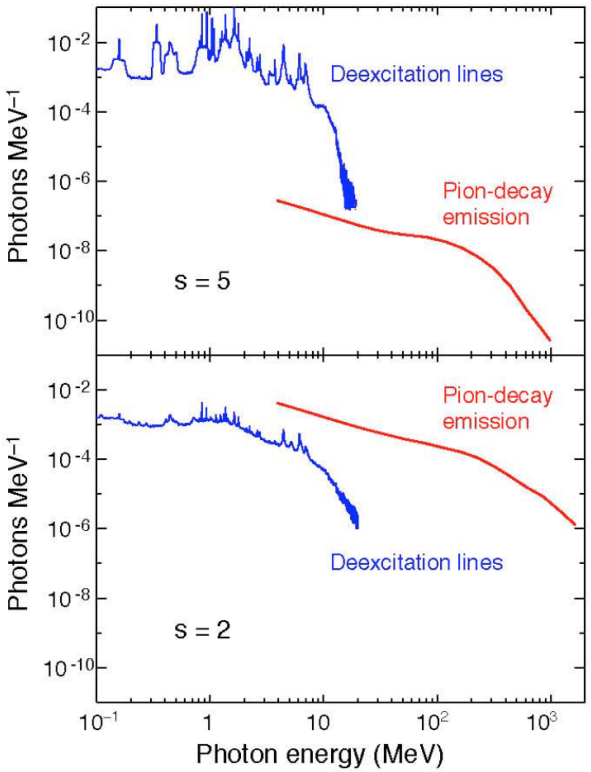

The ratio of pion-decay emission to nuclear deexcitation-line emission depends very strongly on the steepness of the accelerated-ion kinetic-energy spectrum

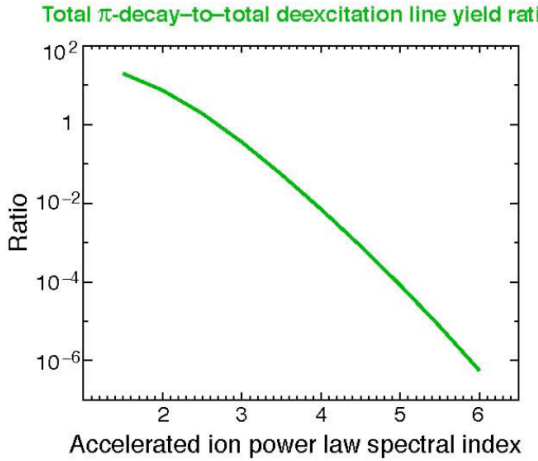

This ratio can be used to determine the accelerated-ion spectral index

Murphy, Poster 16.16

Share 2007

Solar Flares in Gamma-rays

Study particle acceleration and magnetic trapping of high-energy ions from minutes to hours after flares (e.g. EGRET observation on June 11, 1991; Kanbach et al.)

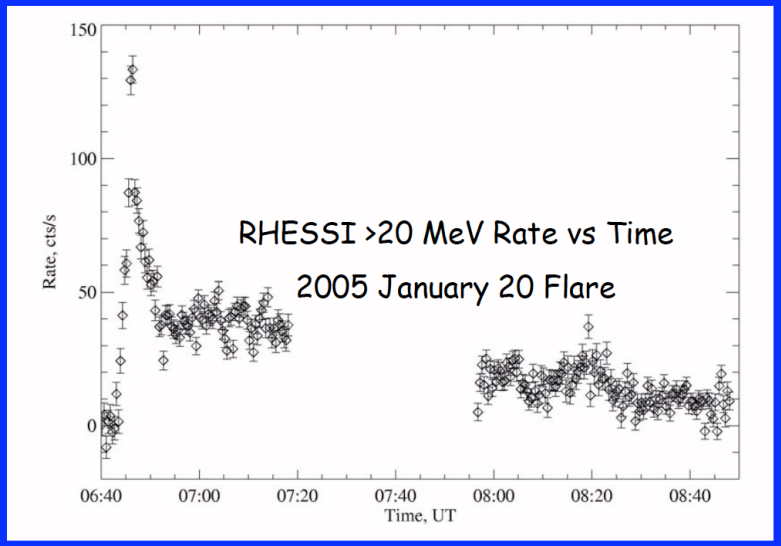

LAT is 10^4 times more sensitive to pion radiation than RHESSI

Share 2007

Solar Flares in Gamma-rays

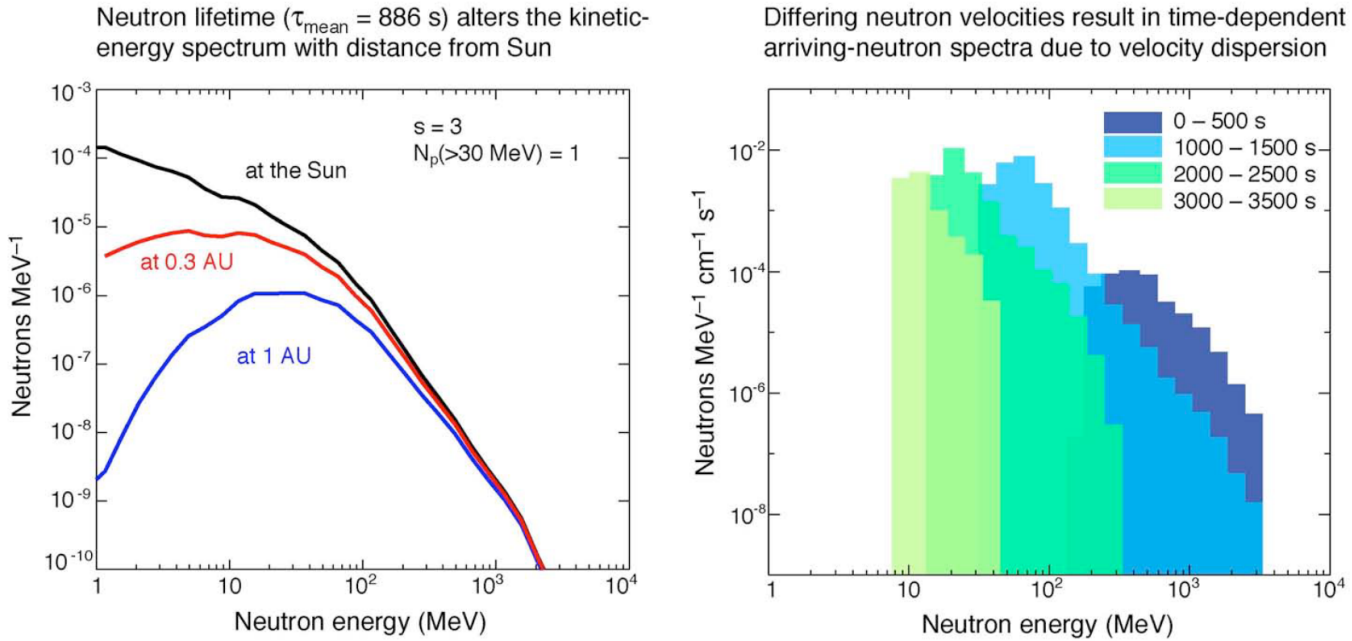

Murphy, Poster 16.16

GBM will also detect an increase minutes after the impulsive phase of the flare.

Share 2007

Solar Flares in Gamma-rays

20 January 2005 06:44-06:56

RHESSI, Hurford et al. 2007

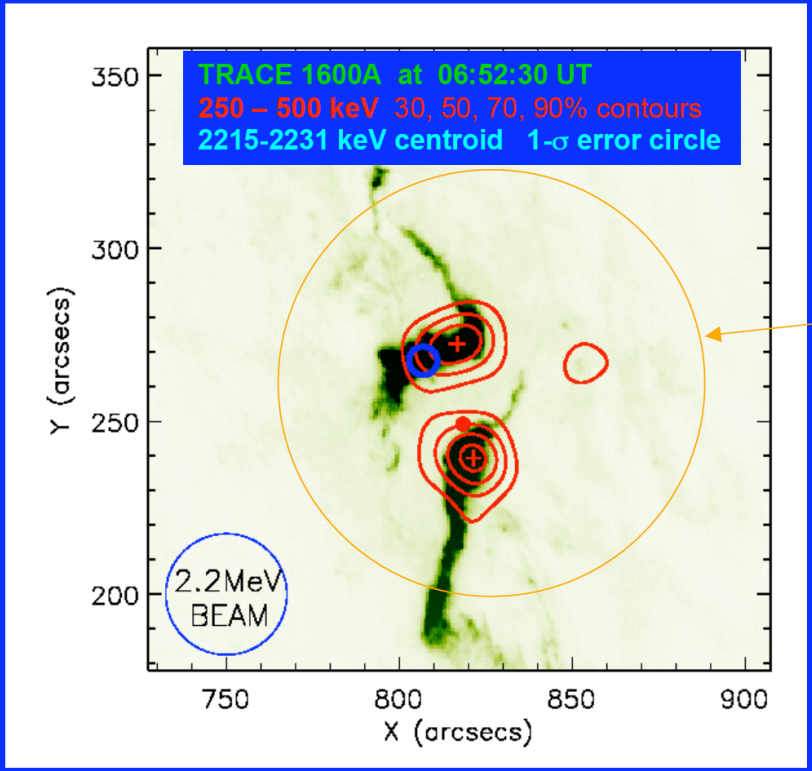

GLAST Location

Localize the source of >1 GeV photons to ~30 arc sec

Share 2007

Astrofisica Nucleare e Subnucleare

Laboratory for Gamma Astrophysics - 1

Fermi Key Features

- Two instruments:
  - LAT:
    - high energy (20 MeV – >300 GeV)
  - GBM:
    - low energy (8 keV – 40 MeV)

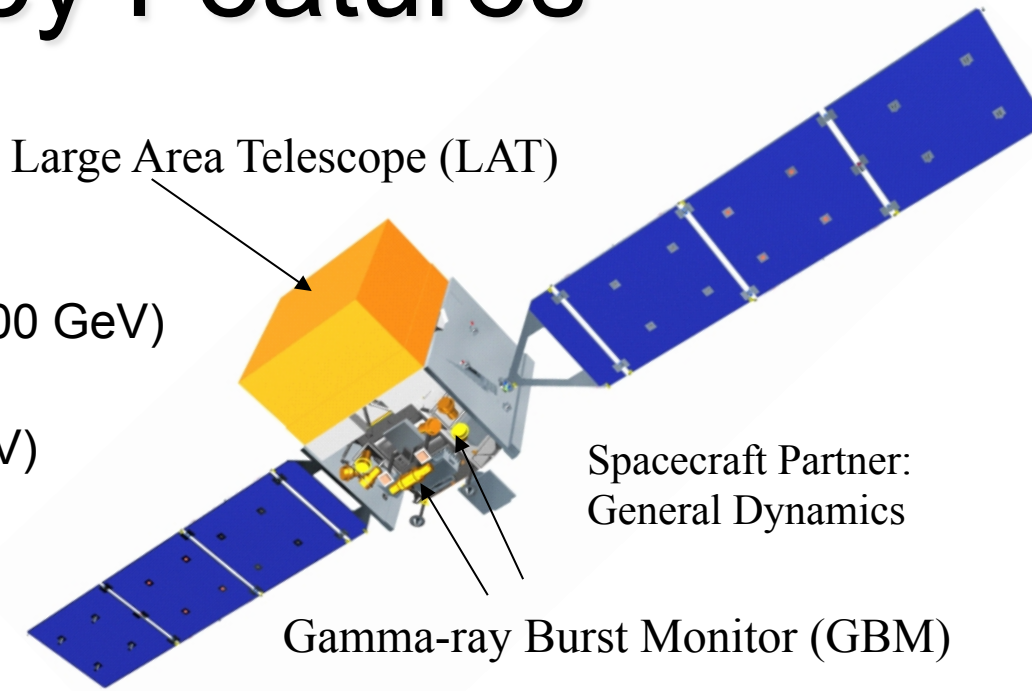

- Huge field of view
  - LAT: 20% of the sky at any instant; in sky survey mode, expose all parts of sky for ~30 minutes every 3 hours. GBM: whole unocculted sky at any time.

The Observatory

Fermi/GBM detector (2008 -- ..)

BGO detector unit

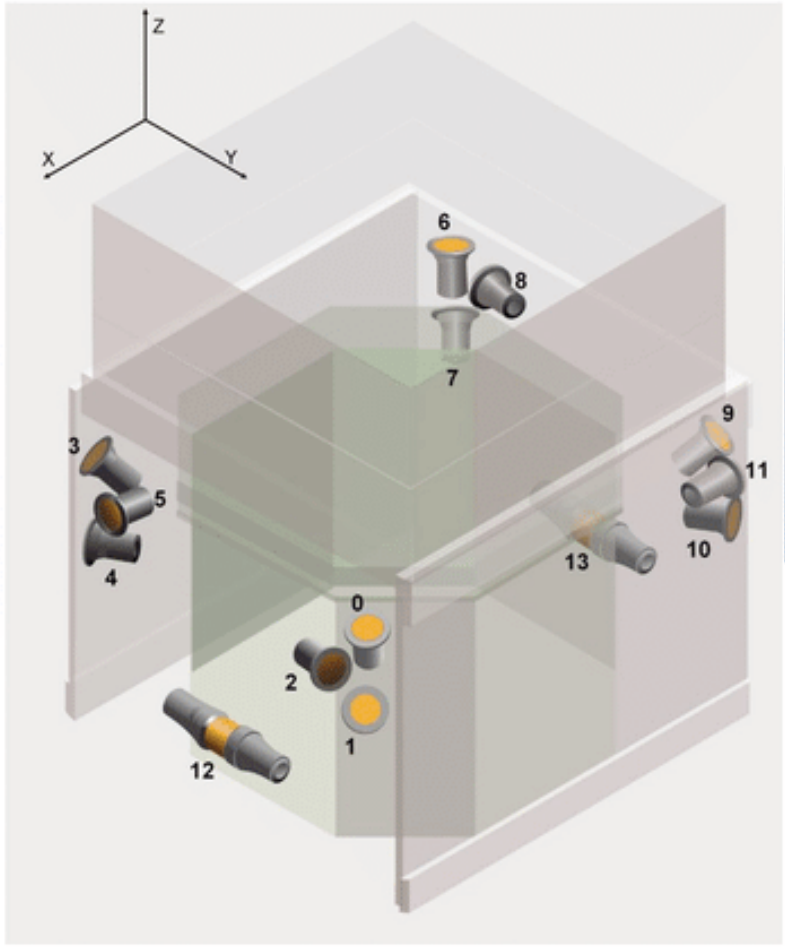

NaI(Tl)-detector flight unit

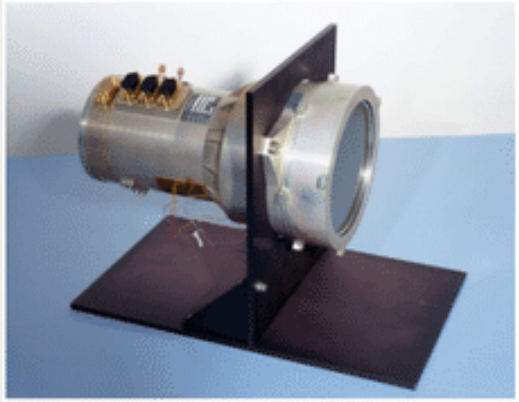

Fermi Data

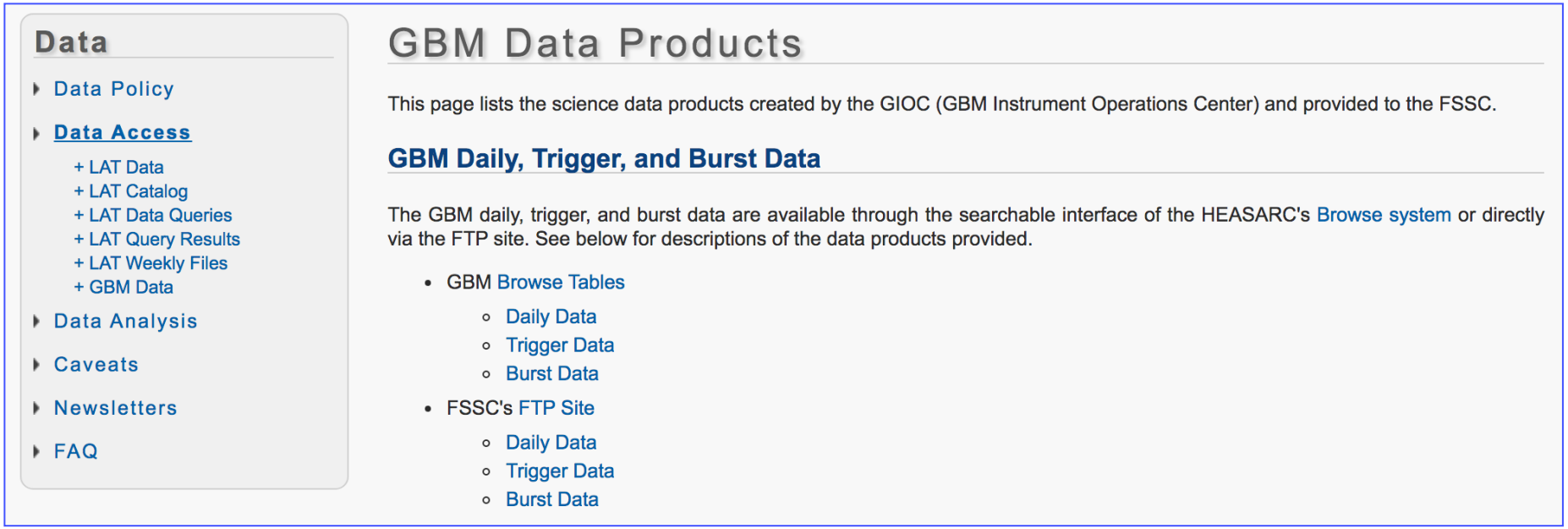

Data

- Data Policy
- **Data Access**
  - + LAT Data
  - + LAT Catalog
  - + LAT Data Queries
  - + LAT Query Results
  - + LAT Weekly Files
  - + GBM Data
- Data Analysis
- Caveats
- Newsletters
- FAQ

GBM Data Products

This page lists the science data products created by the GIOC (GBM Instrument Operations Center) and provided to the FSSC.

GBM Daily, Trigger, and Burst Data

The GBM daily, trigger, and burst data are available through the searchable interface of the HEASARC's Browse system or directly via the FTP site. See below for descriptions of the data products provided.

- GBM Browse Tables
  - Daily Data
  - Trigger Data
  - Burst Data
- FSSC's FTP Site
  - Daily Data
  - Trigger Data
  - Burst Data

https://fermi.gsfc.nasa.gov/ssc/data/access/gbm/

Fermi Data

ID	Name	Description
GS-001	CTIME (daily version)	The counts accumulated every 0.256 seconds in 8 energy channels for each of the 14 detectors.
GS-002	CSPEC (daily version)	The counts accumulated every 8.192 seconds in 128 energy channels for each of the 14 detectors.
GS-003	TTE (continuous version)	Event data for each detector with a time precise to 2 microseconds, in 128 energy channels. The downlink schedule determines how many data files are produced each day. These files are being replaced by the GS-013 hourly TTE files.
GS-005	GBM gain and energy resolution history	History of the detector gains and energy resolutions; required for calculating Detector Response Matrices (DRMs).
GS-006	Fermi position and attitude history	History of Fermi's position and attitude, required for calculating DRMs.
GS-013	TTE (hourly version)	Time tagged events for each detector which occurred during the hour (including up to the last 120 seconds of events from the previous hour) with a time precise to 2 microseconds, in 128 energy channels.

https://fermi.gsfc.nasa.gov/ssc/data/access/gbm/

Fermi Data

ID	Name	Description
GS-101	CTIME (burst version)	For each detector, the counts accumulated every 0.064 s in 8 energy channels
GS-102	CSPEC (burst version)	For each detector, the counts accumulated every 1024 s in 128 energy channels.
GS-103	GBM TTE (burst version)	Event data for the burst. There is one file for each detector.
GS-104	GBM DRMs	8 and 128 energy channel Detector Response Matrices (DRMs) for all 14 detectors. These files may not be produced for all triggers.
GS-105	GBM Trigger Catalog Entry	Classification of GBM trigger with some characteristics (e.g., trigger time, coordinates). This file is used to create the GBM Trigger Catalog.
GS-107	GBM TRIGDAT	All the GBM's messages downlinked through TDRSS. These messages are the basis of the GCN Notices for the burst.
	Quicklook Plots	Lightcurves and spacecraft pointing history files in GIF and PDF format.

https://fermi.gsfc.nasa.gov/ssc/data/access/gbm/

Quick Look

Browse this table...

FERMIGBRST - Fermi GBM Burst Catalog

HEASARC Archive

Overview

When referencing results from this online catalog, please cite von Kienlin, A. et al. 2020, Gruber, D. et al. 2014, von Kienlin, A. et al. 2014, and Bhat, P. et al. 2016.

This table lists all of the triggers observed by a subset of the 14 GBM detectors (12 NaI and 2 BGO) which have been classified as gamma-ray bursts (GRBs). Note that there are two Browse catalogs resulting from GBM triggers. All GBM triggers are entered in the Fermi GBM Trigger Catalog, while only those triggers classified as bursts are entered in the Burst Catalog. Thus, a burst will be found in both the Trigger and Burst Catalogs. The Burst Catalog analysis requires human intervention; therefore, GRBs will be entered in the Trigger Catalog before the Burst Catalog. The latency requirements are 1 day for triggers and 3 days for bursts. There are four fewer bursts in the online catalog than in the Gruber et al. 2014 paper. The four missing events (081007224, 091013989, 091022752, and 091208623) have not been classified with certainty as GRBs and are not included in the general GRB catalog. This classification may be revised at a later stage.

The GBM consists of an array of 12 sodium iodide (NaI) detectors which cover the lower end of the energy range up to 1 MeV. The GBM triggers off of the rates in the NaI detectors, with some Terrestrial Gamma-ray Flash (TGF)-specific algorithms using the bismuth germanate (BGO) detectors, sensitive to higher energies, up to 40 MeV. The NaI detectors are placed around the Fermi spacecraft with different orientations to provide the required sensitivity and FOV. The cosine-like angular response of the thin NaI detectors is used to localize burst sources by comparing rates from detectors with different viewing angles. The two BGO detectors are placed on opposite sides of the spacecraft so that all sky positions are visible to at least one BGO detector.

The signals from all 14 GBM detectors are collected by a central Data Processing Unit (DPU). This unit digitizes and time-tags the detectors' pulse height signals, packages the resulting data into several different types for transmission to the ground (via the Fermi spacecraft), and performs various data processing tasks such as autonomous burst triggering.

The GRB science products are transmitted to the FSSC in two types of files. The first file, called the "bcat" file, provides basic burst parameters such as duration, peak flux and fluence, calculated from 8-channel data using a spectral model which has a power-law in energy that falls exponentially above an energy EPeak, known as the Comptonized model. The crude 8-channel binning and the simple spectral model allow data fits in batch mode over numerous time bins in an efficient and robust fashion, including intervals with little or no flux, yielding both values for the burst duration, and deconvolved lightcurves for the detectors included in the fit. The bcat file includes two extensions. The first, containing detailed information about energy channels and detectors used in the calculations, is detector-specific, and includes the time history of the deconvolved flux over the time intervals of the burst. The second shows the evolution of the spectral parameters obtained in a joint fit of the included detectors for the model used, usually the Comptonized model described above. The bcat files and their time-varying quantities contained in these two extensions are available at the HEASARC FTP site. Quantities derived from these batch fits are given in the bcat primary header and presented in the Browse table, as described below. The main purpose of the analysis contained in the bcat file is to produce a measure of the duration of the burst after deconvolving the instrument response. The duration quantities are:

```
 * 't50' - the time taken to accumulate 50% of the burst fluence starting at the 25% fluence level.
 * 't90' - the time taken to accumulate 90% of the burst fluence starting at the 5% fluence level.
```

By-products of this analysis include fluxes on various timescales and fluences, both obtained using the simple Comptonized model described above. These quantities are detailed in the Browse table using the following prefixes:

```
 * 'flux' - the peak flux over 3 different timescales obtained in the batch mode fit used to calculate t50/t90.
 * 'fluence' - the total fluence accumulated in the t50/t90 calculation.
```

The fluxes and fluences derived from the 8-channel data for these bcat files should be considered less reliable than those in the spectral analysis files described below.

https://heasarc.gsfc.nasa.gov/W3Browse/all/fermigbrst.html

Quick Look

https://heasarc.gsfc.nasa.gov/W3Browse/all/fermigbrst.html

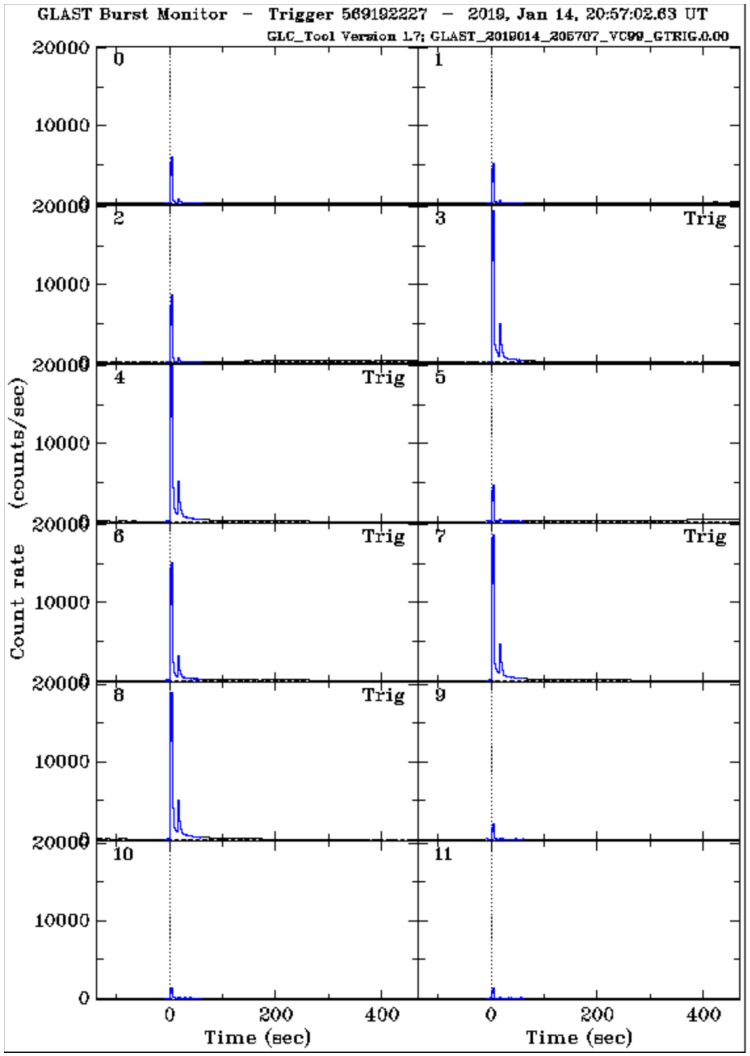

gtburst analysis

Data

- Data Policy
- Data Access
- **Data Analysis**
  - + System Overview
  - + Software Download
  - + Documentation
  - + Cicerone
  - + Analysis Threads
  - + User Contributions
- Caveats
- Newsletters
- FAQ

GTBURST

This tutorial provides a step-by-step guide to using the gtburst GUI for GRB and solar flare analysis of GBM and LAT data. You can also watch a video tutorial

What it is used for?

Gtburst can be used to do the following:

- GBM data:
  - download data from the GBM Trigger catalog, select data analysis interval, and interactively fit the background
  - write out pha and rsp files for spectral analysis in either XSPEC or RMFIT
- LLE data:
  - download data from the Fermi LAT Low-Energy Events Catalog, select data analysis interval, and interactively fit the background
  - write out pha and rsp files for spectral analysis in either XSPEC or RMFIT
- LAT data:
  - download photon events and spacecraft data from the LAT Data server
  - produce navigation plots to allow user to select optimal time intervals and zenith cuts
  - do photon selections based on energy, Region Of Interest (ROI), time, zenith, event class
  - produce counts maps
  - do likelihood analysis given a simple spectral model and background models
  - localization using gtfindsrc or a TS map
  - writes out pha and rsp files for spectral analysis in either XSPEC or RMFIT

https://fermi.gsfc.nasa.gov/ssc/data/analysis/scitools/gtburst.html

gtburst analysis

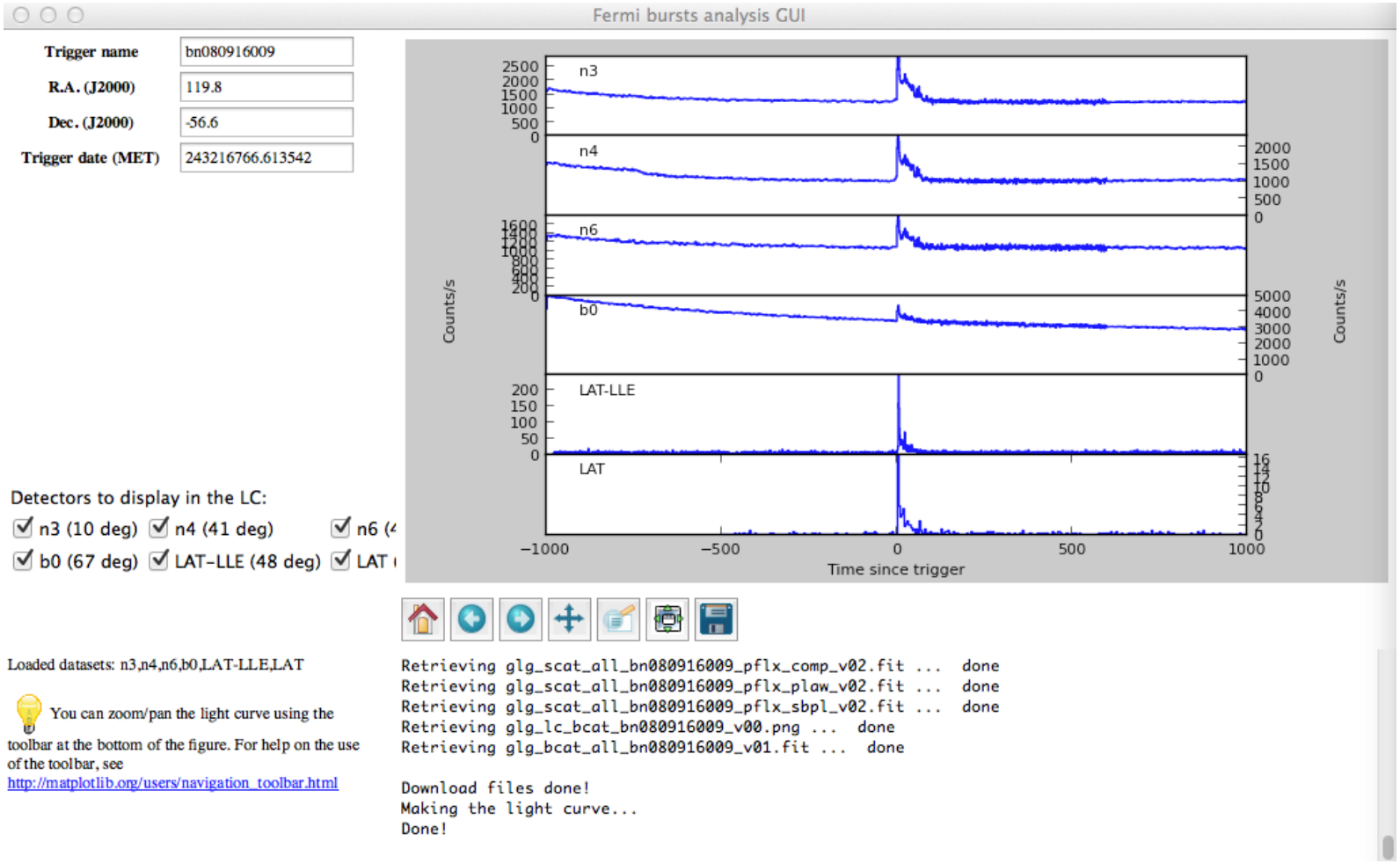

https://fermi.gsfc.nasa.gov/ssc/data/analysis/scitools/gtburst.html

Check the “Navigation” plot

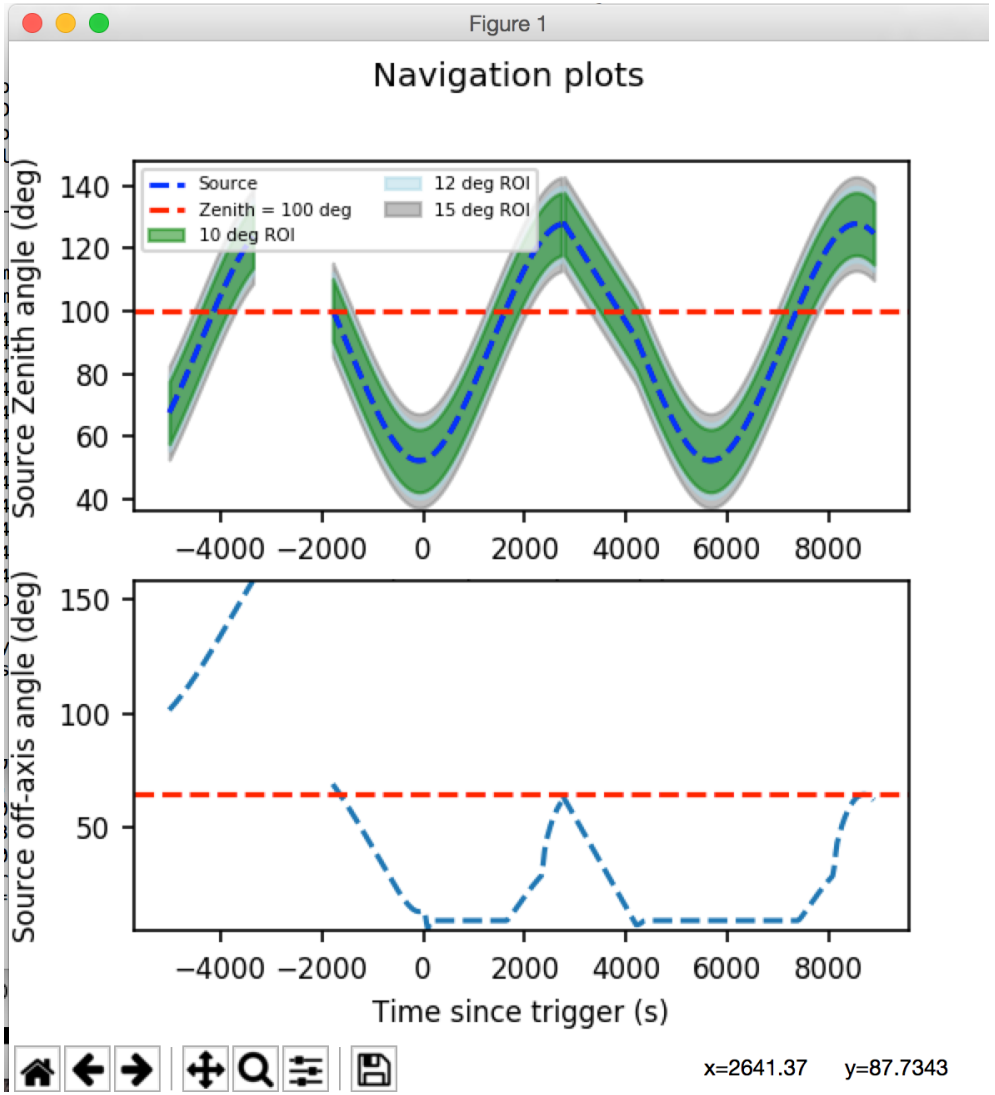

GRB analysis with gtburst

Fermi bursts analysis GUI

Trigger name	bn160905471
R.A. (J2000)	162.245
Dec. (J2000)	-50.801
Trigger date (MET)	494767139.912

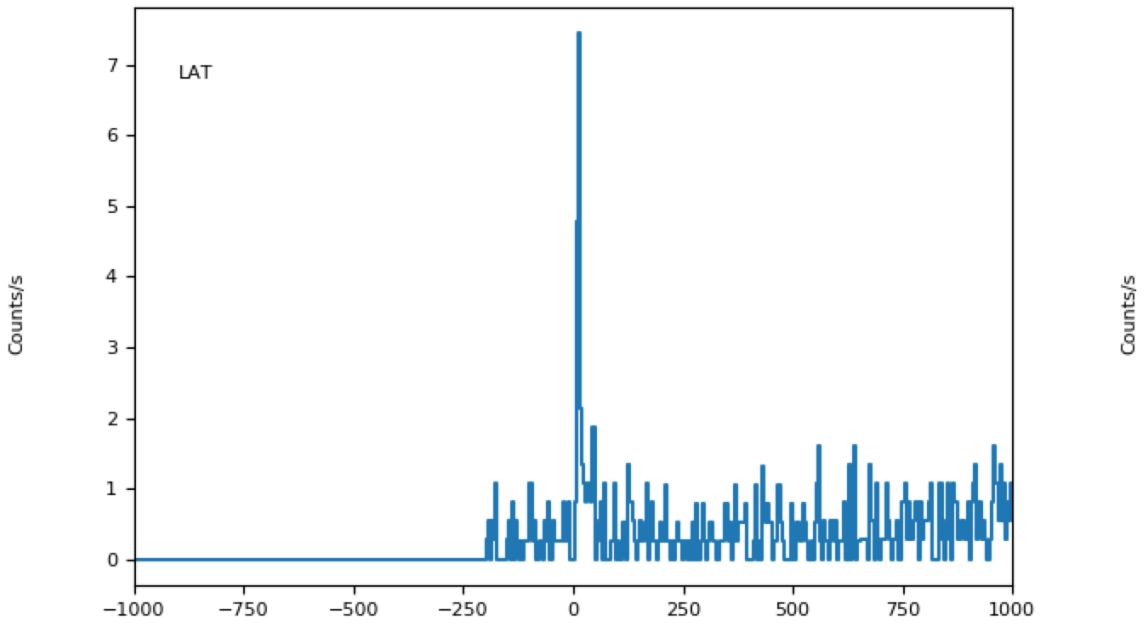

Detectors to display in the LC:

☑ LAT (16 deg)

Loaded datasets: LAT

You can zoom/pan the light curve using the toolbar at the bottom of the figure. For help on the use of the toolbar, see http://matplotlib.org/users/navigation_toolbar.html

```
    done.

 *  Updating keywords in the headers of the CSPEC file...

    done.

gtllebin done!
Making the light curve...
Done!
```

RMFIT analysis

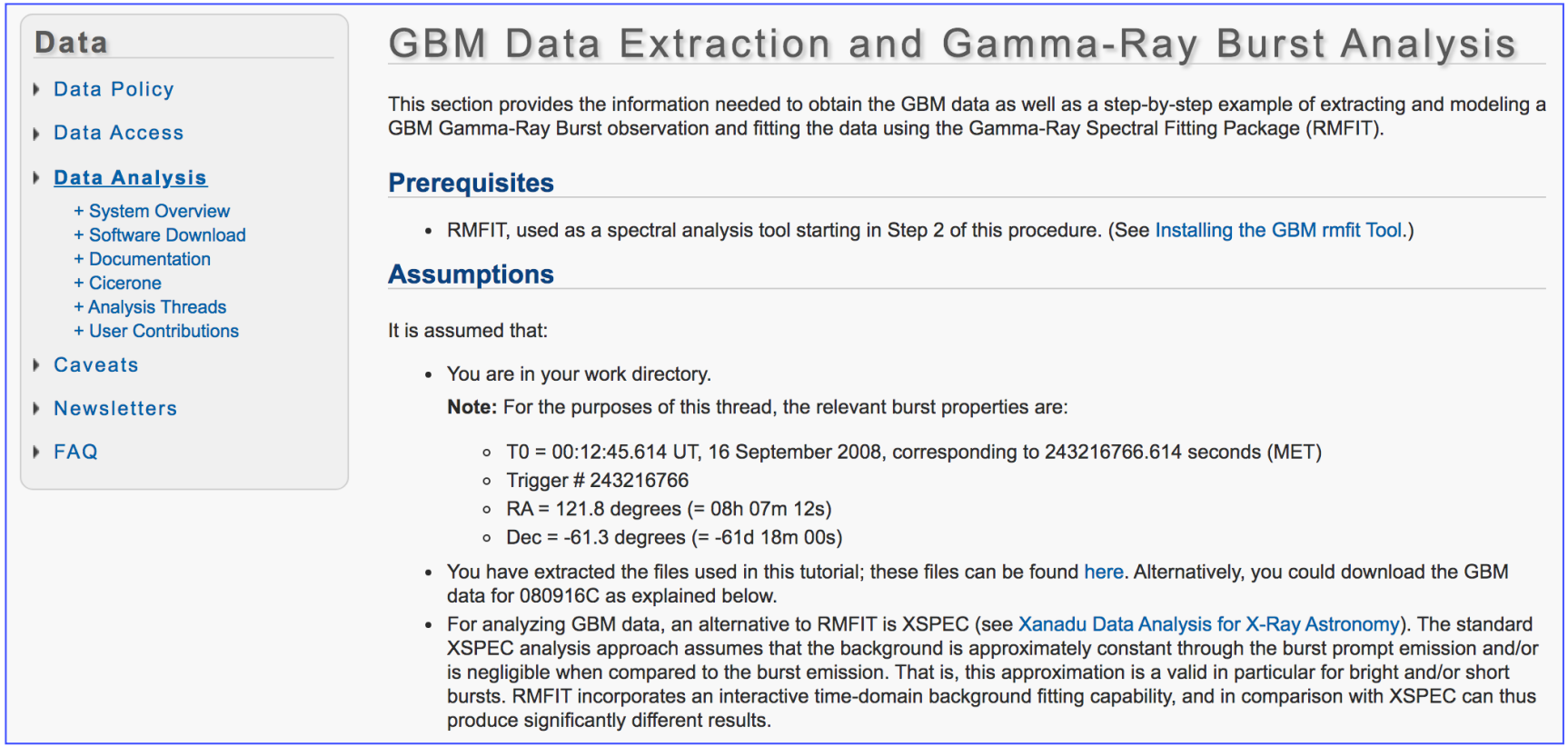

Data

- Data Policy
- Data Access
- **Data Analysis**
  - + System Overview
  - + Software Download
  - + Documentation
  - + Cicerone
  - + Analysis Threads
  - + User Contributions
- Caveats
- Newsletters
- FAQ

GBM Data Extraction and Gamma-Ray Burst Analysis

This section provides the information needed to obtain the GBM data as well as a step-by-step example of extracting and modeling a GBM Gamma-Ray Burst observation and fitting the data using the Gamma-Ray Spectral Fitting Package (RMFIT).

Prerequisites

- RMFIT, used as a spectral analysis tool starting in Step 2 of this procedure. (See Installing the GBM rmfit Tool.)

Assumptions

It is assumed that:

- You are in your work directory.

  Note: For the purposes of this thread, the relevant burst properties are:

  - T0 = 00:12:45.614 UT, 16 September 2008, corresponding to 243216766.614 seconds (MET)
  - Trigger # 243216766
  - RA = 121.8 degrees (= 08h 07m 12s)
  - Dec = -61.3 degrees (= -61d 18m 00s)
- You have extracted the files used in this tutorial; these files can be found here. Alternatively, you could download the GBM data for 080916C as explained below.
- For analyzing GBM data, an alternative to RMFIT is XSPEC (see Xanadu Data Analysis for X-Ray Astronomy). The standard XSPEC analysis approach assumes that the background is approximately constant through the burst prompt emission and/or is negligible when compared to the burst emission. That is, this approximation is a valid in particular for bright and/or short bursts. RMFIT incorporates an interactive time-domain background fitting capability, and in comparison with XSPEC can thus produce significantly different results.

https://fermi.gsfc.nasa.gov/ssc/data/analysis/scitools/rmfit_tutorial.html

RMFIT analysis

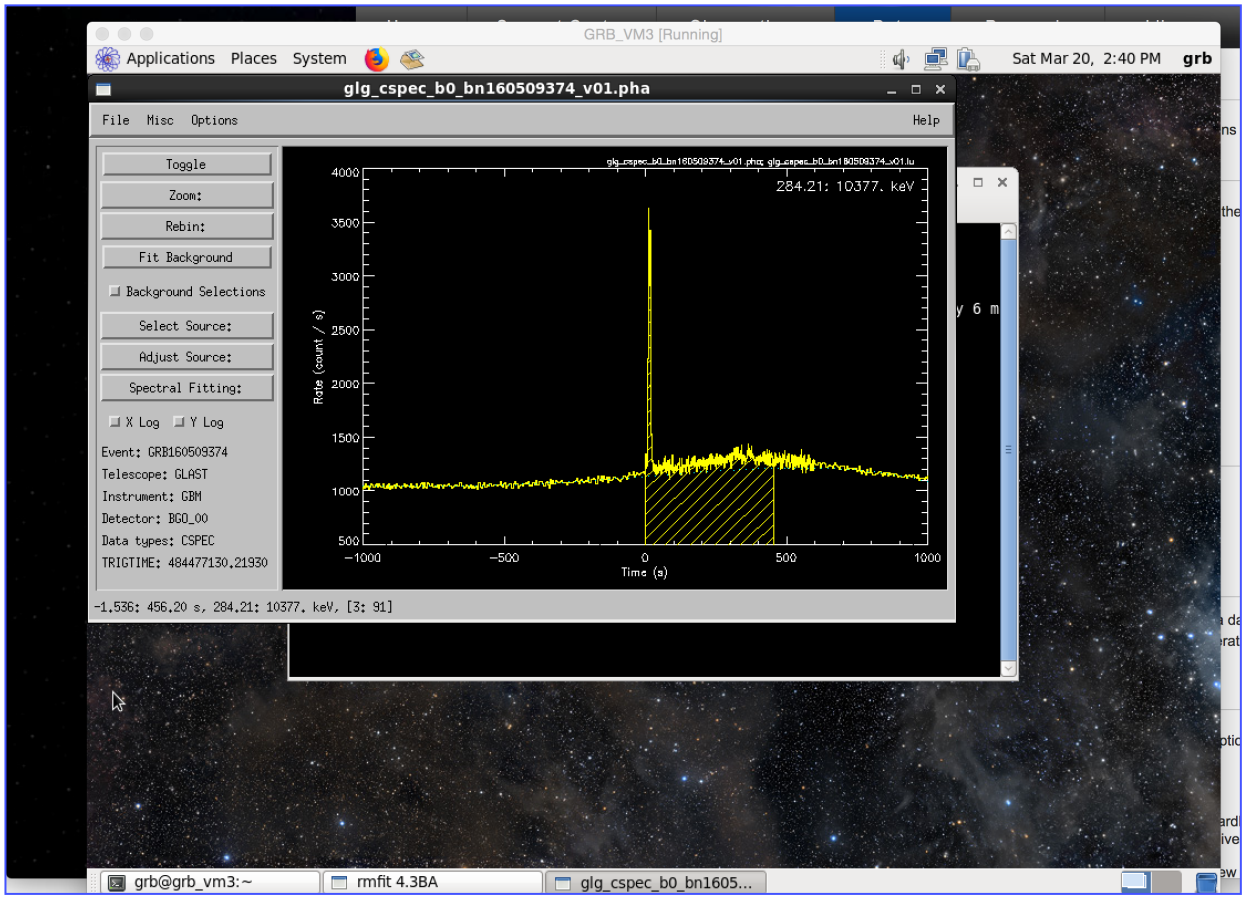

https://fermi.gsfc.nasa.gov/ssc/data/analysis/scitools/rmfit_tutorial.html

RMFIT analysis

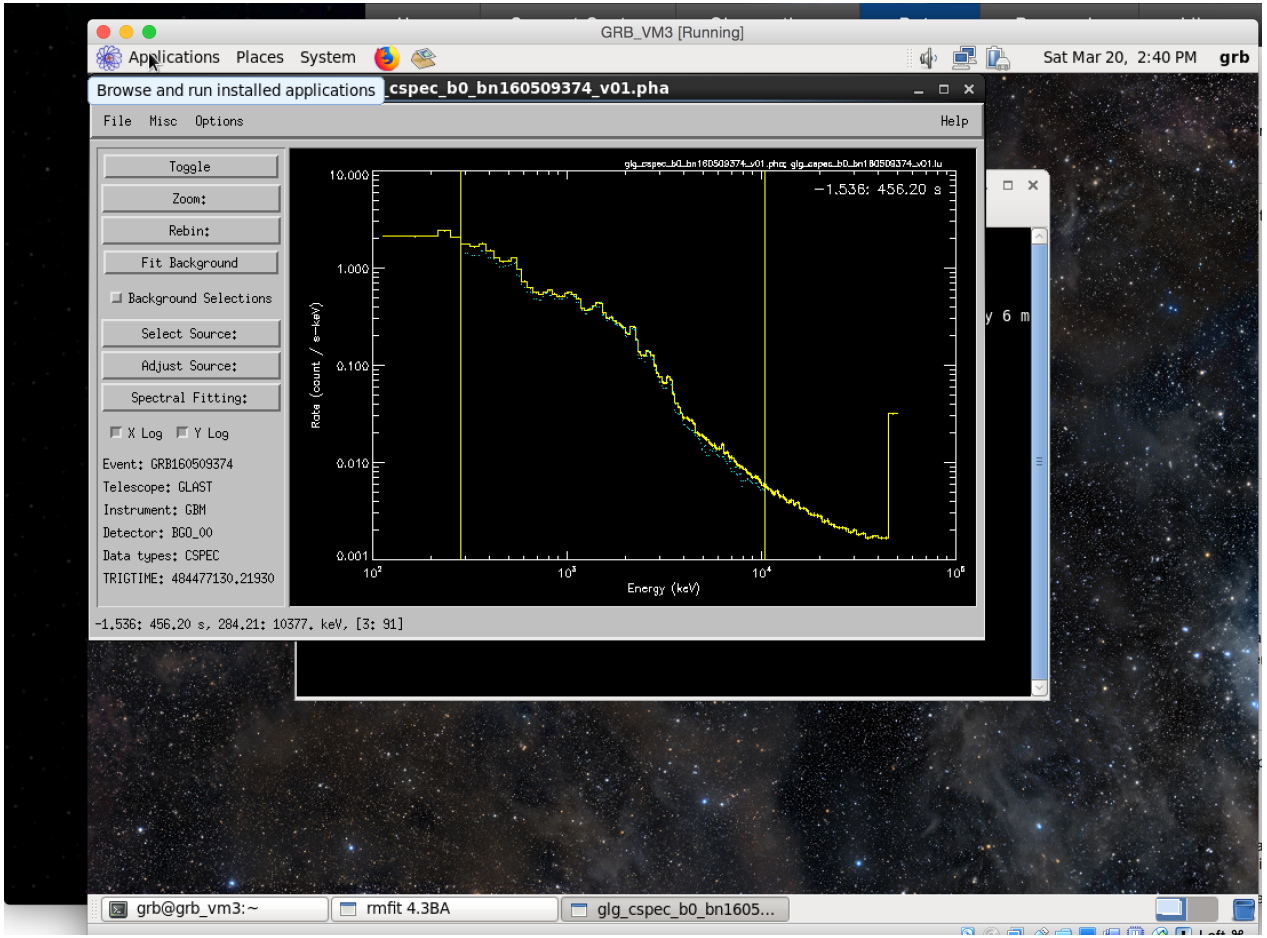

https://fermi.gsfc.nasa.gov/ssc/data/analysis/scitools/rmfit_tutorial.html

GBMDataTools analysis

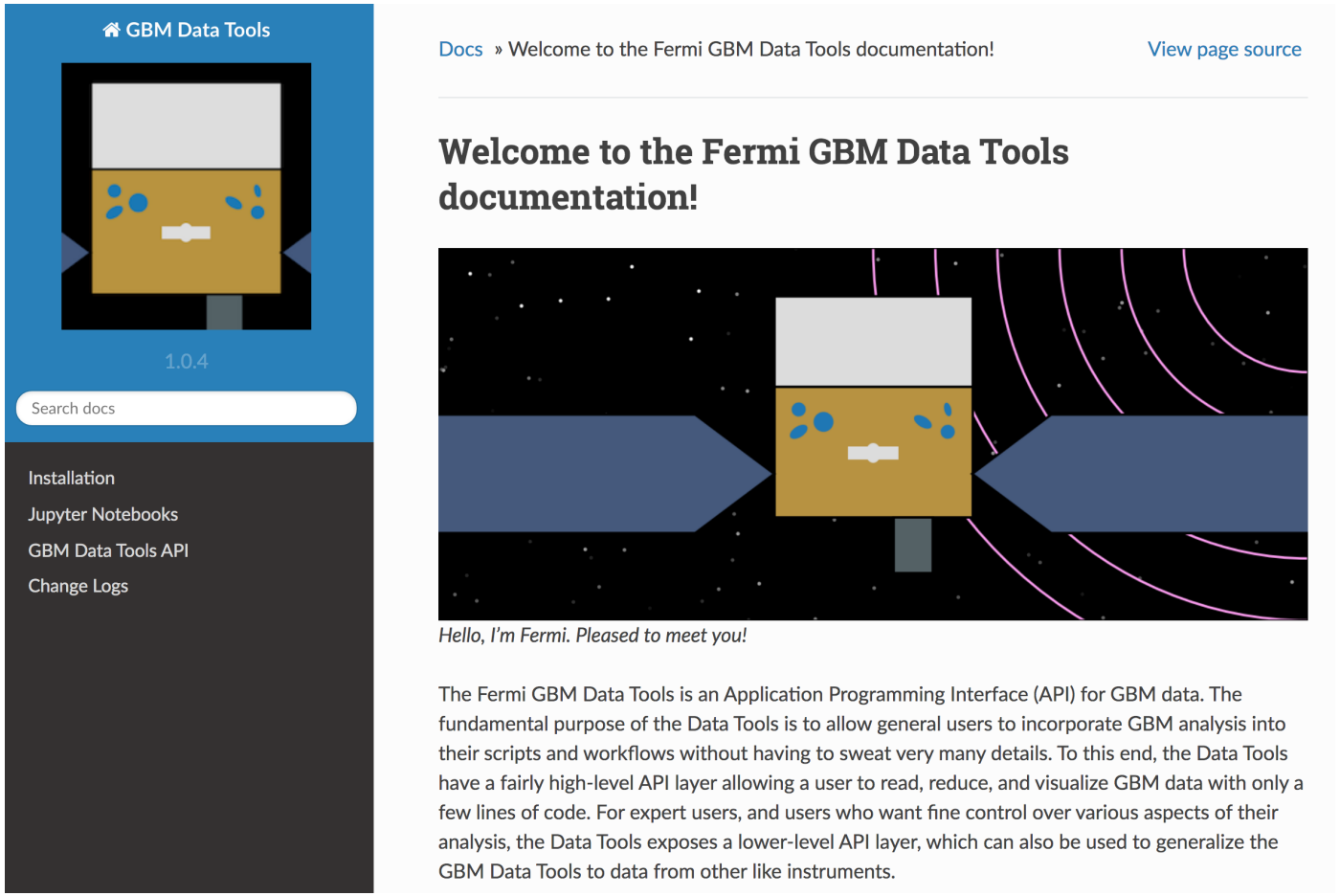

https://fermi.gsfc.nasa.gov/ssc/data/analysis/gbm/gbm_data_tools/gdt-docs/